



Finding the strength of glass

A mechanical and fractographic research
of glass' biaxial strength for structural
purposes

O. van der Velde

Technische Universiteit Delft

FINDING THE STRENGTH OF GLASS

A MECHANICAL AND FRACTOGRAPHIC RESEARCH
OF GLASS' BIAXIAL STRENGTH FOR STRUCTURAL
PURPOSES

by

O. van der Velde

in partial fulfillment of the requirements for the degree of

Master of Science
in Civil Engineering

at the Delft University of Technology
to be defended publicly on Friday July 3, 2015 at 16:00

Supervisor

Prof. ir. R. Nijssen
Dr. ir. F. A. Veer
Dr. O.Çopuroğlu

TU Delft
TU Delft
TU Delft

An electronic version of this thesis is available at <http://repository.tudelft.nl/>

Acknowledgements

This thesis was written as part of the Civil Engineering master curriculum at the Delft University of Technology.

I would like to express my gratitude to all of those who have helped me in completing this master thesis.

Special thanks to Fred Veer, my main supervisor, for sharing his wide expertise on glass and fracture mechanics with me and his patience in answering my questions.

Secondly, I would like to thank Oğuzhan Çopuroğlu for sharing his expertise on microscopy, which resulted in an interesting approach to glass fractography, and for his motivational spirit. I would like to thank Rob Nijse for keeping an eye on the general organisation and giving his feedback on the structural design part.

My appreciation goes out to the technical assistants who helped me: Kees Baardolf, for building the test set up and always having time for a chat, Kees van Beek, for providing the electrical equipment and giving his view on the issues I encountered and Ger Nagtegaal, for endlessly performing the strength tests with me and truly helping me figure out any problems we encountered.

On a personal note, I would like to share my gratitude towards my parents, for always supporting me in my studies both financially and emotionally, towards my friends for their help and motivation and towards my boyfriend for his support and sharp feedback.

O. van der Velde
Delft, June 2015

Abstract

Over the years, glass has been increasingly used as a structural building material. Structural calculations on glass are conservative because the strength is quite uncertain. Weibull plots of the strength of glass can range from 20 MPa to 150 MPa. This is caused by flaws, which are not visible to the human eye and therefore it is difficult to predict glass strength. Because of this uncertainty, in practice, 20 MPa is assumed and a high safety factor is applied. Therefore, more research on glass' strength is important. This thesis focusses on gaining a better understanding of the biaxial strength of glass. This was achieved by performing a literature study and conducting strength tests and microscopic observations.

A ring on ring test was chosen for the tensile biaxial strength testing. 53 cruciform plates were tested of which 5 with a rosette strain gauge. It was found that the ring on ring formula, that gives the biaxial tensile stress within the inner loading ring, deviates around 20% from the strain measurements. This can be attributed to assumptions that were made to derive the formula. Therefore, the formula should be further explored with more strain measurements and, if necessary, finite element modelling . Additionally, there was a variability in the strain measurements, which might have been caused by friction.

Moreover, 30 out of the 53 tested plates showed circumferential cracking at the support ring, which is not mentioned in literature. For these tests, recommended ratios from biaxial testing on ceramics were applied. 10 tests of glass plates with different ratios resulted in no circumferential cracking at the support ring. It was concluded that the recommended ratios should be changed for the application on glass.

A traditional fractographic analysis of glass consists of a fracture pattern analysis by eye and a fracture surface analysis by eye and by microscope. In this research, it was suggested to also study the fracture pattern by microscope. By using a transmitted light microscope with Z axis builder software a multicolour image was obtained representing all flaws and fracture marks throughout the thickness of the glass plates. This turned out to be a valuable addition, because this image revealed fracture marks that would otherwise have been overlooked. These can be used as a quick guide to find the fracture origin and give new insights on the crack propagation.

In future research, it is recommended to optimise the ring on ring test so that certainty is acquired about the strength results. With a fractographic analysis, different flaw types can be characterised. It is expected that when these flaw types are related to the strength data, more sensible Weibull plots can be made. This information can then be used as an input for a better glass strength assessment and improvement.

Contents

1	Introduction	1
1.1	Problem definition	1
1.2	Scope	1
1.3	Objective	2
1.4	Research questions	2
1.5	Thesis outline	2
2	Glass	3
2.1	Introduction	3
2.2	Chemistry of glass	3
2.2.1	Atomic structure	3
2.2.2	Conclusions	7
2.3	Manufacturing of glass	7
2.3.1	Production process	7
2.3.1.1	Drawn glass	7
2.3.1.2	Rolled glass	7
2.3.1.3	Float glass	8
2.3.2	Mechanical processing of glass	8
2.3.2.1	Cutting	9
2.3.2.2	Grinding	9
2.3.2.3	Drilling	9
2.3.3	Thermal processing	9
2.3.3.1	Annealing	9
2.3.3.2	Tempering	9
2.3.3.3	Heat-strengthening	10
2.3.4	Conclusions	10
2.4	Glass as a structural material	10
2.4.1	Strength of glass	11
2.4.2	Flaws in glass	14
2.4.3	Conclusions	16

3	Failure and fracture of glass	17
3.1	Introduction	17
3.2	Materials failure	17
3.2.1	Von Mises criterion	17
3.2.2	Tresca criterion	18
3.2.3	Coulomb-Mohr	18
3.2.4	Drucker-Prager	19
3.2.5	Christensen's criterion	20
3.2.6	Conclusions	21
3.3	Fracture mechanics	22
3.3.1	Energy approach	22
3.3.2	Stress intensity approach	23
3.3.3	Fracture mechanics of flaws	24
3.3.4	Crack tip plasticity	25
3.3.5	Conclusions	26
3.4	Statistics of glass	27
3.4.1	Weibull analysis	27
3.4.2	Weibull analysis of glass	27
3.4.3	Conclusions	28
4	Testing methods	29
4.1	Introduction	29
4.2	Biaxial testing	29
4.2.1	Biaxial testing on concrete	29
4.2.2	Biaxial testing on ceramics	31
4.2.3	Biaxial testing on glass	32
4.2.4	Conclusions	32
4.3	Forensic analysis	32
4.3.1	Fracture pattern analysis	32
4.3.2	Fracture surface analysis	34
4.3.2.1	Fracture origin	36
4.3.3	Microscopy	37
4.3.3.1	Stereo microscope	37
4.3.3.2	Compound light microscope	38
4.3.3.3	Scanning electron microscope	39
4.3.4	Other instruments	40
4.3.5	Conclusions	41
5	Experiment	43
5.1	Introduction	43
5.1.1	Specimens	43
5.2	Ring on ring test	43
5.2.1	Test outline	44
5.2.1.1	Strain measurement	45
5.2.1.2	High speed camera	45
5.2.1.3	Compressive tensile test	45
5.2.2	Test conditions	46
5.2.2.1	Dimensions	46
5.2.2.2	Environmental conditions	47
5.2.2.3	Friction	47

5.2.3	Results	49
5.2.3.1	Strain measurements	49
5.2.3.2	Biaxial tensile test	51
5.2.3.3	High speed camera	55
5.2.3.4	Compressive tensile test	55
5.2.3.5	3mm thick glass	56
5.2.4	Conclusions	58
5.3	Fractographic analysis	59
5.3.1	Test outline	59
5.3.2	Results	59
5.3.2.1	Fracture pattern analysis	59
5.3.2.2	Microscopic analysis - qualitative	59
5.3.2.3	Microscopic analysis - quantitative	64
5.3.3	Conclusions	66
6	Application in Practice	67
6.1	Introduction	67
6.2	Safety philosophy	67
6.3	Case I	68
6.3.1	Portal design	68
6.3.1.1	Beam design	69
6.3.1.2	Roof design	70
6.3.1.3	Column design	70
6.3.1.4	Loads and factors	71
6.3.2	Calculation portal version A	71
6.3.2.1	Roof	71
6.3.2.2	Beam	72
6.3.2.3	Column	73
6.3.3	Calculation portal version B	74
6.3.3.1	Roof	74
6.3.3.2	Beam	75
6.3.3.3	Column	75
6.4	Case II	75
6.4.1	Window pane design	75
6.4.2	Calculation window pane version A	75
6.4.2.1	Biaxial bending	78
6.4.2.2	Double glazing	78
6.4.3	Calculation window pane version B	79
6.5	Material use	79
6.6	Conclusions	80
7	Conclusions	81
8	Recommendations	85
	Appendices	97

Introduction

1.1 Problem definition

Glass is more and more used as a structural material in the building industry. Whereas it is considered aesthetically pleasing, it can be challenging to work with glass. The main difficulty with glass is the uncertainty of its strength. A large variability occurs in most results, making it impossible to pinpoint an average strength. Glass researchers collectively agree this is to blame on flaws that occur in glass, such as inclusions or scratches [1, 2, 3, 4]. The most critical flaw determines the glass' strength. In the general research, glass strength has never been lower than 20 MPa. As a safe approach, this value is therefore applied in practice [1]. However, strength values have been reported as high as 150 MPa [4]. Due to this uncertainty in the strength, generally a high safety factor is chosen for glass: 5 to 7. A lot of material would be saved if this uncertainty could be taken away, resulting in both a lower safety factor and a higher strength value.

Quinn [5] states that the type of flaw that is most critical is just as important as the strength value in understanding the behaviour of glass. Therefore, research is needed in which both the mechanical properties as well as the fractographic processes of glass are taken into account.

1.2 Scope

A literature study was performed to gain a broad sense of all aspects that are of importance when studying glass' strength.

The mechanical part of the research was covered by biaxial strength tests. It was chosen to test on biaxial strength over uniaxial strength because:

- Not many biaxial strength tests on glass have yet been performed.
- It is more directly related to structural applications.
- The influence of the orientation of flaws is reduced.

The fractographic part consisted of a fracture pattern analysis and a microscopic examination. For the latter a transmitted light microscope and a stereo microscope were used.

There are several types of glass, depending on the ingredients used and the processes applied.

As this research is performed for structural purposes it will focus on the most common type in the building industry: Annealed soda silica lime glass.

There are three categories of flaws depending on their location in the glass: edge, surface and inside [3]. Because edges are line shaped they are best tested in a uniaxial strength test. Therefore, this research will focus at surface and volume defects. Due to the size of these defects, optical microscopy will be of help in this part.

1.3 Objective

The main goal of this study is to gain a better understanding of the biaxial strength of glass. An overview of all factors that influence glass' strength was expected to give a basic understanding. The biaxial tests are a measure of determining the glass strength and gave insight on glass' behaviour in structural applications where different load combinations occur. The fractographic analysis will reveal what happened at the microscale that caused the glass to fail.

1.4 Research questions

Main question: How can the biaxial strength of float glass be understood through a mechanical and fractographic research?

Subquestions:

- Which factors influence the strength of glass?
- How can models describe the strength of glass?
- How can the strength be mechanically determined?
- How can the strength be fractographically interpreted?
- What is the benefit for structural purposes?

1.5 Thesis outline

The first three chapters are the result of the literature study. Chapter 1 covers all aspects that influence the strength of glass, ranging from its chemical composition to the production process and from final processing to its life cycle. Each section finishes with a conclusion stating the influence on glass' strength. Chapter 2 gives an overview of relevant models that can describe glass' strength. The complexity of modelling glass failure is set out. The use of fracture mechanics at a local level in glass is elaborated. The chapter ends with the fact that glass failure is a statistical problem which can be best described by the Weibull analysis. Chapter 3 explains the possible testing methods, both for the biaxial strength testing as for the fractographic analysis. For each, a founded choice is made.

The set up, results and conclusions of these experiments are described in Chapter 4.

In Chapter 5 two cases show the application of glass in structural design and the impact of improving glass' strength assessment on the material savings.

The thesis ends with conclusions, recommendations and the appendices.

Glass

2.1 Introduction

In this chapter, basic knowledge of glass is obtained. The first section deals with glass' chemical composition and reaction. Then, different methods of manufacturing glass are set out, including mechanical and thermal process that are performed to alter glass' properties. Both of these sections end with a conclusion on how the topic covered affects the strength of glass. The last section is about glass as a structural material and elaborates how flaws drastically influence the strength of glass.

2.2 Chemistry of glass

There are numerous types of glass. In fact, any material which is heated to a melt and shows glass transformation behaviour when cooled down is a glass [6]. Glasses are characterised by not having a long range periodic atomic arrangement, which is what makes them different from crystals. If cooled fast enough, there is insufficient time for the melt to form such a periodic arrangement, leading to the fact that almost any material can form a glass.

For the building industry, generally only the transparent types are of interest. Soda-lime silicate is the most common, but others occur [1]. Borosilicate is chosen when fire resistance is important, due to its low thermal expansion coefficient. Low-iron or soda-lime glass is opted when a higher transparency is required. Additives can be used to give the glass a colour, usually these only comprise 1% of the mix. Glass used in the building industry is composed of almost 75% of silica. The melting temperature of silica is 1713°C. Adding 25% of soda lowers the melting temperature to 793°C [2]. Soda, however, is prone to ion migration. Lime is added to prevent this and thereby improve the chemical resistance of the glass. This is the reason soda-lime silica glass is most used and therefore this research will focus on that type of glass.

2.2.1 Atomic structure

To reach a better understanding of the properties and structure of glass, this section will begin at the lowest level possible to analyse: at the atom level. As was said, most common glass consists of silica (SiO_2), soda (Na_2O), lime (CaO) and potentially some additives. The base

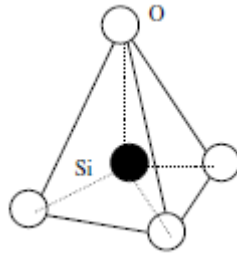


Figure 2.1: A silicon atom bonded to four oxygen atoms [2]

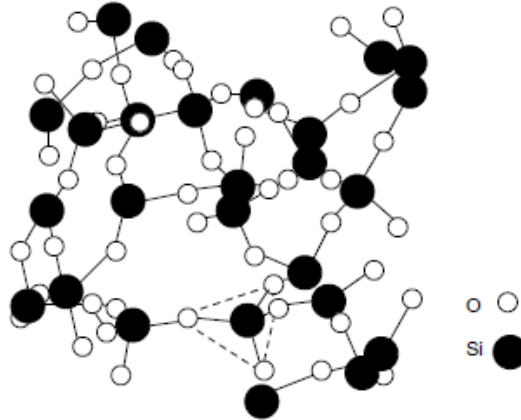


Figure 2.2: A silicon dioxide network [2]

element, silicon, tends to bond to four oxygen atoms in a tetrahedral shape [2]. See Figure 2.1. The glass structure is built up by these tetrahedra. They are connected to each other by sharing the oxygen atoms at their corners, forming a SiO_2 network. See Figure 2.2. This is more clearly represented in a 2D projection of such networks in Figure 2.3. Two tetrahedra meet only at one corner, but each oxygen atom is shared by two silicon atoms, causing all corners of tetrahedra to be shared. Figure 2.3a shows the structure of silica when it gets the time to form a long-range ordered crystalline solid. This network consists only of rings containing 6 silicon atoms which arrange themselves into a honey grid pattern. Therefore every atom's position can be predicted in this solid.

Figure 2.3b shows the structure of silica glass. The silica was not able to form a long-range ordered structure. In this case the network consists of rings containing 4 or more silicon atoms, without a predictable pattern. It is called short-range because the atomic arrangement is regular at short distances [7]. In other words, it is amorphous and has formed a glass. An amorphous material has no phase boundaries at which the light rays are scattered and therefore glass appears transparent [1].

Figure 2.3c shows the structure of silica soda glass. The sodium atom (Na^+) is called a modifier because it modifies the silica network. Na^+ ions are charged positively with $+e$. This charge is compensated by a negative charge e from a non-bridging oxygen atom, which bonds the sodium to the network [2]. Na^+ ions migrate easily. Lime is added because the Ca^{2+} ions prevent this. Apart from lowering the melting temperature, soda reduces the viscosity of molten silica glass making it easier to work with. X-ray techniques have suggested that the Na^+ ions occupy some of the free spaces left in the silica open structure. This would explain the increase in density of glass, when soda is added. The material that is added to glass controls the atomic packing

density of the glass which plays an important role in glass properties. For example, metallic glasses show a much higher Young's modulus; their packing density is 0.7 compared to 0.5 for common glasses.

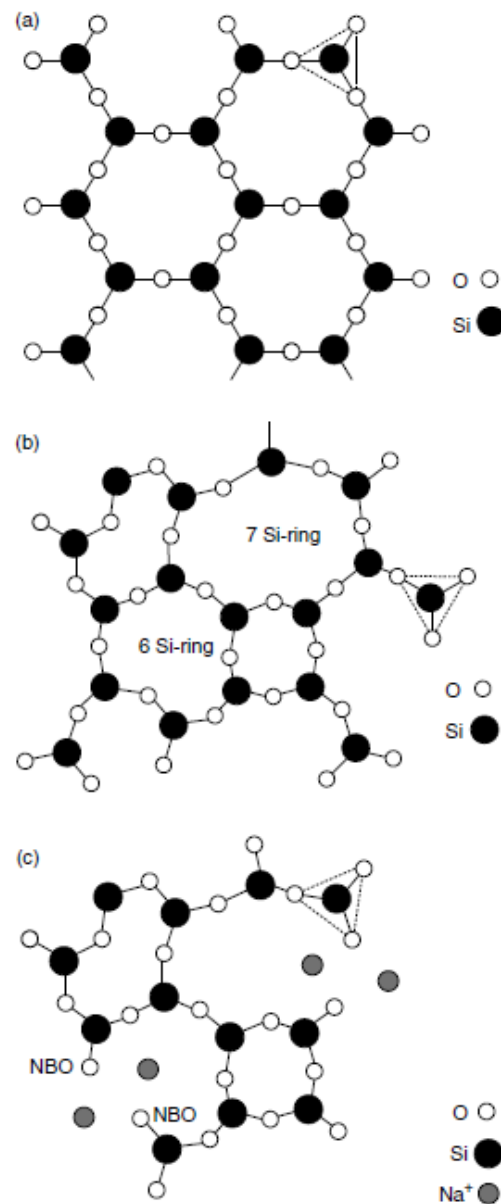


Figure 2.3: (a) A crystalline SiO_2 network, (b) an amorphous SiO_2 network, (c) A soda silica glass network [2]

The atomic structure of the surface of glass can look different than that of the glass bulk [2]. An interaction between the surface and the atmosphere takes place. Gas molecules can penetrate the open glass structure and may react with the glass. Moreover, glass can react with water [8] as is schematised in Figure 2.4. In the case of soda silica glass, the glass will undergo ion exchange, which means the Na^+ is leached from the glass [2]. The diffusion of Na^+ increases the alkalinity, thus the pH, of the aqueous solution at the surface of the glass. When pH reaches 9 silica bonds can react with hydroxide ions. This reaction is called glass corrosion because

it depolymerises the glass. See Figure 2.5. These reactions are problematic because they can change the surface properties dramatically. They are enhanced by Na_2O -, K_2O - and CaO -rich glasses and can be limited by B_2O_3 -, ZrO_2 - and TiO_2 -rich glasses, as these latter oxides act as barriers.

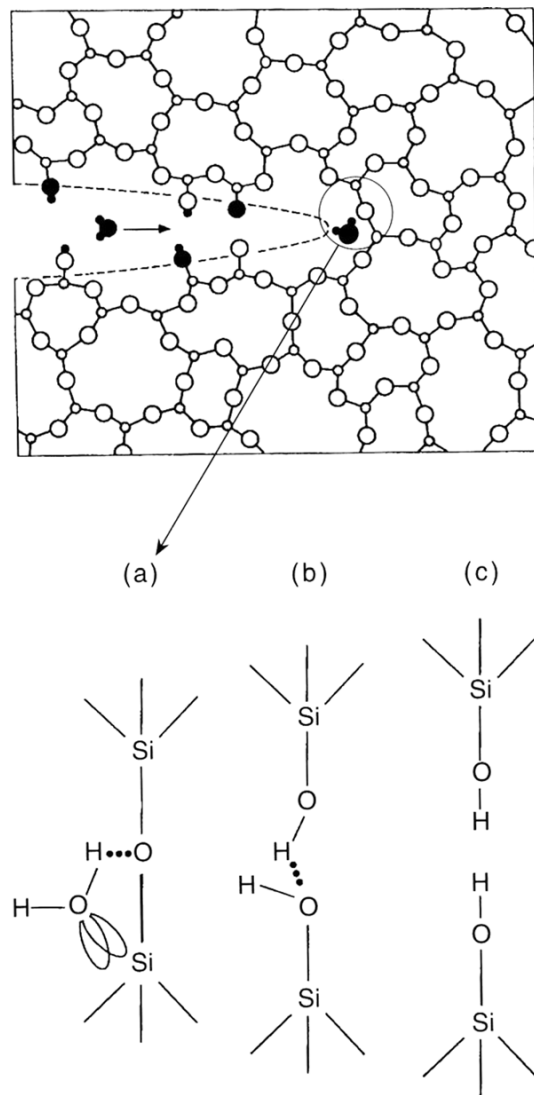


Figure 2.4: Water molecules deteriorating the glass structure [8]

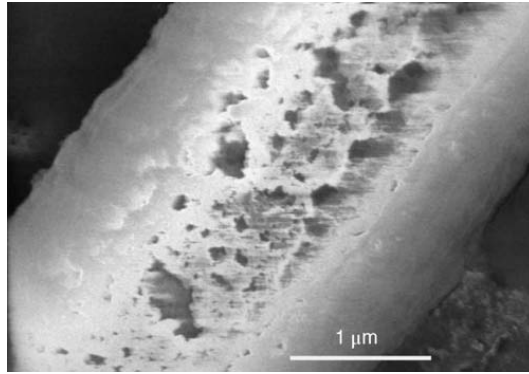


Figure 2.5: Corroded glass [2]

2.2.2 Conclusions

- The recipe of glass influences its strength. Adding soda, increases the density which results in a higher Young's Modulus. However, soda can alter the surface, which makes it weaker. Adding lime prevents this.
- The nature of the environment influences the quality of the glass surface, which can affect the strength.

2.3 Manufacturing of glass

From the point where the recipe of the glass is determined to the moment it can be applied in practice, several steps are taken by the manufacturer. Glass has to be shaped into an element that is suitable for practice and there are several processes which can be undertaken to improve its quality. They are presented in the paragraphs below in historical order.

2.3.1 Production process

After determining the recipe of the glass, the materials need to be heated to a melt and then produced in their desired shape. Since the building industry mainly uses flat glass, the theory presented here will only consider the manufacturing processes of that type of glass.

2.3.1.1 Drawn glass

In this process a sheet of glass is drawn vertically out of the melt, see Figure 2.6b, and moved up by rollers, during which time it is cooled slowly to avoid residual stresses [1]. With this technique it is possible to produce special glasses: thin glass (<1.8mm), thick glass (>19mm) and glass with a wide range of colours. The width is limited to about 1.9 meters but the length can go up to 24 meters.

2.3.1.2 Rolled glass

In this process two rollers continuously pull a sheet of glass out of a glass melt [1], see Figure 2.6a. The sheet continues on consecutive rollers where it cools down and is cut to 2.50m x 4.50m sizes. It is possible to print a pattern on the first two rollers to create ornamentation on the glass. Wired glass can be produced by adding a wire mesh to the sheet of glass when

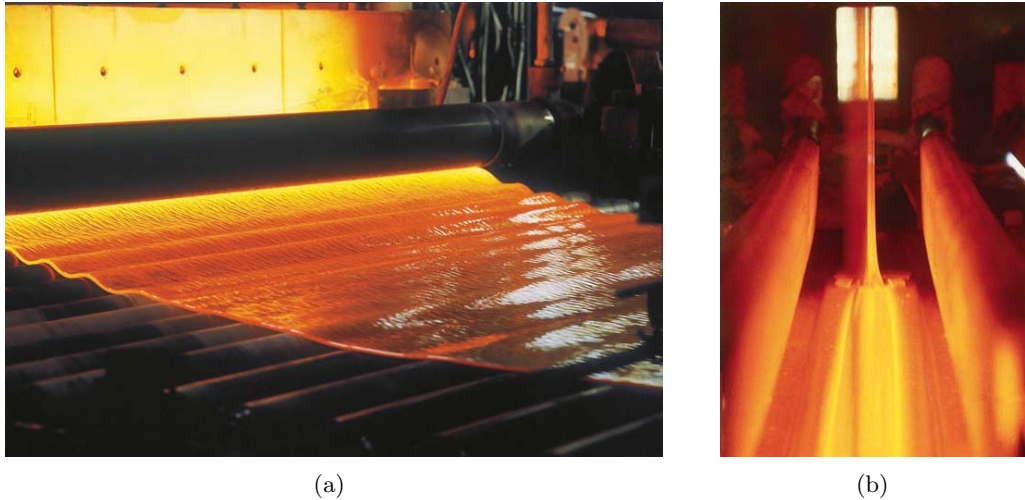


Figure 2.6: (a) A sheet of molten glass is pulled through rollers (b) Molten glass is pulled vertically from the melt into a sheet [1]

it is pulled through the rollers. Thicknesses of 4 to 19 mm are possible and a large selection of colours is available.

2.3.1.3 Float glass

90% of the flat glass production is manufactured by the float method [2]. This technique consists of a large furnace with a large bath of molten tin inside. Molten glass is poured on top of the tin. See Figure 2.7. Because of the difference in density between the two materials, the glass

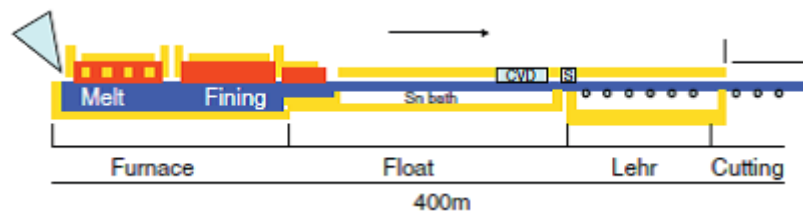


Figure 2.7: A schematic overview of the float glass process [2]

literally floats on top of the tin. The amount of molten glass that is poured and the speed of the rollers determine the thickness [4]. It is poured at 1100°C and it solidifies at 600°C [1]. After cooling most factories cut the glass to jumbo size panes of $3.21\text{m} \times 6\text{m}$. Also, the glass is inspected on flaws by optical sensors. Plates that contain flaws which are visible by eye are taken out, because these are not suitable for use in façades and other applications that require clear visibility. Flaws smaller than the eye can see ($<0.2\text{ mm}$) remain in the glass.

Rolled and drawn glass can be used in buildings for architectural reasons, but from a structural viewpoint float glass is the most suitable. Also, it appears the most transparent of the three. This is because the other two production processes cause more dispersion in the glass.

2.3.2 Mechanical processing of glass

There are several reasons to manipulate glass mechanically: to make it into a desired size, to include holes or to improve its quality. The mechanical alterations are done before any thermal

processing takes place. The most relevant techniques are mentioned in this section. Often a combination of these techniques is performed.

2.3.2.1 Cutting

Cutting is mostly done by a diamond scratching wheel with an accuracy of about 0.1 millimetres [1]. This happens after the glass has cooled down. It is transported over rollers, the wheel scratches a line over the glass which is then bent or heated so that tensile stresses break the glass. This damages the glass locally, reducing its strength. The quality is also very dependent of the machinery used [4]. An alternative is water jet cutting [1], which uses a high pressure water jet in which abrasive particles are mixed. The accuracy is higher than that of a diamond cut, although angular inaccuracies can occur. However, this technique is generally only used for special applications as it is time and cost consuming.

2.3.2.2 Grinding

Grinding the edges or surface of glass is done with metal tools that have diamond or carborundum coatings. Grinding is done in several phases, starting with rougher abrasives and ending with fine grains [1]. This results in a matt straight edge. Final polishing makes the edge transparent. Sometimes the corners are rounded to avoid stress concentrations. Grinding transforms a rough edge or surface into a smooth one and it is therefore believed that it results in a higher strength. However, there are several causes why this is not always the case. Grinding itself also causes damage [5]. The finer abrasives are supposed to reduce this damage, but if not enough refinement is applied grinding cracks are left behind. On the other hand, the first abrasive should be deep enough to remove entire cracks. If it is not, it only removes the top part of the crack while the deeper part stays inside the material. Lastly, if machinery is not properly maintained, grinders can also reduce the strength [4]. Additionally

2.3.2.3 Drilling

This technique is used to create holes in the glass. These are often used to create connections between glass elements. The holes alter the stress distribution of the glass plate, resulting in stress concentrations.

2.3.3 Thermal processing

Thermal processing is executed to improve the strength of glass.

2.3.3.1 Annealing

Annealing is always done. It is the process of cooling the glass down once it comes out of the oven. This needs to be done slowly to prevent residual stresses building up inside the glass. Improper annealing can result in glass cracking on the cutting table [4].

2.3.3.2 Tempering

The glass is heated to approximately 650°C, then cooled down by blowing air on both sides [1]. The cooling down is done at such a rate that the outer part of the glass cools faster than the inner part, causing the outer shell to be under compression, see Figure 2.8a. This is convenient because now the outer part can take a higher tensile load than before because the compressive stress compensates for it.

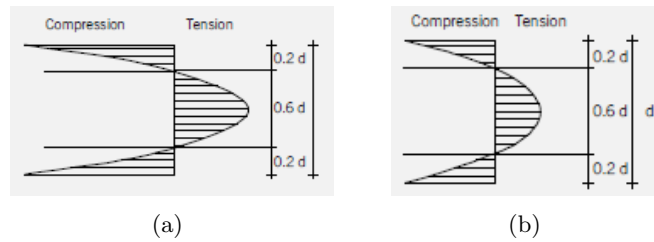


Figure 2.8: (a) The surface is put under compression when glass is tempered (b) Heat-strengthening has the same effect but less intense [1]



Figure 2.9: A tensile load in the outer fibers is compensated by the compressive stress [1]

2.3.3.3 Heat-strengthening

This method is also called partial tempering, because it works on the same principle, only the cooling down is done slower, thereby creating less compressive stresses at the surface [1], see Figure 2.8b. Figure 2.9 illustrates how the compressive surface compensates tensile stresses when a glass element is loaded in bending. The characteristic minimum strength of this type of glass is half that of tempered glass but twice that of annealed glass. Yet it is still attractive to opt for heat-strengthened glass rather than tempered glass, because of the difference in fracture. The high built-up stress in tempered glass causes it to break into small pieces at failure which disintegrate. When tempered glass is applied as a beam these pieces could fall down and cause injuries. The fracture pattern of heat-strengthened glass is much more like non-tempered glass. Therefore it is mostly preferred in constructive elements. See Figure 2.10. If the extra strength is not required, annealing suffices. It can be preferred because the other thermal processes negatively influence the transparency and planarity of glass.

2.3.4 Conclusions

All of these processes influence the quality and thereby the strength of the glass. Therefore the strength is dependent on:

- The type of mechanical processing.
- the type of thermal processing.
- The manufacturer. Each have different standards and machinery.

2.4 Glass as a structural material

Glass has a long-standing history of being used as a façade element in the building industry. However, in modern days it is used more and more as a construction element. One of the most common ways of using the bearing strength of glass is by applying it in a laminated beam. Lamination is a good way of using glass structurally. Melting the glass in one beam is problematic because of residual stresses that form during cooling. This problem can be avoided

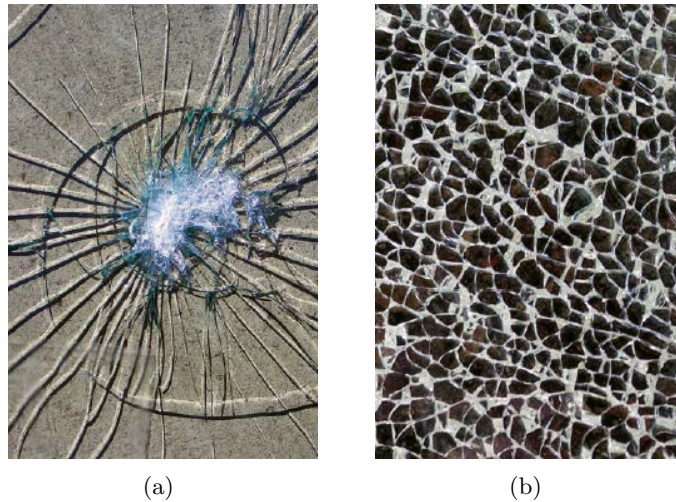


Figure 2.10: Fracture pattern of heat-strengthened (a) and tempered glass (b)[1]



Figure 2.11: Laminated glass with sacrificial outer layers [1]

when producing glass in plates. The required thickness can be obtained by gluing the glass together. Obviously the type of glue is important. It should be stronger than the glass itself to avoid failure by shear stresses. Another requirement is that it is transparent. Bonding materials that fulfil these requirements are [1]:

- Polyvinylbutyral (PVB).
- Cast-in-place resin (CIP).
- Ethylene vinylacetate (EVA).
- SentryGlas Plus (SGP).

A laminated glass element is convenient for structural application, because when one of the glass plates breaks, instead of falling down, the glue holds the pieces together, ensuring structural safety. To ensure that the element can still carry the calculated load, often the outer glass layers are designed as sacrificial panes that are allowed to break. See Figure 2.11. The middle layer is ended a certain distance before the edge, to protect it from damage. Steel reinforcement can be applied to make the glass even stronger and safer [9]. The design of a construction made of glass is different compared to that of a construction made of traditional building materials. This is due to the fact, that only a few standardized codes exist and that the rules differ per country. It is hard to prove to the authorities that the construction is safe. Often this is done by demonstration tests and computer analyses.

2.4.1 Strength of glass

In structural design the strength of a material determines its dimensions. In theory, glass has a very high strength. Orowan formulated a rupture criterion in 1949 [2], containing the following

expression for the theoretical tensile strength:

$$\sigma = \sqrt{\frac{E\zeta}{r_0}} \quad (2.1)$$

where E is the Young's modulus, ζ the surface energy and r_0 interatomic spacing, which is the equilibrium distance between atoms forming a bond. In the case of soda lime silica glass: $E = 70$ GPa, $\zeta = 0.6$ J/m² and $r_0 = 0.15$ nm (Si-O distance). This results in a strength of 16 GPa. However, in practice, values as low as 20 N/mm² are applied [1]. Additionally, an extremely high safety factor is employed of 5 to 7.

Strength of a material can be found in several ways. Common tests are the three-point bending and four-point bending tests. Veer [4] used these methods in different experiments conducted over seven years on soda lime glass. These experiments differ in the way the glass was mechanically processed, the size of the specimens, the number of specimens, the type of test and the type of glass. From these experiments he drew the following conclusions:

- The failure strength of glass can only sometimes be described by a Weibull distribution (see Section 3.4).
- The way the glass is processed influences the behaviour of each data set.
- The minimum value of all data sets used is 20 MPa, which is a lower boundary.
- A maximum strength of annealed float glass of 110 MPa follows from the results.
- The higher the specimen, the lower the strength. This is probably caused by the fact that this results in a larger tension area. In a previous experiment Veer had already concluded that the edge strength is dependent on the edge quality, which follows from the type of mechanical processing [10].

Veer concluded that the lowest failure strength values are caused by a critical defect which can occur in the glass. This is reported by several more researchers [1, 2, 3]. They all agree that the tensile strength of glass is mostly based on the amount of damage and defects to the glass. This is supported by Griffith's theory of flaws being the nuclei of fracture [11]. Also see Section 3.3. Flaws lead to cracks and due to the brittle behaviour, these can rapidly lead to failure. During its lifetime, glass can suffer multiple flaws. Therefore its tensile (or bending) strength is not a constant value. The following factors contribute to this effect:

- Size of the element. Glass fibers are much stronger than flat glass because there is a lower probability they contain a critical flaw [2]. See Figure 2.12.
- Age of pane; the older, the more flaws [1].
- The manufacturer. Each delivers a different quality and their location might influence their temperature control [4].
- The handling of the glass; careless handling can lead to surface flaws [2].
- Location of the glass element from the jumbo plate. At the long sides more flaws occur [12]. See Figure 2.13.
- The side of the float glass that was lying on the tin bath is stronger than the side in contact with the air. It is unknown if this is caused by flaws.

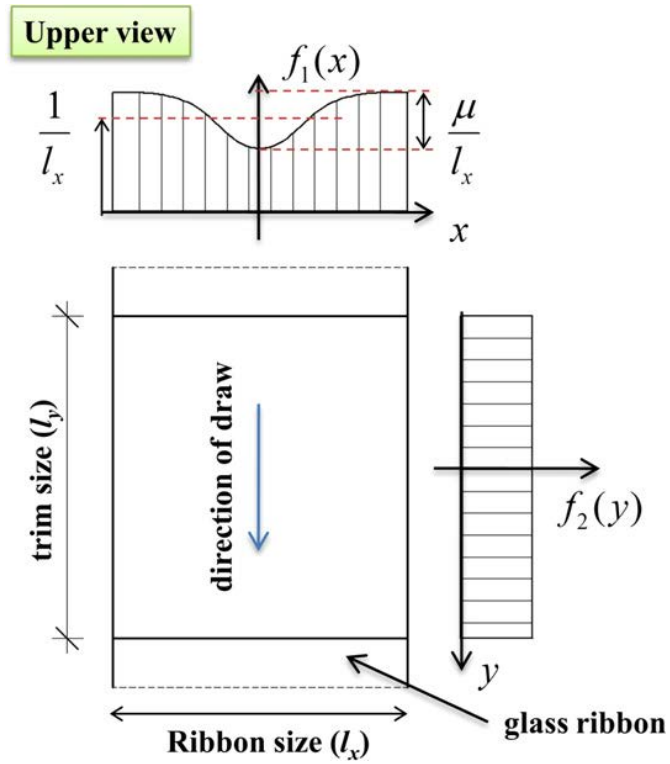


Figure 2.13: The distribution of flaws over the surface of a float glass plate [12]

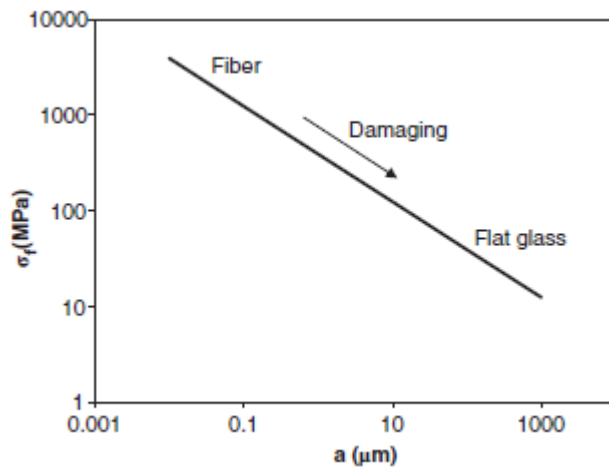


Figure 2.12: Size effect [2]

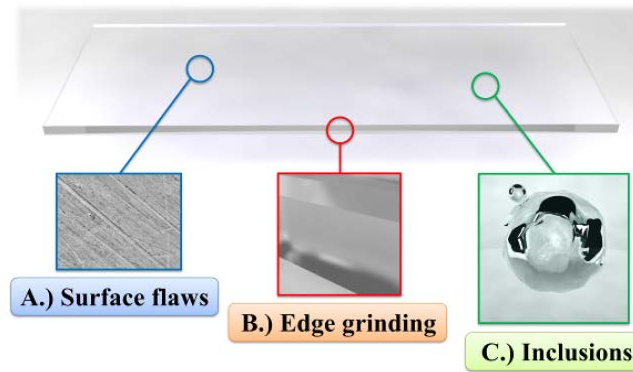


Figure 2.14: Three types of flaws [3]

2.4.2 Flaws in glass

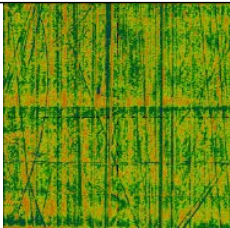
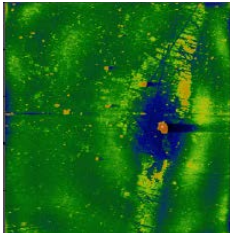
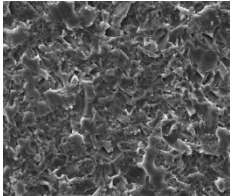
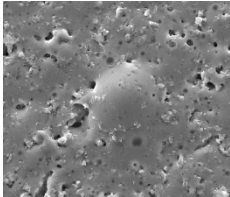
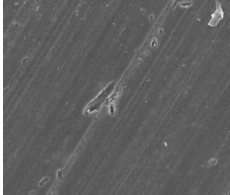
Molnár et al. [3] described the inhomogeneities by sorting them in three regions of the glass: the surface, the edge and the inner volume. See Figure 2.14. One important notion is to be made here. When glass fractures at its surface or edge this does not necessarily mean the flaw was of a surface or edge type [5]. Volume flaws can end up at the surface or edge in the production process or due to the way glass components are cut from the bulk.

Molnár et al. built an FEM model in ANSYS in which they compared several flaw types to a reference glass, which contained no flaws. This way they were able to evaluate the impact of a flaw numerically, by determining its contribution to strain peaks in the glass. Table 2.1 shows a summary of their findings and results.

A few things should be noted about these results:

- It is implied edge flaws result in the largest strain peaks. However, Molnár et al. [3] state that with further polishing this can be reduced, which would make intrinsic defects the governing flaws. On the other hand Le Bourhis [2] reckons that bubbles can be avoided as an origin of failure by modern fining processes and that the governing defects are at the surface of the glass because damage to the glass is inevitable. The smallest bubbles take longer to rise to the surface and can therefore not be taken out as easily during the fining period, it being too short.
- The air bubbles they found were of a few millimetres length. The size of air bubbles in glass highly depends on the manufacturer. Some production plants do not allow glass plates to be produced with air bubbles larger than 1 mm. It is not clear what the effect of smaller bubbles is.
- These results are based on numerical calculations and have not been verified by experiments. Questions can be asked about the calculation methods and boundary conditions that have been used to create the model and to which extent these simulates reality.

Table 2.1: Effect of flaws in glass

Type	Photo	Effect
<i>Surface</i>		After production there are barely any flaws, giving a strain peak of 8%. Processing results in nanoscratches and a strain peak of 37%
		After 3 years of use: scratches are gone, but small pits have appeared due to weathering, which generate strain peaks of 70%. After 15 years this value is 97%, so the majority of the peak increase is in the first few years.
<i>Edge</i>		Edge quality depends on its finishing. The grinded specimen shows a much rougher texture than the polished edge. Additionally, the strain peaks for edges are much higher than for the glass surface: 350%.
		An acid etched edge results in similar strain peaks as a grinded edge, so it brings no benefit. Consequently, acid etching should not be used for glass surfaces because it could increase their strain peaks significantly.
		The polished edge shows much fewer flaws and consequently yields a lower strain peak of 200%. Still this is much higher than that of a glass surface.
<i>Volume</i>		The air bubbles Molnár et al. had found were of a prolate spheroid shape. According to their calculations an air bubble of a few millimeters can create strain peaks of 290%
		Molnár et al. photographed one stony inclusion. It is of oblate spheroid form and consists of imperfectly melted material compounds, making it hard to find because it has a similar density as glass. According to Le Bourhis such an inclusion nucleates when silica crystallizes locally [2].

Molnár et al. are not the only ones to have studied flaws in glass. Next to scratches and pits other flaws that are known to occur at the glass' surface are [5]:

- Voids, created during the production process, similar to pores only they are at the surface.
- Impact flaws from either a blunt or a sharp object.
- Grinding cracks. These are tricky. Whereas scratches caused by grinding are mostly diminished by polishing, the cracks go deeper and might not be removed in the finishing process.

Edge type flaws are not further discussed here, as glass tested in biaxial tests usually break due to surface or volume flaws. As said, these volume flaws are either air bubbles (pores) or inclusions. However, the glass community has specified these further:

- Devitrification inclusions form if the glass crystallises.
- Stones come from broken off material of the furnace.
- Blisters is the name given to large air bubbles.
- Seeds is used as the term for small air bubbles.
- Striae are streaks of inhomogeneous glass. Intense striae are termed cords and appear as strands.

Finally, sometimes flaws come from the most unexpected sources, such as hair, insect carcasses and dandruff, just to name a few.

2.4.3 Conclusions

- Theoretically, glass has a very high strength.
- Due to large scatter in test results it is hard to assign an average strength to glass.
- Flaws are the cause of this high scatter and can cause a very low strength when it is a critical flaw.
- It is hard to pinpoint which type of flaw has the most severe effect on the glass' strength, as this also depends on its dimensions and characteristics. It might be necessary to create subtypes.

Failure and fracture of glass

3.1 Introduction

This chapter deals with the models that can be used to describe the failure and fracture of glass theoretically. The first section covers a few models that describe the failure of materials. It is written based on the views of Christensen. The second section describes how flaws and cracks that occur at the small scale can lead to failure, based on the theories of Griffith and Irwin. In the third section it is recognised how strength is a matter of probability and the Weibull analysis is discussed.

3.2 Materials failure

As this research will study the failure of glass it is useful to know more about the existing theories of failure. Over the years, scientists have tried to describe the failure of materials with theoretical models, of which some have found a wide range of application. Below, the most common and accepted of these are mentioned and summarised. Despite their accepted use, Christensen [13] argues that none of them achieves to be a complete model to describe materials failure. In his view a general theory for materials should be applicable to all isotropic and homogeneous materials ranging from the most brittle to the most ductile material.

Below the compressive strength is denoted as C , the tensile strength as T , the principal stresses as σ_i and the shear strength as S .

3.2.1 Von Mises criterion

Von Mises stated that a material fails when the deviatoric stress reaches a limit value [14]. He based this on the observation that a material barely reacts to a change in the isotropic part of the stress, but is much more sensitive to changes in the deviatoric part of the stress. His criterion reads:

$$\frac{1}{2}[(\sigma_1 - \sigma_2)^2 + (\sigma_2 - \sigma_3)^2] + (\sigma_3 - \sigma_1)^2 \leq T^2 \quad (3.1a)$$

$$C = T \quad (3.1b)$$

$$S = \frac{T}{\sqrt{3}} \quad (3.1c)$$

The resulting failure envelope is presented in Figure 3.1. Christen [13] acknowledges that the Von Mises criterion is of lasting significance. However, it only applies to very ductile materials and therefore he deems it unsuitable to be used as a criterion for all materials.

3.2.2 Tresca criterion

Tresca assumed that a material fails when the shear stress exceeds a critical value [14]. This results in:

$$\frac{1}{2}(\sigma_1 - \sigma_3) \leq S \quad \text{for } \sigma_1 \geq \sigma_2 \geq \sigma_3 \quad (3.2a)$$

$$C = T \quad (3.2b)$$

$$S = \frac{T}{2} \quad (3.2c)$$

The criterion is plotted within the Von Mises criterion in Figure 3.1. The corners of the Tresca formulation are caused by describing the maximum shear stress in three principal coordinate planes [13]. These corners are associated with dislocation movement at the crystal level. However, more complex behaviour at aggregate level should involve averaging over a wide variety of physical conditions and effects. This averaging has a smoothing effect that is much more supportive of the smooth Von Mises criterion than of the non-smooth Tresca form. Therefore Von Mises is preferable over Tresca in Christensen's opinion.

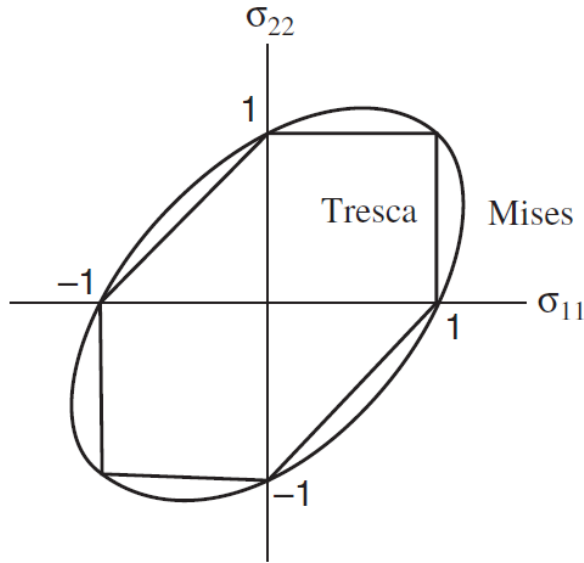


Figure 3.1: Failure envelope according to the Von Mises and the Tresca criterion [13]

3.2.3 Coulomb-Mohr

This model is based on the fact that stresses acting on different planes can be related to one another using the equilibrium equations [15]. Mohr discovered that these equations can be represented by a circle. The ratio of shear stress to normal stress differs along the circle because the ratio varies for different planes. The straight lines indicate the Coulomb envelop. When Mohr's circle touches this envelope the material starts to fail. The criterion reads:

$$\frac{1}{2} \left(\frac{1}{T} - \frac{1}{C} \right) (\sigma_1 + \sigma_3) + \frac{1}{2} \left(\frac{1}{T} + \frac{1}{C} \right) (\sigma_1 - \sigma_3) \leq 1 \quad (3.3)$$

The criterion is plotted in Figure 3.2. Christensen [13] demonstrated examples for which the Coulomb-Mohr criterion allows unlimited compressive stress, making it unsuitable for a general theory. He does recognise the good applicability in the geological area.

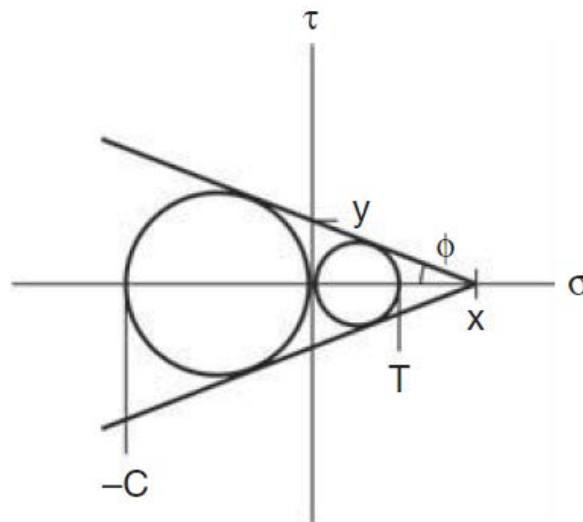


Figure 3.2: Failure theory based on Mohr and Coulomb [13]

3.2.4 Drucker-Prager

In the principal stress space, the Von Mises criterion looks like a cylinder, see Figure 3.3. The Drucker-Prager criterion attempts to add a limit to this formulation by replacing the open end by a point, creating a cone. In formula, this reads:

$$\frac{1}{2} \left(\frac{1}{T} - \frac{1}{C} \right) (\sigma_{11} + \sigma_{22} + \sigma_{33}) + \frac{1}{2} \left(\frac{1}{T} + \frac{1}{C} \right) \left\{ \frac{1}{2} [(\sigma_{11} - \sigma_{22})^2 + (\sigma_{22} - \sigma_{33})^2 + (\sigma_{33} - \sigma_{11})^2] + 3(\sigma_{11}^2 + \sigma_{22}^2 + \sigma_{33}^2) \right\}^{\frac{1}{2}} \leq 1 \quad (3.4)$$

The symmetry axis of the cone makes equal angles with the three principal axes. When $T = C$ the failure surface becomes the circular cylindrical form of Von Mises. Christensen deems Drucker-Prager inappropriate for representing materials failure. For $\frac{T}{C} < \frac{1}{3}$ unlimited compressive stress is allowed, which cannot be true.

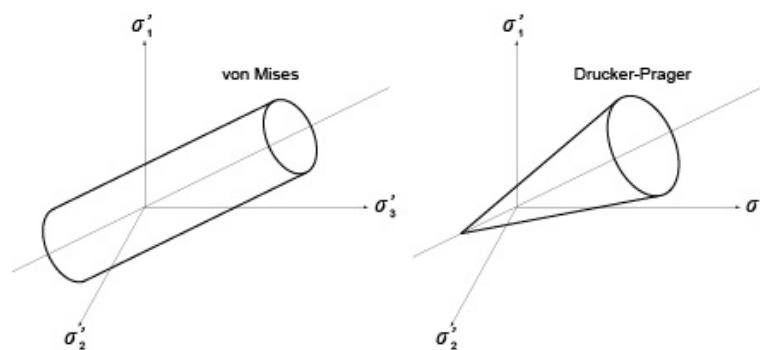


Figure 3.3: Failure envelope according to Drucker and Prager

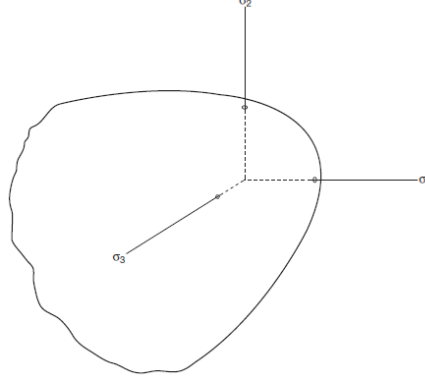


Figure 3.4: Paraboloid resulting from Christensen's polynomial-invariants criterion [13]

3.2.5 Christensen's criterion

Christensen [13] argues that a general theory for materials failure should be calibrated by only a few failure properties. If more parameters get involved, the whole process would be merely reduced to that of fitting parameters to a specific situation and the model loses its scientific meaning. He decided to use the ratio of the materials' tensile strength, T , and their compressive strength, C , as an organising structure. All isotropic materials fall within the range $0 \leq \frac{T}{C} \leq 1$, where $\frac{T}{C} = 1$ is the ductile limit and $TC = 0$ is the brittle limit.

Christensen then points out that with the Coulomb-Mohr and Drucker-Prager criterion being linear or quasi-linear, but failing to be suitable failure theories, one can conclude a proper failure theory should include non-linear effects. Because the Von Mises criterion has proven to work for ductile cases he takes the fact that it is in a quadratic form as a basis for his own theory. He starts by giving a polynomial-invariants criterion, which indicates the effective limit of linear elastic behaviour:

$$\left(1 - \frac{T}{C}\right)\hat{\sigma}_{ii} + \frac{3}{2}\hat{s}_{ij}\hat{s}_{ij} \leq \frac{T}{C} \quad (3.5)$$

No matter whether the material fails in a ductile or a brittle manner, the principle is the same: the end of elastic behaviour. In terms of principal stresses, Equation 3.5 can be written as:

$$\left(1 - \frac{T}{C}\right)\hat{\sigma}_{ii} + \frac{1}{2}[(\hat{\sigma}_1 - \hat{\sigma}_2)^2 + (\hat{\sigma}_2 - \hat{\sigma}_3)^2 + (\hat{\sigma}_3 - \hat{\sigma}_1)^2] \leq \frac{T}{C} \quad (3.6)$$

Graphically, this results in a paraboloid, see Figure 3.4. However, this criterion does not hold for all types of isotropic materials. There is much evidence that brittle materials have a three-fold symmetry in their failure envelope, rather than axial symmetry, as is currently portrayed here. If a maximum normal stress type fracture criterion is added, this would result in additional parameters. According to Christensen, that is the dead-end path followed by most previous failure criteria developments. He therefore states that a fracture criterion can only be added if it does not add new parameters. Additionally, the criterion should not introduce any discontinuous behaviour to the envelope that is found. The one criterion that satisfies these conditions is for $\frac{T}{C} \leq \frac{1}{2}$:

$$\sigma_1 \leq T \quad (3.7a)$$

$$\sigma_2 \leq T \quad (3.7b)$$

$$\sigma_3 \leq T \quad (3.7c)$$

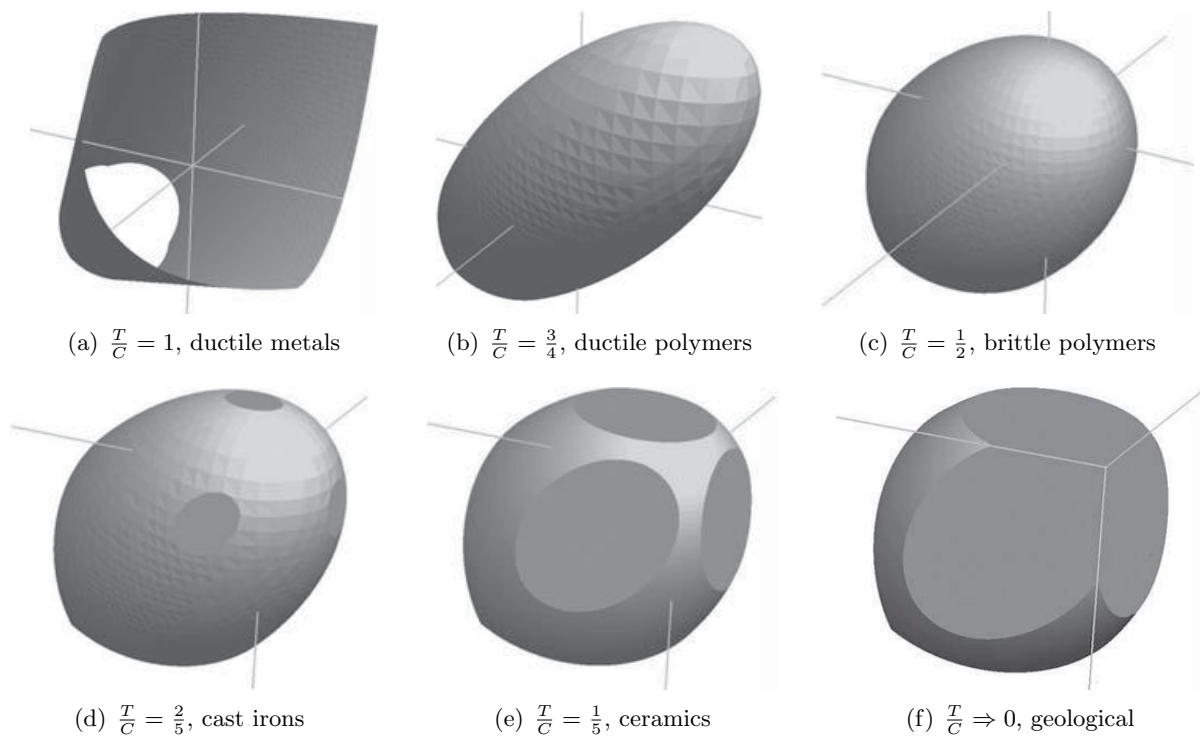


Figure 3.5: Paraboloids for different values of T/C [13]

So we have two criteria, the polynomial-invariants criterion (Equation 3.6) and the fracture criterion (Equation 3.7). At a given stress state, the criterion that is the most limiting of the two is the controlling failure condition at that stress state. Figure 3.5 shows the graphical representation of several values of $\frac{T}{C}$, including the corresponding type of material. $\frac{T}{C} = 1$ is the ductile limit, which takes the shape of the Mises cylinder. $\frac{T}{C} \Rightarrow 0$ is the brittle limit, but it is practically never reached.

For glasses, Christensen suggests $\frac{T}{C} = \frac{1}{8}$, which looks like Figure 3.6. Although, this research will cover only the biaxial failure envelope, which can be created by taking one of the principal stresses to be zero.

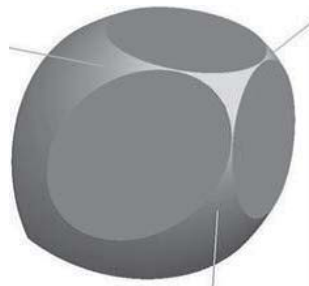


Figure 3.6: $T/C = 1/8$, glasses [13]

3.2.6 Conclusions

The field of materials failure has been explored by many researchers, all coming up with different theories. The model of Christensen gives a sense of what can be expected from glass. It will be interesting to see if the biaxial failure envelope of glass can be described by this theory.

3.3 Fracture mechanics

Glass fails because tensile stresses cause cracks which propagate through the rest of the material, reducing its strength down to a level too low to carry the applied load. The field of fracture mechanics attempts to describe this phenomenon at local level.

There are three modes of crack surface displacements [16], see Figure 3.7. Here, only the first mode will be covered, since it is the governing mode for most practical cases, including glass.

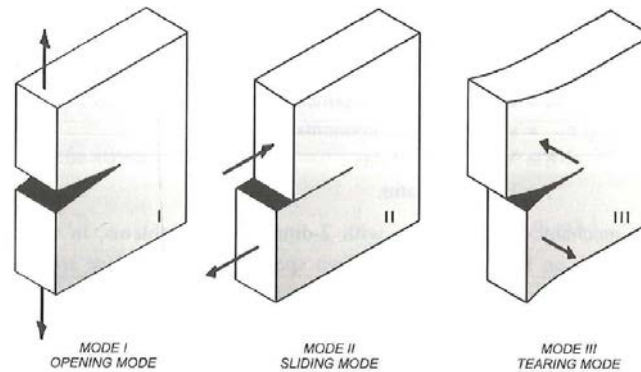


Figure 3.7: The three modes of crack surface displacements [16]

3.3.1 Energy approach

The first accepted theory of fracture mechanics was formulated by Griffith in 1920. He considered an infinite plate loaded by a uniform tensile stress σ containing a crack of length $2a$. See Figure 3.8. He stated that the crack will propagate if this causes the total energy of the

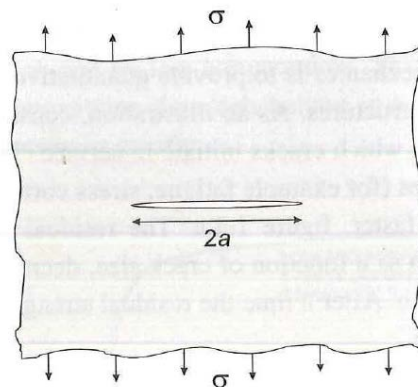


Figure 3.8: Crack in an infinite plate [16]

system to be lowered and he formulated the following balance of energy to calculate this:

$$U = U_0 + U_a + U_\gamma - F \quad (3.8)$$

In which U is the total energy of a plate and its loading system with a crack. U_0 is the total energy of a plate and its loading system without a crack, so this is a constant value. U_a is the change of the stored elastic strain energy. The stress around a crack will decrease and become zero. This will decrease the elastic strain energy by “volume of stress free material” times “original value of the stored elastic strain energy”. U_γ is the energy needed to create new

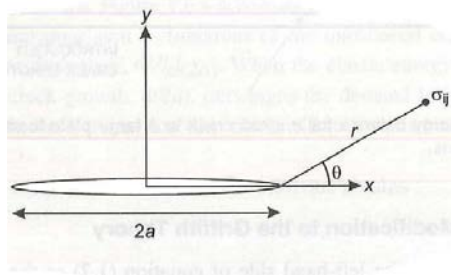


Figure 3.9: Polar coordinates for stresses near the crack tip [16]

crack surfaces, which is “crack surface area” times “surface tension”. The surface tension is the surface energy per unit area. F is the work by load, so load times displacement.

Griffith assumed the stress free material to be in a circle around the crack. The stored elastic strain energy in a material is half times stress times strain. So if the crack has a length of $2a$ and assuming linear elastic material behaviour:

$$U_a = \frac{-\pi\sigma^2 a^2}{E} \quad (3.9)$$

The surface of a crack is two times its length times the thickness. So in this case, the crack surface area per unit thickness is $2 * (2a) = 4a$. The surface tension is given by γ_e . The energy required to create new surfaces is:

$$U_\gamma = 4a\gamma_e \quad (3.10)$$

For a fixed grip condition, where F is zero, Griffith showed that the following expression is the criterion for crack extension:

$$\frac{\pi\sigma^2 a}{E} > 2\gamma_e \quad (3.11)$$

Irwin wrote this as $G > R$, where G is the energy release rate and R is the crack resistance.

3.3.2 Stress intensity approach

The energy approach is limited to ideally sharp cracks and is unable to describe slow stable crack growth. Irwin overcame these difficulties by introducing the stress intensity approach in 1950 [16]. He first formulated an expression for the stresses near the crack tip:

$$\sigma_{ij} = \frac{K}{\sqrt{2\pi r}} f_{ij}(\theta) \quad (3.12)$$

See Figure 3.9 for the polar coordinates. f_{ij} is a dimensionless parameter that varies with the load and geometry. K is a new parameter, the stress intensity factor, which gives the magnitude of the elastic stress field at the crack tip:

$$K = C\sigma\sqrt{\pi a} * f(a/w) \quad (3.13)$$

For an infinite plate $f(\frac{a}{w}) = 1$ and $C = 1$, so $K = \sigma\sqrt{\pi a}$.

For a finite plate both C and $f(\frac{a}{w})$ have to be determined by stress analysis. When K reaches the value of the critical stress intensity, crack extension takes place. This is formulated in the criterion:

$$K > K_c \quad (3.14)$$

If the value of the critical stress intensity can be determined, the fracture stress can be calculated by [2]:

$$\sigma_f = \frac{K_c}{Y\sqrt{a}} \quad (3.15)$$

The lower K_c , the lower the stress at which the material will fracture. The stress intensity factor is introduced in the energy approach by:

$$G_c = \frac{K_c^2}{E} \quad (3.16)$$

The critical stress intensity can be experimentally determined and that fact is what makes the stress intensity approach so powerful [16]. Actually, it is customary to work with the fracture toughness K_{Ic} instead of K_c . The fracture toughness is a material property that is independent of the specimen thickness. K_c is dependent of the thickness constraint. However, at a certain point a maximum constraint has been reached. Even if the thickness is increased, it does not add up to the constraint anymore. From that point K_{Ic} can be used for different geometries. For several types of glass the fracture toughness is given in Table 3.1 [2]. For comparison, the

Table 3.1: Fracture toughness of different types of glass [2]

Glass	$K_{Ic}[MPa\sqrt{m}]$
Silica	0.74 - 0.81
Soda-lime-silica	0.72 - 0.82
Borosilicate	0.75 - 0.82
Aluminosilicate	0.85 - 0.96
Lead-silicate	0.62 - 0.73

fracture toughness of metallic glass is around $50MPa\sqrt{m}$.

3.3.3 Fracture mechanics of flaws

The above theory is only applicable to cracks, but it was stated before that flaws can induce failure. Insight on what is happening there can be obtained from the following formula Griffith gave for an elliptical flaw [16]:

$$\sigma' = \sigma\left(1 + \frac{2a}{b}\right) \quad (3.17)$$

In which $2a$ is the flaw length, $2b$ the flaw width, σ the uniform applied stress and σ' the maximum stress at the tip of the flaw. The flaw concentrates stresses at the points of minimum curvature. This means that the sharper a flaw, the higher the stress peak. When $\sigma' > \sigma_f$ a crack will start at the flaw tip and propagate until specimen fracture.

Mecholsky [17] stated that even when the source of fracture is an inclusion, the fracture is caused by a crack at the boundary of the material and the inclusion. Relating this to the above theory, this can be translated to that the stress peak at a flaw causes a small crack which initiates failure.

3.3.4 Crack tip plasticity

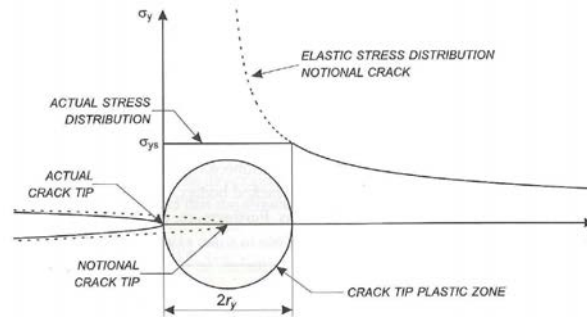


Figure 3.10: Plasticity zone at the crack tip [16]

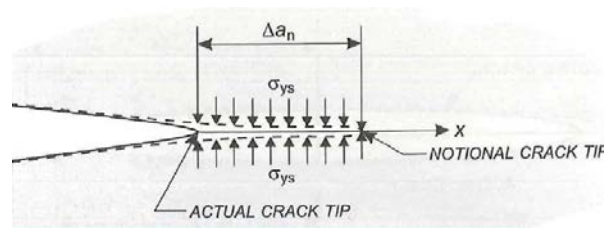


Figure 3.11: The strip-yield model [16]

Consider equation 3.12 again. This expression suggests that when r approaches zero the stress becomes infinite. In other words, the stress at the crack tip is infinitely high. This solution is for a crack with a crack tip radius of zero. However, in reality materials contain cracks with crack tips that have a minimum radius of at least the interatomic distance [16]. So the elastic solution is not always applicable. To overcome this, Irwin suggested that a plastic zone exists at the crack tip under tensile loading, which causes the crack to behave as if it is longer than it actually is. He proposed a model in which this plastic zone is circular with a diameter of $2r_y$ and where the crack tip ends at r_y . After $2r_y$ the elastic solution can be used. In the plastic zone the stress has a constant value, namely that of the stress at $2r_y$. Figure 3.10 shows how the plastic crack tip reaches until the centre of the circular plastic zone. Dugdale proposed a different but quite similar model, also based on the assumption that the crack behaves longer than it actually is. He did not suggest a geometry for the plastic zone, but merely specified a strip in which plastic deformation concentrates. He denoted the length of this strip by Δa_n , see Figure 3.11, which can be calculated by:

$$\Delta a_n = \frac{\pi}{8} \left(\frac{K_c}{\sigma_{ys}} \right)^2 \quad (3.18)$$

In which σ_{ys} is the yield stress. However, glass is known to show no yielding behaviour. Le Bourhis suggested basing the yield stress on the nanohardness of glass [2]. When indenting glass with a nanoindenter it produces a zone that is permanently deformed. See Figure 3.12. From this experiment the hardness H was calculated as the mean pressure over the indentation contact. He then stated that for elastic-perfectly plastic materials the yield stress Y can be calculated by:

$$H \approx 3\sigma_{ys} \quad (3.19)$$

In this case he found $\sigma_{ys} \approx 2$ GPa. Putting this in the Dugdale formula results in $a_n \approx 50$ nm. For the Irwin formula, this would give $2r_y \approx 40$ nm.

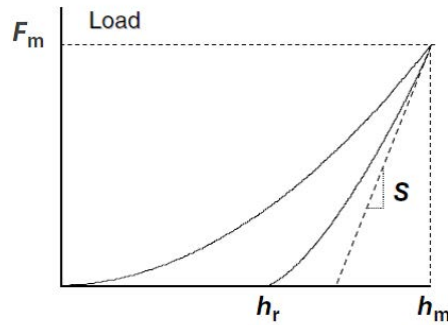


Figure 3.12: The loading-unloading curve shows the specimen has deformed plastically [2]

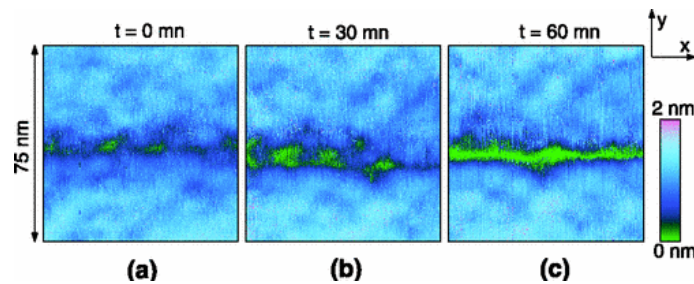


Figure 3.13: Cavities develop ahead of the crack tip [18]

Le Bourhis argued that this emphasises the brittle behaviour of glass. Contrary to a metal, which has $\Delta a_n \approx 1$ millimetre, only a few bonds support the high stress concentration at the crack tip.

On a macroscale glass has never shown plastic behaviour. But the results above suggest some plasticity occurs at the nanoscale. Using atomic force microscopy, Célarié [18] found that cavities develop ahead of the crack tip at the nanoscale, see Figure 3.13. Because this behaviour has been widely observed for metallic materials at the microscale, he stated that glass breaks like metal, only just at a very small scale.

3.3.5 Conclusions

A glass specimen contains a lot of flaws and cracks. Fracture mechanics describes the development of one crack in a material. Some of the models developed assume a certain amount of plasticity near the crack tip. Research has shown this actually seems to be case for glass. Because the models focus on one crack, fracture mechanics is only applicable for glass at a local level, but can still be of help. For example:

- The size of the critical flaw can be calculated with fracture mechanics and checked with the dimensions of the critical flaw found in the fractographic analysis, for verification [5].
- The sharper the tip of a flaw, the easier it is for a crack to propagate. This is an important notion, because this would imply that in a constant stress state the flaw with the sharpest tip will be the critical flaw.
- Finding out which flaws are the most critical could improve the strength assessment of glass.

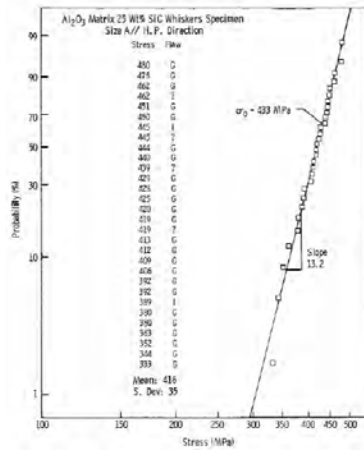


Figure 3.14: A Weibull plot of the strength of an aluminium. The points fit well on the line with slope m [5]

3.4 Statistics of glass

The above text concerned itself with physical models describing the behaviour of glass. In the end however, it is a matter of probability whether a critical flaw happens to be present in an area of maximum stress [4]. It is generally accepted that the Weibull analysis has proven to be a good descriptor of brittle failure. It is based on the idea that a body will fail due to the weakest link present, which relates well to the presence of a critical flaw in glass. Yet glass researchers have trouble fitting their data to a Weibull model. Glass breaks due to flaws, but as was mentioned in Chapter 1 there are different type of flaws. Quinn states that glass specimens that have their fracture origin due to different types of flaws are not statistically comparable [5]. Each flaw type has its own distribution.

3.4.1 Weibull analysis

The most common Weibull distribution is the two-parameter distribution [5]:

$$P_f = 1 - \exp\left(-\left(\frac{\sigma_a}{\sigma_\theta}\right)^m\right) \quad (3.20)$$

where P_f is the probability of failure, σ_a is the applied stress, m is a constant called the Weibull modulus and σ_θ is another constant called the characteristic strength of the specimen which is determined by the fracture stress of the specimen at a probability of 63.2%. If the data fits the Weibull distribution it should fit a straight line with slope m and $\sigma_a = \sigma_\theta$ at the probability of 63.2%.

Weibull himself stated that his distribution function only sufficed as long as it fitted best compared to other functions [19]. He had approached the problem mathematically and had not based it on physical theory, but simply on the assumption of a body containing small elements with their own strength of which one is the weakest link. This long remained the case, until Jayatilaka and Trustum derived it from fracture mechanics and gave it a physical basis [5].

3.4.2 Weibull analysis of glass

A Weibull figure is supposed to look like Figure 3.14. A Weibull plot for glass, however, often looks like Figure 3.15. This plot is a result of the strength tests done by Veer [4] that were discussed in Section 2.4. He found that mostly it is the lowest values of failure strength that cause the Weibull plot to be invalid. As was stated it is flaws in the glass that cause the great

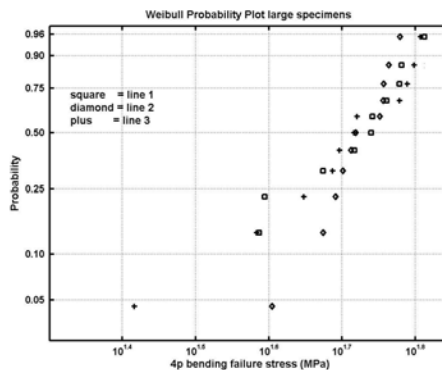


Figure 3.15: No straight Weibull line is achieved with the data from glass strength tests [4]

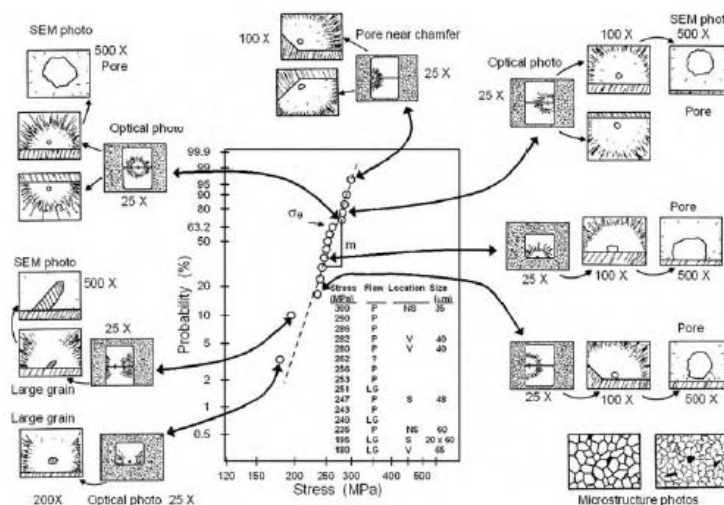


Figure 3.16: A fractographic montage of a ceramic [5]

variability of its strength. Veer suggests splitting the data according to their cause might yield more significant results. The next chapter will describe how to find flaws in glass. Figure 3.16 shows a Weibull plot of a ceramic [5] and a so called fractographic montage. For each point it is indicated which flaw was found to be the origin of failure. It can be seen how pores near a chamfer resulted in the highest strengths and large grains caused the lowest. A similar system could be applied to glass.

3.4.3 Conclusions

The strength of glass is a statistical problem. It is a matter of probability whether a critical flaw will lie in the highest stressed part. Weibull analysis has proven to be a good describer of the probability of the weakest link in a body. However, flaws in glass behave so differently that they do not result in a proper Weibull plot. This might be solved if the flaws are characterised and their corresponding strength data are plotted separately. To the knowledge of the author, this has not been tried before for glass.

Testing methods

4.1 Introduction

This chapter is divided into two parts. The first part covers the possible strength tests to bring biaxial stresses in a material. A choice is made which test will be performed in this research. The second part elaborates on the most relevant methods that can be conducted in a forensic analysis of glass. This part focusses mainly on equipment that is available at the Faculty of Civil Engineering at Delft University of Technology.

4.2 Biaxial testing

To find the biaxial strength of glass the specimens need to be loaded in three combinations of stresses:

- Compression & compression.
- Compression & tension.
- Tension & tension.

Creating a biaxial stress state is not a new field of expertise. Over the past decades, researchers have conducted similar experiments, which can be educative for this research. A literature study has been performed of biaxial testing on materials with similar material and strength properties as glass, such as ceramics and concrete.

4.2.1 Biaxial testing on concrete

For concrete, this field of research goes back as far as the early seventies. Kupfer seems to be the first researcher who found a biaxial failure envelope for concrete. Figure 4.1 shows his results [20].

Because concrete and glass have a similar compressive strength/tensile strength-ratio, it can be expected to get a similar envelope for glass. After Kupfer, more researchers conducted these kind of experiments in various ways on various types of concrete [20, 21, 22]. Figure 4.2 shows the different setups used in these experiments. Kupfer [20] applied a biaxial stress by two frames

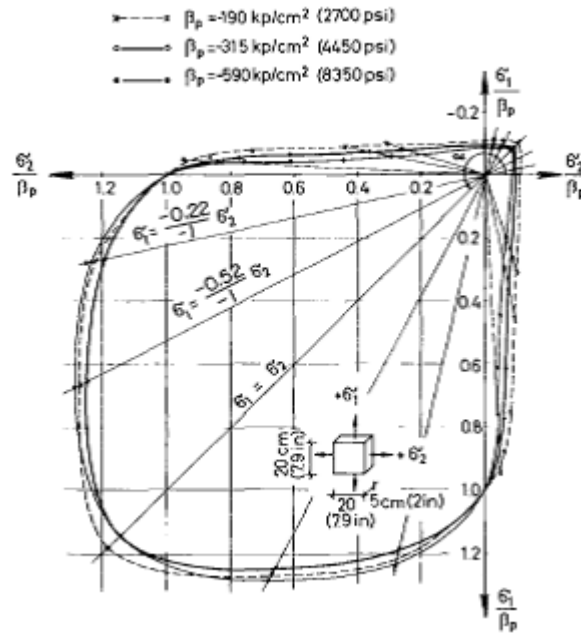


Figure 4.1: Biaxial failure envelope of concrete [20]

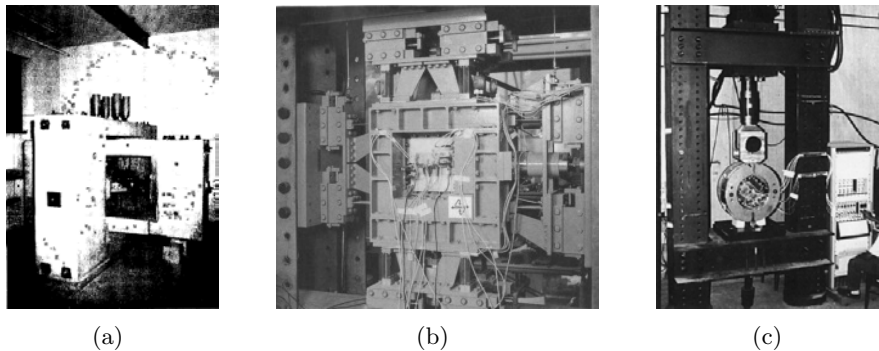


Figure 4.2: Possible setups for biaxial testing [20, 21, 22]

perpendicular to each other, see Figure 4.2a. Nooru-Mohammed [21] used two frames parallel to each other, see Figure 4.2c. Both Kupfer and Nooru-Mohammed ensured tensile stresses by glueing the specimen to the frame. Lastly, Yin came up with an ingenious set up where biaxial compression is induced through uniaxial compression by placing the specimen in a specially designed ring. However, this is rather complicated to built and cannot apply tensile stress. Glueing the specimen will be hard because the glass plates might not have enough thickness to do this properly. Another possibility would be to clamp the glass, but glass surface is very smooth, therefore it is expected to be rather difficult. Still, some useful notions could be learnt from these experiments, namely how to ensure a homogeneous stress state. This can be done by taking the following precautions:

- Take care of the boundary conditions. Friction between the boundary conditions and the specimen can cause differences in the stress state.
- Calculate the expected stress state.
- Measure the stress state during the experiment to verify the calculated stress state.

The biaxial tests performed on concrete are performed on a bigger scale than is necessary for glass, due to the size of aggregates. The biaxial compressive tests can be translated to a smaller scale to apply on glass. However, inducing tensile stress in the specimen by gluing its side to the frame is expected to be less successful for glass.

4.2.2 Biaxial testing on ceramics

In the research field of ceramics smaller scale experiments are performed. A wide range of equibiaxial tensile tests can be found. Most of these tests make use of a combination of rings, balls and pistons, such as ring on ring or piston on three balls. These tests work on a similar principle as the four point bending test, but then in a circular set up. In the inner circle a constant biaxial tensile stress is created. Table 4.1 summarises the advantages and disadvantages of three types of these experiments, based on various research articles. [23, 24, 25, 26] From the

Table 4.1: Conclusions biaxial flexure tests [23, 24, 25, 26]

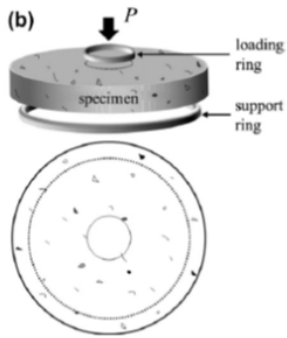
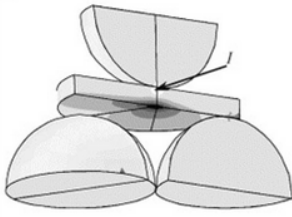
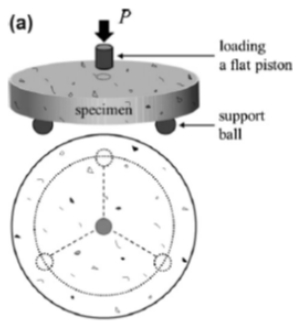
Ring on ring		Ring/ball on 3 balls		Piston on ring/balls	
					
<i>Pros</i>	<i>Cons</i>	<i>Pros</i>	<i>Cons</i>	<i>Pros</i>	<i>Cons</i>
Equibiaxial stress distribution in inner ring	Friction at rings causes a variation in the results Hard to determine failure stress if failure starts under loading ring	Tolerance for non-smoothness Fewest friction	Uncertain stress distribution	Tolerance for warpage Fewer friction	Uncertain stress distribution

table it follows that friction and assuring the correct stress state, again, are important issues in biaxial strength testing. The ring on ring (RoR) test performs best in applying a constant biaxial tensile test in a larger area, but performs worst in reducing friction. Since glass breaks due to a flaw, it is important to put a significant area of glass in tension. The surface of glass is smoother than that of most ceramics, therefore the friction effects might be less of a problem for glass.

4.2.3 Biaxial testing on glass

The field of biaxial testing for glass is smaller than that of ceramics, but some testing has been done. Quinn [5] and Pepi [27] both suggest a RoR test to determine the biaxial tensile strength of glass. Overend published a paper [28] with a set up and results of a RoR test on glass. The context of the research was different from this one, but the goal of determining the biaxial tensile strength of glass was the same. Overend states two additional advantages of the RoR test: edge failure and the influence of flaw orientation are eliminated.

In the European standards EN 1288-2 [29] and EN 1288-5 [30] the RoR test is also proposed. No literature on biaxial compressive tests or compressive tensile tests was found. However, this does not mean this has not been done. Also, this is not problematic because compressive testing seems to be more straightforward than tensile testing.

4.2.4 Conclusions

In biaxial testing it is important to minimise friction at the boundary conditions and to assure the actual stress state in the material. The ring on ring test is chosen to perform the tensile biaxial strength test. For the following reasons:

- A substantial area is loaded in equibiaxial tension, which increases the chance a critical flaw is present in that part of the glass.
- Edge failure and influence of flaw orientation are eliminated.
- Problems with clamping or glueing the glass (as was done in concrete tensile testing) are avoided.
- It is expected that friction will not be a problem for glass.

It has to be said that the RoR test will result in equibiaxial stress states only, so combinations of different tensile stresses cannot be examined. However, the fully tensile part of the biaxial failure envelope is expected to be quite small. Therefore, it is probably still possible to draw the envelope with only one point.

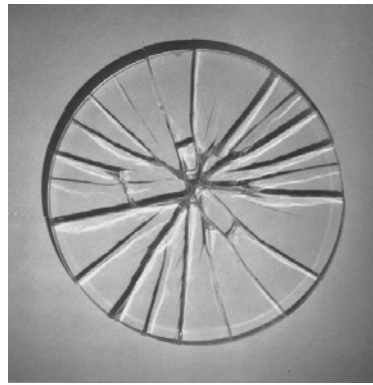
The compressive stress can be applied in a similar way as was done in the biaxial testing on concrete.

4.3 Forensic analysis

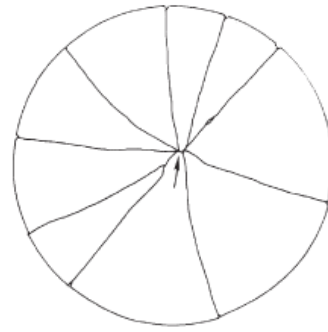
The term forensic indicates that the analysis takes place after fracture has occurred and is focussed on discovering the cause. There are several techniques available that could be of use. They are illustrated below. The expectation is that near the fracture point defects will be found which were the cause of the failure. The hypothesis is that a relationship can be found between certain types of flaws and low or high strengths.

4.3.1 Fracture pattern analysis

The first step in any forensic analysis is an assessment of the fracture pattern. For glass, a lot can be learned from it. A first general rule is that the crack propagates normal to the direction of the tensile stress [5]. This is not so helpful in the biaxial tensile test, but when compression is added, this should reflect in the fracture pattern. Secondly, fracture always starts as one single crack that separates the specimen into two pieces, which then branches into multiple propagating



(a) Glass disc tested in a ring-on-ring test



(b) Fracture pattern and origin

Figure 4.3: Fracture pattern analysis of a disc broken in a biaxial tensile test [5]



Figure 4.4: The analysis of crack branching can supply useful information [5]

cracks. This fact helps finding the fracture origin, see Figure 4.3 The crack branching indicates the direction of crack propagation. The fracture origin is typically halfway between the first branches, see Figure 4.4. Furthermore, the angle of the branches is dependent on the stress state. Uniaxially stressed specimens fork at 45° . Equibiaxially stressed specimens are supposed to fork at 180° . However, additional research has shown that disk specimens tested in a RoR test have smaller angles from 120° to 150° . Only specimens that are very strong and have a lot of stored elastic energy reach 180° .

In Figure 5.10, possible patterns are shown for ring on ring tests on brittle materials. As can be seen, the higher the failure stress, the more branching cracks. The arrows indicate the likely fracture origin. Quinn [5] made two useful remarks on these patterns. Firstly, in low strength specimens the larger remnant is likely to break in bending right after biaxial fracture has taken place. Secondly, moderate to high strength disks often show secondary circumferential cracking near the loading ring.

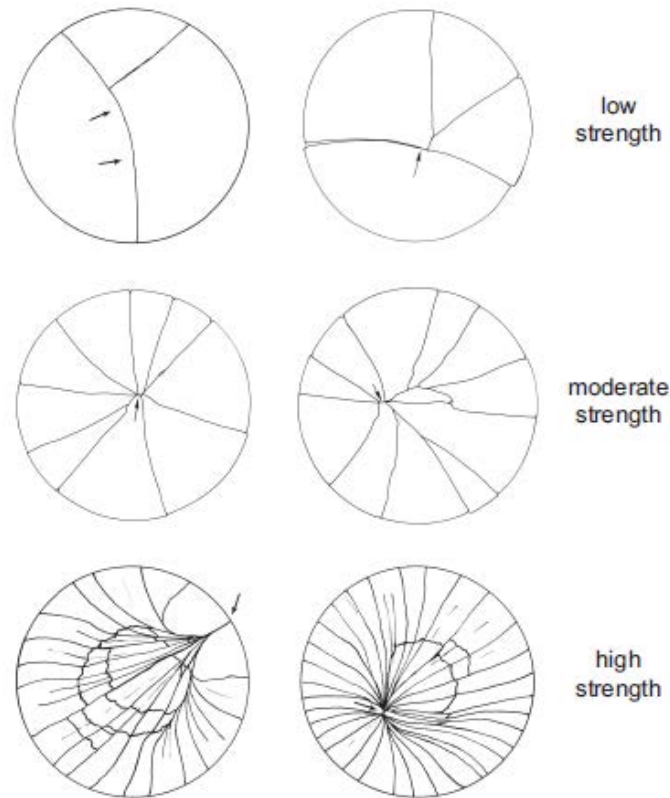


Figure 4.5: Typical fracture patterns in ring on ring tests [5]

To be able to study the glass fracture pattern, the glass should be kept together by an adhesive transparent foil. Another option is to reassemble the fractured pieces, but this is time consuming and small pieces might get lost during the experiment. However, Quinn warns not to put foil at the tensile stressed part of a specimen or at the place where the rings touch the glass.

Actually the best way to find the fracture origin is to film the fracture. This will be tried during the experiment with a GoPro 240 fps camera.

4.3.2 Fracture surface analysis

Traditional glass fractography focusses on fracture surface analysis. This can be performed by taking the fragments apart. Useful fracture markings, that can be observed either by eye or by microscope, are Wallner lines, see Figure 4.6. Irregularities at the surface, such as flaws, produce elastic waves that interact with the stress at the crack front [31]. These superimposed shear waves cause the plane of crack propagation to tilt slightly, thereby producing ripples on the fracture surface [32]. In other words, the crack wobbles. These ripples are perceived as lines, due to the way light reflects on them [33], see Figure 4.7. The two positions indicate the depth at which the microscope is focussed on so that the clearest contrast is obtained. The space between the Wallner lines can be used to calculate local crack velocity [32]. More importantly, the Wallner lines are concave towards the fracture origin [31]. Therefore, they can be used to find the direction of the crack propagation and, if followed all the way back, the origin and thereby the cause of fracture. This is illustrated by Dutt [34] in Figure 4.8.

The front of a propagating crack has different shapes depending on the stress state. Wallner lines follow this shape. See Figure 4.9.



Figure 4.6: Wallner lines at the fracture origin. The arrows indicate the crack propagation direction [31]

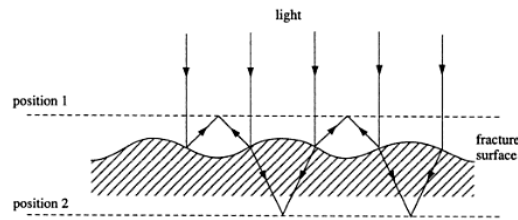


Figure 4.7: The reflection of light causes the ripples to look like lines [33]

There are several more features in fractured glass that can give an indication of what has occurred there that led to the failure. There are marks close to the critical flaw, where the crack starts to grow [17]. See Figure 4.10a. The small half-circle at the middle marks the initiation point of the crack. The horizontal line shows the direction of the crack propagation. The surrounding area can be divided into the following regions:

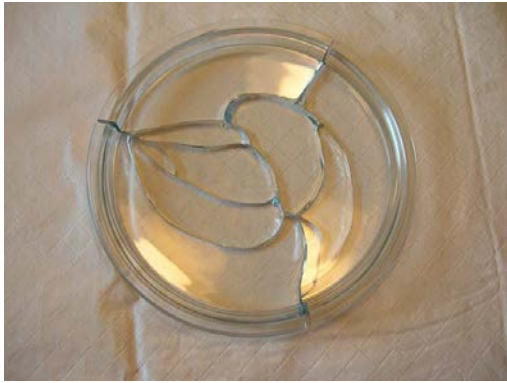
- Up to $2b_{cr}$: Stable crack growth until rapid propagation commences (dashed lines).
- $2b_{cr}$ to r_1 : Mirror region – crack propagates in a relatively smooth plane. Low stress intensity levels, crack propagates at low speed.
- r_1 to r_2 : Mist region – crack propagation gets rougher. The “mist” is a result of defects nucleating ahead of the main crack front. High stress intensity levels.
- r_2 to r_3 : Hackle region – It gets rougher. The cracks are similar to the ones in the mist region but larger. The cracks interact with each other causing branching. Very high stress intensity levels.

The higher the crack propagation speed, the more surface area is needed to dissipate the potential strain energy. The glass accommodates this by creating rougher irregular faceted surfaces [2]. Consequentially, if the failure stress is lower, there are fewer fracture marks and they are therefore harder to interpret.

Figure 4.10b shows these zones in a glass fibre under the microscope. There is a relation between the size of these zones and the applied far field stress at fracture:

$$\sigma_f r_j^{\frac{1}{2}} = M_j = \text{constant} \quad (4.1)$$

So for r_1 a mirror constant M_1 can be found. For most common glasses M_1 is about $2 \text{ MPa}/\sqrt{m}$. For soda lime silica glass it is 2.05.



(a) Assemble the shards back in the original form



(b) Find the Wallner lines on the fracture surface of each of them



(c) Find the direction of the crack propagation



(d) Determine the origin point of the fracture

Figure 4.8: Using Wallner lines in a fractography analysis [34]

There is usually (exceptions exist) one mirror region in a fractured specimen [5]. The crack reaches its final (terminal) velocity within the mirror region. Researchers have shown this can be up to 2500 m/s. This acceleration takes place in microseconds. A mirror region tends to be fully circular in specimens broken in tension, for specimens broken in bending it is often shaped as a half circle. Mirrors that are not circular indicate stress gradients, residual stresses or elongated flaws at the origin. Although mirrors can also be elongated by bending stresses.

4.3.2.1 Fracture origin

The above methods should all lead to finding the location of the fracture origin. But the fracture origin is also an object, the critical flaw. The following tips can help in determining which flaw caused the fracture:

- Examine both fracture halves [5]. Sometimes the flaw first appears to have been a pore, but when considering the other half an inclusion might be found which merely left its mark on the first half.
- When finding a mirror region close to or at the surface, tilt the specimen so that the exterior surface is visible and look for surface type flaws such as scratches or pits. If none are found consider the possibility that the cause is intrinsic.
- Sometimes scratches are no longer visible at the exterior surface since the surface has been polished smooth. Yet the damage beneath the surface remains.

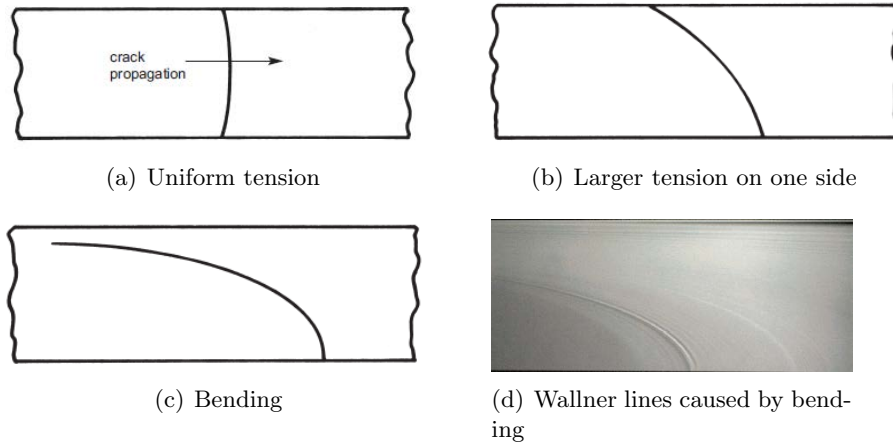
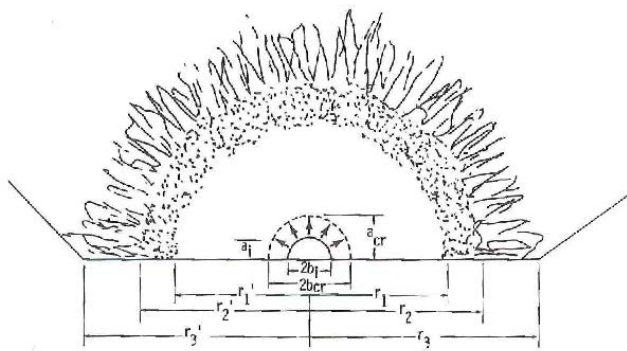
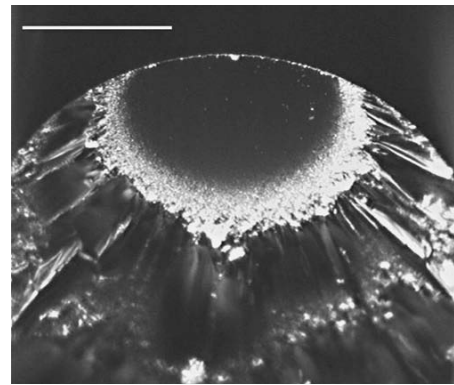


Figure 4.9: Different crack fronts and Wallner lines per stress state [5]



(a) Regions around the starting point of fracture [17]



(b) Mirror, mist and hackle region in a glass fibre [2]

Figure 4.10: Crack initiation marks

- In RoR tests scratches can be tricky to diagnose because the crack can run normal to the scratch for a certain distance, due to the fact that there is always a tensile stress perpendicular to the scratch's orientation.
- Look at the rest of the surface for other surface type flaws. If they are present this can be a clue that the fracture also originated at a surface flaw.
- When more flaws are present at the origin, consider the possibility that a combination of them caused the fracture.

4.3.3 Microscopy

The above mentioned phenomena are best studied with the proper microscopic instruments. The ones that can be useful in glass fractography are described below.

4.3.3.1 Stereo microscope

The stereo microscope provides a low magnification, which makes it suitable to give a general overview of the material [35]. Its advantage is that it has a good depth of field and therefore

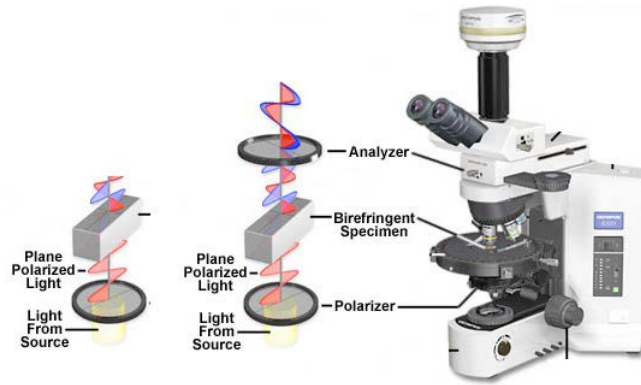


Figure 4.11: A schematic of a polarised light microscope [35]

it is suitable to observe fracture surfaces where it is important to distinguish three-dimensional effects [5].

4.3.3.2 Compound light microscope

This microscope gives a high magnification (25x to 600x) at a very good resolution. However, its depth of field is limited, making it hard to bring a fracture surface in focus [5]. This is overcome when the compound microscope is used in combination with Z-axis scanning software. The image from the objective lens is filmed by a camera, which is shown live on screen with the appropriate software. With Z-axis scanning, the software interprets which parts of the image are in focus. Then, when the vertical position of the microscope is changed, it does this again building a three dimensional virtual image which is represented in a two dimensional image on the computer screen.

The compound microscope available at the faculty of Civil Engineering at Delft University of Technology is a polarised light microscope. This type of microscope can only be used to examine translucent materials. It is often used in concrete petrography. The concrete specimens have to be cut and polished to a very thin section to make it translucent [35]. As glass is transparent, thick sections can be used. A detailed analysis of fractured glass can be performed to find the critical defect. The inclusion and bubbles found by Molnár et al. (see Chapter 1) were around 0.5 mm in diameter [3].

It is called a polarised light microscope because it contains two polarising lenses, see Figure 4.11 [35]. The lower lens, the polariser, is always in place and lets through plane polarized light (PPL). The second lens is called the analyser. It is positioned at an angle of 90 degrees compared to the polariser. The combination of the two lets through no light. A translucent specimen can be placed in between. PPL will simply pass through, and shows the material in its actual colours. When the analyser is added, an isotropic material will let the PPL through in one ray of light which is then blocked by the analyser and no light reaches the objective, resulting in a dark image for the viewer. However, if an anisotropic material lies in between the lenses the PPL is split in two rays, see Figure 4.12, which can pass the analyser. This light is called cross polarised light (XPL). The difference between the angles of refraction of these rays is called birefringence. XPL makes the material appear in a different colour, called the interference colour. By the help of these colours the composition of the material can be analysed. Glass is an isotropic material and appears dark through the analyser. However, the inclusions in glass can be of crystalline composition [12]. Therefore the analyser can be of help in glass research to distinguish inclusions from air bubbles. Broken glass will not appear dark

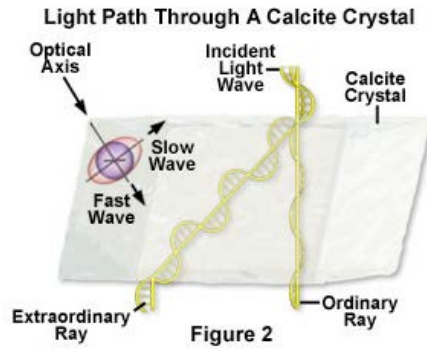


Figure 4.12: An anisotropic material splits light in two rays, a slow and a fast one [35]

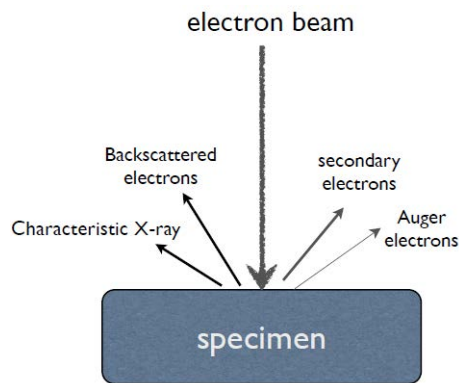


Figure 4.13: The interaction between the beam and the specimen [36]

in XPL light, because the light is refracted by the fracture planes inside the glass.

4.3.3.3 Scanning electron microscope

When the critical defect is found, the question may arise what it consists of. Bubbles probably just consist of air, but it might be interesting to investigate the inclusions further. As was stated the interference colour can be of help here, but this may be hard to pinpoint and only anisotropic components will be shown. Another useful device is a Scanning Electron Microscope (SEM) [36]. This is a device that shoots an electron beam at the specimen. The beam interacts with the specimen, which releases different types of electrons and characteristic x-rays, see Figure 4.13. For the electrons and x-rays to be properly released, the specimen must have no protruding parts that can block the reflected beams. In concrete fractography specimens are polished extremely flat. In his guide to fractography of glasses and ceramics however, Quinn only mentions placing the fracture surface of the specimen perpendicular to the incident beam [5]. Additionally, the component that has to be analysed has to be at or close to the surface. It is expected that the critical flaw will be close to the fracture surface. Lastly, a protective coating such as gold or carbon should be sprayed over the specimen. This is to protect the specimen from damage by the electron beam.

There are several analyses that can be performed with a SEM. Two are relevant in this case. The first is creating an image from backscattered electrons. These are the primary electrons that are released when the electron beam interacts with the specimen. They lose energy in the process, which is characteristic for the chemical composition. The SEM translates this to

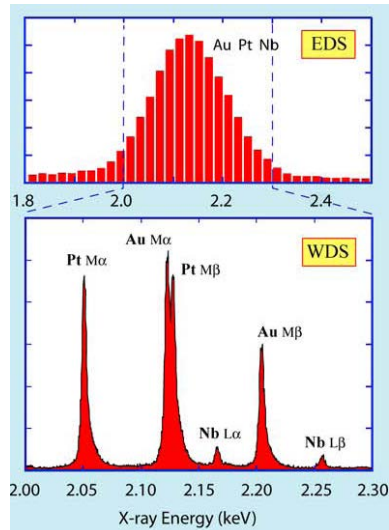


Figure 4.14: Energy resolution of EDS vs WDS [36]

a grayscale image of the specimen's components. The higher the atomic number of the phase, the brighter it will appear in the image. So the image that can be analysed is similar to the interference colour, except now isotropic materials can be analysed as well. Also it gives a much more detailed image. The second technique is the X-ray analysis. The SEM needs additional detectors to identify the X-rays that are released after the electron beam interacted with the specimen [37]. There are two types: Energy Dispersive Spectroscopy (EDS) and Wavelength Dispersive Spectroscopy (WDS). These detectors measure the intensity of the energy or the wave length of the x-rays and translate them into a graph like the lower graph in Figure 4.14. When the atomic numbers are close EDS has trouble distinguishing the peaks, creating the upper graph. However, WDS damages the specimen and has a higher cost and time consumption. So if the glass contains no overlapping components, EDS is preferred. The value of the energy or wave length can be compared to characteristic values of elements, to determine which element is present in the specimen. To determine the composition of an inclusion, Quinn recommends scanning the inclusion and then scanning a part of the glass next to it and compare both graphs [5].

4.3.4 Other instruments

There are numerous other instruments that can be of help in a fractographic analysis. Two more examples are:

- Nano-indenter: to determine the Young's modulus locally. This could give insight in what is happening around a defect.
- Micro CT-scanner. Molnár et al. [12] used such a scanner to measure the exact dimensions of the defects.

The ones mentioned in this section were chosen because they are commonly used and present at the faculty of Civil Engineering of Delft University of Technology and therefore at the disposal of the author. However there are many more instruments which have proven to be very useful. An extensive list of possible instruments can be found in Quinn's guide to fractography of ceramics and glasses [5].

4.3.5 Conclusions

There are some techniques that can be very useful in glass research. The polarised light microscope will be used for analysing the fracture marks and finding the defect at the origin. The other techniques will mainly be necessary when it is desirable to know more about the composition of the defect, which shall follow from the first analysis.

Experiment

5.1 Introduction

The experiment consists of a mechanical and a fractographic part. The mechanical part is a biaxial strength test, which means three strength tests should take place:

- A biaxial tensile test.
- A tensile compressive test.
- A biaxial compressive test.

The former will be done by a ring on ring test. The second will be a variation on the RoR test where a compressive force is added in one direction. The latter can be performed by compressive forces in two directions. In the end, not enough time was left to fully perform the tensile compressive and biaxial compressive test. But a set up was proposed.

As Quinn [5] stated, the flaw type that caused failure might be just as important as the strength found and therefore it is wise to include a fractographic analysis. This consists of a fracture pattern analysis and examination with a polarisation microscope.

5.1.1 Specimens

A hundred specimens were ordered from a manufacturing plant in China. They are cruciform-shaped, so that it is possible to add a compressive stress. See Figure 5.1.

The thickness of the plates is 3.9 mm. Some plates had chipped edges, but all of these were a sufficient distance from the middle of the plates.

5.2 Ring on ring test

The principle of this test is of a flat specimen lying on a support ring and a load ring pressing down on it, creating an equibiaxial flexure stress in the material within the loading ring. This method can be compared to the four point bending test, but then circular, ensuring the same stress in all directions.

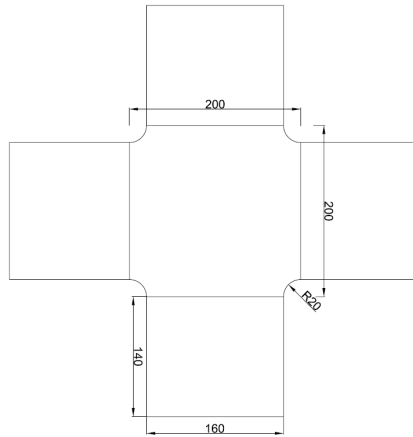


Figure 5.1: Ring on ring test values

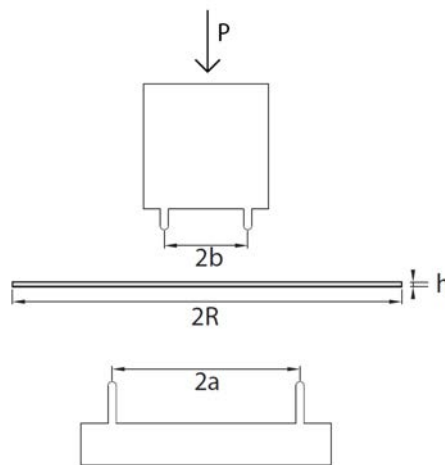


Figure 5.2: Ring on ring test values

The ring on ring test is described by the following formula:

$$\sigma_b = \frac{3P}{2\pi h^2} \left\{ (1 - \nu) \frac{a^2 - b^2}{2R^2} + (1 + \nu) \ln \frac{a}{b} \right\} \quad (5.1)$$

Most of the values in this formula are given in Figure 5.2. σ_b is the biaxial stress within the loading ring for the given load P . The value of P at failure gives the strength of the specimen. ν is the poisson's ratio.

5.2.1 Test outline

The ring on ring test is going to be performed in a loading device Instron 8874, which can load up to 10 kN. The dimensions have to be such that for all possible glass strengths the specimens will break before the maximum load is achieved. With these dimensions the lowest recorded strength of 20 N/mm^2 would occur for a load a little under 0.7 kN. The expected maximum load of 150 N/mm^2 would occur at approximately 5 kN.

All specimens were cleaned with ethanol and then wrapped in transparent adhesive foil, so that the shards stay together making post-fracture analysis more convenient. See Figure 5.3 for the set up. It is quite important that the support and loading rings are coaxial to a high precision

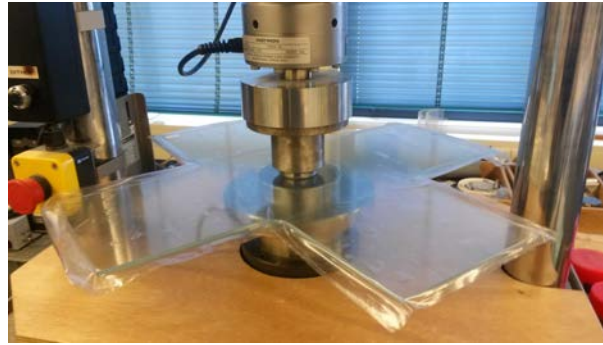


Figure 5.3: Ring on ring test set up

[26]. This was assured by a plastic ring, of which the outer rim fits exactly in the steel support ring and the inner rim fits exactly around the steel load ring. The glass plates were placed centrally inbetween these rings by marking the required position of the rings at the centre of the glass.

All plates were tested with the air side down, which is slightly weaker than the tin side and thereby governing for glass' strength. The tin and air side can be distinguished with ultraviolet light.

5.2.1.1 Strain measurement

6 plates were tested with a strain gauge rosette to check if the measured strain corresponds with the stress that follows from the ring on ring formula. A rosette was chosen because it measures the strain in three directions. It was glued at the tensile side of the glass at the middle of the loading ring zone. The output wires were connected to an A/D-converter so that the strain could be measured.

5.2.1.2 High speed camera

It would be ideal to determine the starting point of fracture by capturing it with a high speed camera. The Go Pro 3 Black edition was used, which can shoot videos at 240 frames per second in 848x480 resolution. The test set up was made suitable for this by drilling a hole in the support ring and placing an additional light source. See Figure 5.4a. The support ring was raised on two u-profiles so that the camera could be placed underneath. See Figure 5.4b. A nice feature of the camera was that it could be controlled by an app with a smartphone or computer, thereby it could be left underneath the ring during the experiment.

5.2.1.3 Compressive tensile test

The compressive stress was added by a pressure cell with a capacity of 10 kN, controlled with a hand pump. The stress inside the cell was measured and displayed on a computer screen so that the desired value could be applied. The load from the cells was transferred to the glass by plastic profiles. A piece of foam fubber was placed inside the u-profiles to incorporate unevenness of the glass' edge. The profiles were placed at the cruciform's arms, which were cut to the size necessary. The specimens were deliberately ordered with longer arms, so that they would have sufficient length to add the compressive stress. See Figure 5.5 for the set up.

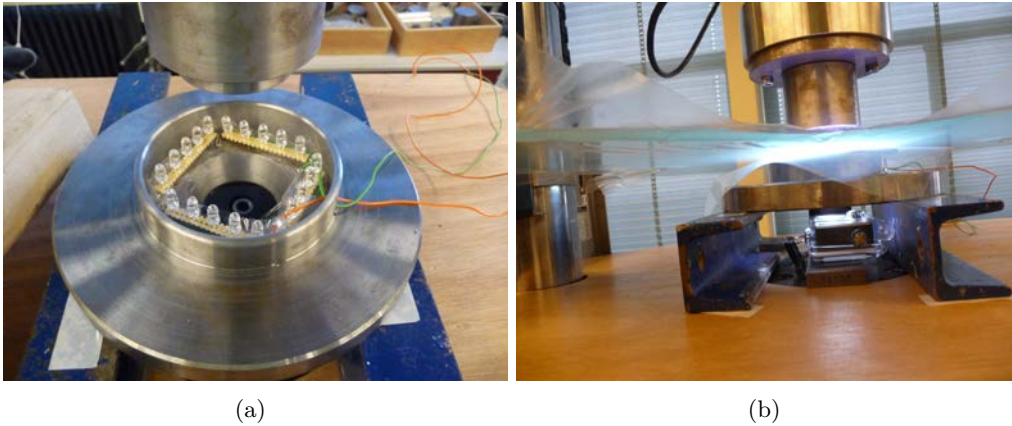


Figure 5.4: High speed camera set up



Figure 5.5: Compressive tensile test set up

5.2.2 Test conditions

In any scientific research, it is important to report the conditions during an experiment and keep them the same or note deliberate changes in consecutive tests. The conditions used in this experiment are documented in the following paragraphs.

5.2.2.1 Dimensions

Over the years the RoR test has been developed and optimised by several researchers. It appeared that the test works best for certain ratios of the dimensions used.

- Outside the support ring the stress drops sharply. Still to avoid failure at the support $R/a > 1.25$ is recommended [38].
- $b/a = 0.5$, this ratio follows from a compromise to get a sufficiently big uniformly stressed region, without getting troubles with the concentricity or shear stresses.
- To be able to use linear analysis, the maximum deflection should be small. This is achieved by applying a ratio of $a < 50h$ [26].
- To avoid wedging effects and the need for corrections: $a > 10h$.
- To avoid failure at the edge, the overhang should either be small $\frac{R-a}{h} < 1$ or large $\frac{R-a}{h} > 5$.
- To minimize friction the radius of the rounded ring should be $h/2$ [38].

Most tests use square or circular specimens. However, there is no difference between these shapes for the stress distribution within the support ring [39]. For square specimens an equivalent radius of half the average of the edge and diagonal lengths can be taken. In this case the specimen is cruciform shaped. It is assumed half the diagonal length of the middle square can be taken as an equivalent radius.

EN 1288-2 proposes an RoR test for large specimens in which $a = 400$ mm and $b = 300$ mm [40]. For the purposes of this thesis, this is far too big to also perform a microscopic analysis. EN 1288-5 proposes an RoR test for small specimens in which $a = 45$ mm and $b = 9$ mm. However, the radius of the loading ring is on the small side to the liking of the author. A larger radius is preferred to obtain a larger area that is stressed in tension.

Following the above recommendations the dimensions of the ring on ring test and the specimen were determined. See Tables 5.1 and 5.2.

Table 5.1: Dimensions

Quantity	Value	Unit
ν	0.22	-
h	4	mm
a	45	mm
b	20	mm
R	141	mm

Table 5.2: Ratios

Ratio	Recommended	Applied
R/a	> 1.25	3.14
a/b	0.5	0.44
a/h	$10 < a/h < 50$	11.25
(R-a)/h	> 5	24.11

5.2.2.2 Environmental conditions

As was reported in Section 2.2.1, water can have a negative effect on glass. In some tests [28], the glass is placed in a nitrogen atmosphere to avoid any contact with water. It is expected the effect of moisture can be neglected as the test will be performed rather quickly. However, it is wise to keep environmental conditions constant among different tests, as big changes could have an effect. Therefore, the humidity was held around 30% and the temperature was kept between 20 and 25 degrees.

5.2.2.3 Friction

Friction can be a difficult issue in ring on ring testing [26]. Several options were tried to minimise friction in this research. For each specimen it is mentioned what kind of interface was applied between the rings and the glass. These interfaces are specified in Table 5.3.

Table 5.3: Interfaces applied to minimise friction

Interface	Specification
Cut foil	The book foil (that was wrapped around the glass) was cut away at the positions where the rings touch the glass.
Vaseline	Vaseline was smeared at the rings.
Rubber	3 mm thick rubber was placed between the rings and the glass. The rings leave an imprint so the rubber had to be replaced regularly.
Lubricant	Dow Corning 7 release compound was smeared at the rings.
Polypropene	3 mm thick polypropene was placed between the rings and the glass. Polypropene has the properties of being both very smooth and very tough, so that the rings barely leave an imprint in the material.
Delrin rings	Rings made of delrin were placed in the steel rings, see Figure 5.6. According to Pepi [27] they minimise friction and local stress concentration, because they are more compliant than the steel rings.
Sharpened rings	Recommended by Overend [41] as used in his research [28]. See Figure 5.7.
Hinged	A circular hinge was placed between the load ring and the Instron machine to make sure the load ring does not touch the glass under an angle and to incorporate unevenness [41, 28].
Strain gauge	The strain gauge might have an effect on the stiffness and therefore it is mentioned as an interface here.

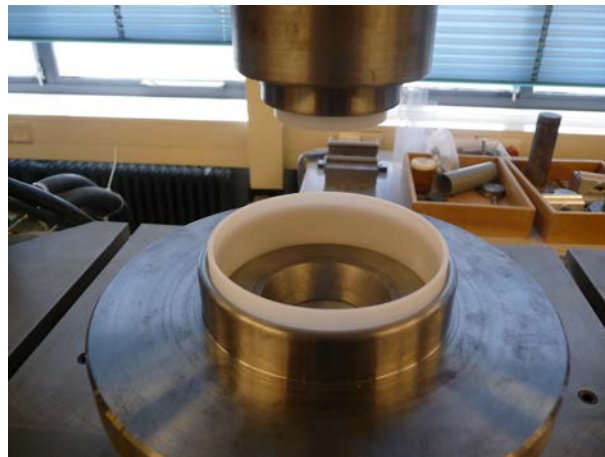


Figure 5.6: Delrin rings were tried as they are more compliant than steel

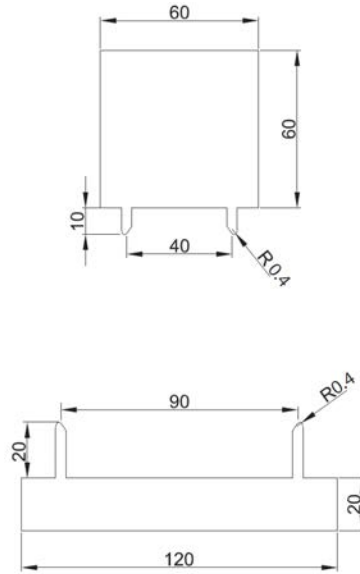


Figure 5.7: Alteration of the steel rings to make a sharper edge

5.2.3 Results

In total 56 out of the 100 plates were RoR tested. 3 of them were tested in a compressive tensile test. Additionally, 10 different plates of 3 mm were tested. All results are discussed in the below paragraphs.

5.2.3.1 Strain measurements

The purpose of the strain measurements was to determine whether they corresponded with the stress that was calculated by the RoR formula. This was checked by the means of the Young's Modulus through the formula:

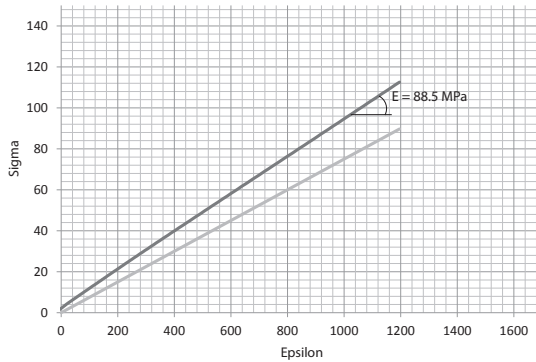
$$\sigma = E\epsilon \quad (5.2)$$

First the Young's Modulus of the glass had to be determined. This was done by a four point bending test on a square piece of the same glass. Two specimens were tested, one with and one without foil. The specimen without foil yielded a Young's Modulus of 74 GPa. The Young's Modulus of soda-lime silica glass can range from 70 to 74 GPa [2], so this is a realistic value. The difference is caused by the choice of additives to the glass mix, such as aluminium. The specimen with foil yielded a Young's Modulus of 75.8 GPa. It seems the foil adds a little stiffness.

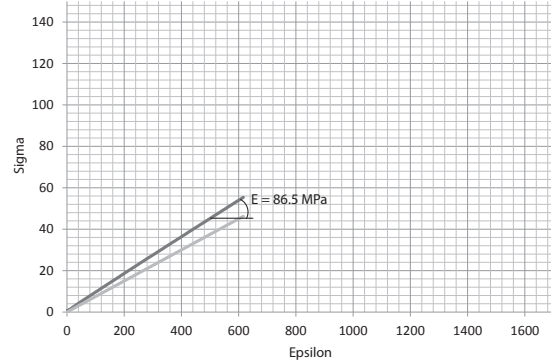
7 cruciform plates were RoR tested with a strain gauge of which 5 were broken. The rosette strain gauge measures the strain in three directions. For all plates, the three different strain values were pretty similar. So it can be concluded that a biaxial stress is successfully achieved in this set up. The strain value used for the calculations was taken to be the average of those three strain values. However, they yielded surprisingly high values of the Young's Modulus as is summarised in Table 5.4. This is visualised in the graphs on the next pages. The $\sigma - \epsilon$ line for the expected Young's Modulus of 75.8 GPa (glass with foil) is plotted too to show the difference. The stops in the first five graphs indicate the point of fracture, the stops for the graphs of TT30 and TT26 indicate the abortion of the test. For this reason, a different axis division was chosen for these two graphs. There are a few possible explanations for these results. First of all, it is seen for specimen TT26 that using a smaller strain gauge gave a lower

Table 5.4: Young's Modulus calculated by RoR stress and measured stress

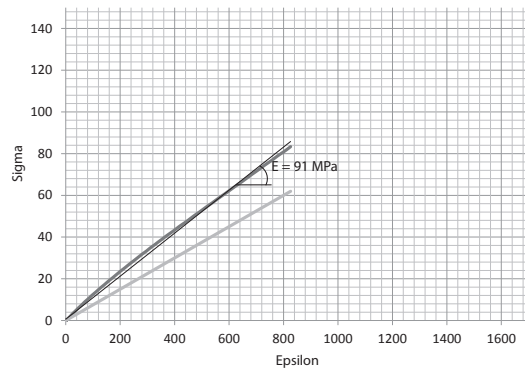
Specimen	[MPa]	E [GPa]	Deviation	Interface
TT1	109.21	88.5	17%	In foil
TT2	53.75	86.5	14%	In foil
TT27	80.87	91	20%	Teflon and vaseline
TT28	76	89.5	18%	Rubber
TT29	143.09	94	23%	Cut foil and vaseline
TT30	N/A	87	14%	Rubber and teflon
TT26	N/A	83	9%	Rubber, teflon, a small strain gauge and no foil



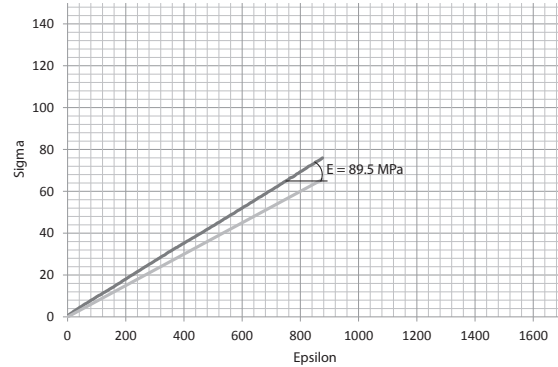
(a)



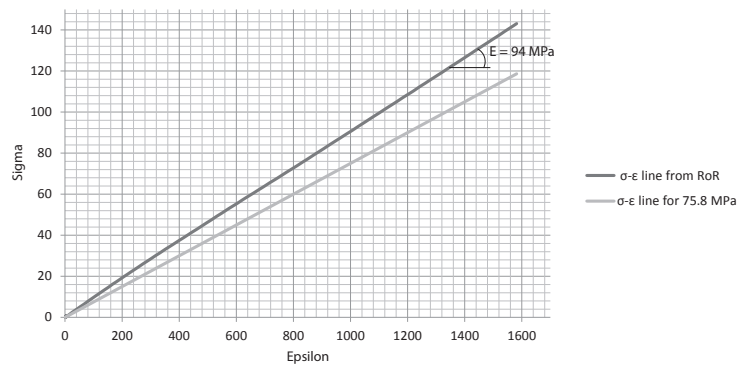
(b)



(c)



(d)



(e)

Figure 5.8: Graphs of the Young's Modulus of (a) TT1 (b) TT2 (c) TT27 (d) TT28 (e) TT29

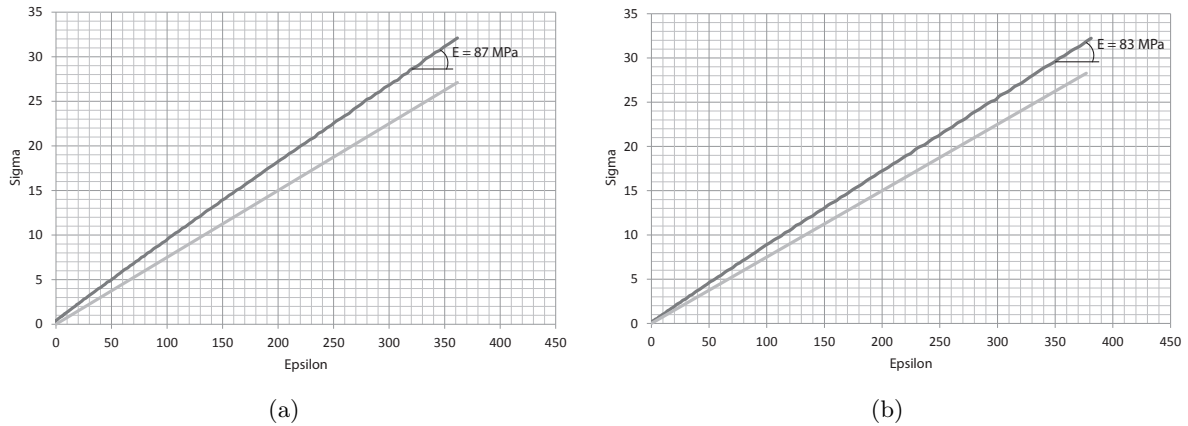


Figure 5.9: Graphs of the Young's Modulus of (a) TT30 (b) TT26

Young's Modulus. It seems that the strain gauge rosette increases the stiffness of the glass locally. A second explanation can be found in friction. If there is friction, a part of the load will be transferred to the support ring. Friction is assumed to be zero in the RoR formula. So if friction is present the formula will give a higher value of failure stress than is actually present in the glass. According to Morrell [26] ignoring friction can lead to overestimation of the strength by a few percent for specimens with $a = 20h$ and tens of percent for specimens with $a < 5h$. For this research, $a = 11.25h$ because Morrell recommended $a > 10h$ but it is clear friction can play a big role. The author thinks this, at the very least, explains the variability in the results, which is also striking. But it is uncertain if it explains the general large deviation of the actual Young's Modulus. In a personal conversation [42] it was discussed the RoR formula assumes zero thickness of the rings, which can be an explanation of the large deviation causing such high values. A correction factor should be applied. However, due to the variability, it was not possible to derive such a factor from these results. Further testing and perhaps even finite element modelling will have to determine this factor.

It was decided to proceed with the strength tests, keeping in mind the RoR stress is probably higher than the actual failure stress. The results can still be valuable because they give an indication of which plates have a low or a high strength.

After all strength tests were performed, further literature research suggested that a large overhang of the specimen stiffens the specimen against deflection [26]. It is therefore encouraged to explore this in future research.

5.2.3.2 Biaxial tensile test

53 plates were fractured in the biaxial tensile RoR test. The matrix in Table 5.5 gives an overview of each tested plate, its interface and the failure load and stress. The horizontal lines divide the plates that were broken in one session. In the strain measurement tests, two plates were not fractured. TT30 was fractured in a later test, TT26 was not and is therefore missing in this list.

Table 5.5: Applied boundary conditions and resulting failure stress and fracture mechanism per specimen

#	Load rate	Cut foil	Vaseline	Rubber	Teflon	Special grease	Polypropene	Delrin rings	Sharpened rings	Hinged	Strain gauge	Fracture	Failure load [kN]	Failure stress [N/mm ²]
TT1	0.01		x								x	I	3.41	109.21
TT2	0.01		x								x	I	1.68	53.75
TT27	0.01		x		x						x	RS	2.39	80.87
TT28	0.01			x							x	I	2.37	76.00
TT29	0.01	x	x								x	RS	4.46	143.09
TT21	0.01			x	x							RS	2.33	74.60
TT22	0.01			x	x							RS	3.04	97.49
TT23	0.01		x	x	x							I	2.48	79.66
TT19	0.01	x				x						I	3.00	96.16
TT20	0.005	x				x						RS	2.95	94.53
TT24	0.005					x						I	2.00	64.16
TT25	0.005					x						I	2.05	65.72
TT30	0.005	x				x				x		IS	2.82	90.42
TT14	0.005					x						RS	2.34	79.13
TT15	0.005					x						RS	3.76	126.86
TT16	0.005					x						RS	2.65	85.02
TT17	0.005					x						R	2.33	74.56
TT18	0.005					x						RS	2.82	90.35
TT10	0.01			x	x	x						I	1.71	57.59
TT11	0.01			x	x	x						R	2.8	89.81
TT12	0.01			x		x						RS	3.45	110.66
TT13	0.01			x	x							RS	4.01	128.61
TT3	0.01		x	x	x							I	1.30	41.79
TT4	0.01		x	x	x							RS	3.26	104.64
TT5	0.01		x	x	x							R	1.96	62.36
TT6	0.01						x					I	2.47	79.14
TT7	0.01						x					RS	3.05	97.73
TT8	0.01						x					IS	3.21	102.83
TT9	0.005						x					I	1.82	58.20
TT31	0.005						x					R	2.39	76.76
TT32	.005							x				R	2.18	72.88
TT33	0.005						x	x				RS	2.91	96.92
TT34	0.005							x				RS	2.88	95.96
TT35	0.005						x	x				I	2.50	83.30
TT36	0.005						x					R	2.47	79.32
TT37	0.005						x					RS	3.02	96.78
TT38	0.005						x					RS	3.18	101.80
TT42	0.005	x							x			I	1.92	61.63
TT43	0.005	x							x			RS	3.56	114.11
TT44	0.005	x							x			I	2.99	95.85
TT45	0.005	x							x			RS	2.91	93.42
TT46	0.005	x							x			RS	2.86	91.63

Table 5.6: Continuation of Table 5.5

#	Load rate	Cut foil	Vaseline	Rubber	Teflon	Special grease	Polypropene	Debrin rings	Sharpened rings	Hinged	Strain gauge	Fracture	Failure load [kN]	Failure stress [N/mm ²]
TT39	0.005	x						x	x			I	3.39	108.53
TT40	0.005	x						x	x			I	1.75	56.16
TT41	0.005	x						x	x			IS	4.29	137.67
TT47	0.005	x						x	x			RS	4.47	143.31
TT48	0.005	x						x	x			IS	3.95	126.73
TT49	0.05	x						x	x			I	2.93	93.85
TT50	0.05	x						x	x			RS	2.89	92.64
TT51	0.05	x						x	x			RS	3.38	108.28
TT52	0.05	x				x		x	x			IS	3.42	109.53
TT53	0.05	x					x	x	x			IS	4.01	128.64
TT54	0.02	x						x	x			IS	2.63	84.30

The lowest strength value is 41.79 MPa and the highest 143.31 MPa.

The tested specimens can be divided into two main categories according to their fracture patterns. The first category contains plates whose fracture origin lies in the loading ring (noted I) and the second category is for plates whose fracture started at or outside the loading ring (noted R). These plates can be further divided into two subcategories: the plates either showed a ringshaped fracture along the support ring or not (if so a letter S is added). Quinn [5] states that secondary circumferential cracking occurs close to the loading ring in plates that fail at a medium to high strength, which is seen in a lot of plates in this research too, but nothing is mentioned about this type of cracking at the support ring. See Figure 5.10. In Figure 5.11 a plate of each fracture category is shown. All fracture patterns of each plate can be found in Appendix A. Plates in category I failed as is expected from a RoR test: at a flaw within the loading ring, where the tensile stress is highest. Plates in category R have two possibilities: either they broke from a flaw at or just outside the ring (the tensile stress at those points is still pretty high) or they broke from a contact point at the ring. Fractographic analysis should conclude this. If the former is the case, the fracture started at the bottom of the plate. Is the latter the true scenario, fracture started at the top.

To the knowledge of the author, there are two possibilities of the circumferential cracking at the support ring seen in categories IS and RS. The first possibility is that this is due to a punching shear mechanism. This was initially thought to be the case with friction between the rings and the glass as the cause. For this reason, the different boundary conditions were tried to minimise this friction. An analysis of the boundary condition is made in Table 5.7. As can be seen, none of them had a significant effect. The second possibility is a more complicated one. When the loading condition in a brittle material suddenly changes, a shock wave will travel through the material [43]. Keeping this in mind, one can imagine that when the first cracks appear on the tension side, this can induce small shock waves that travel through the glass. These waves deform the glass locally. If such a deformation occurs at the ring, this could lead to a local stress concentration causing fracture. This all happens in microseconds. So the glass fails at a flaw but due to the dynamic effects the fracture patterns also exist at the rings. Which of the two scenarios actually took place might follow from microscopic analysis.

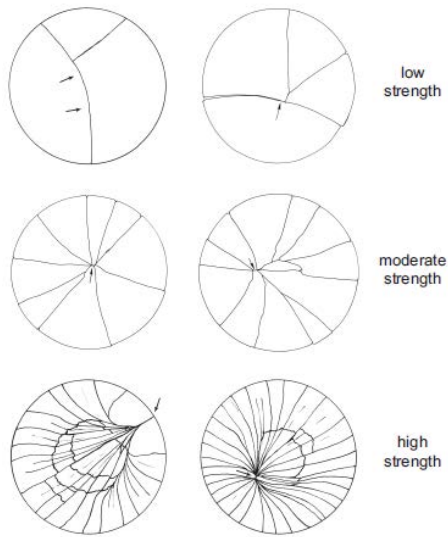
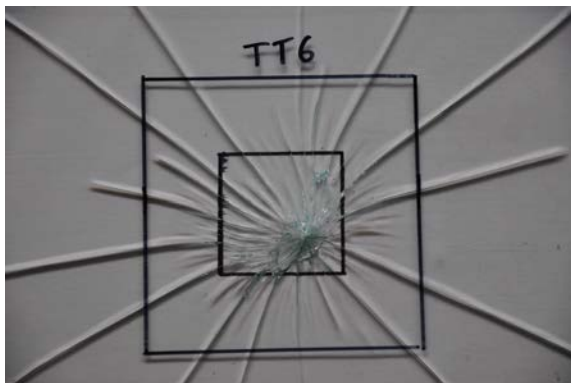
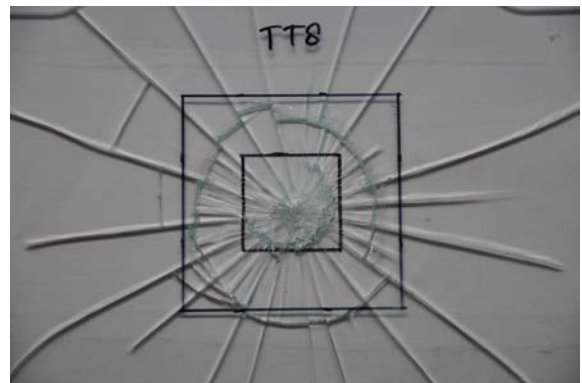


Figure 5.10: Expected fracture patterns in RoR tested plates [5]



(a) TT6, category I



(b) TT8, category IS



(c) TT17, category R



(d) TT16, category RS

Figure 5.11: Fracture pattern categories

Table 5.7: Resulting categories for combinations of boundary conditions

	Rate	I	R	IS	RS
Rings cut/sharp/hinge	0.005	2		2	1
	0.05	1		2	2
	0.02			1	
Rings cut/sharp	0.005	2			3
Delrin	0.005		1		1
Delrin + polypropene	0.005	1			1
Polypropene	0.01	1		1	1
Polypropene	0.005	1	2		2
Vaseline+rubber+teflon	0.01	2	1		1
Compound (some rings cut)	0.005	2	1	1	5
	0.01	1			
Strain gauge + vaseline	0.01	2			1
Gauge+vaseline+teflon	0.01				1
Gauge+rubber	0.01	1			
Rubber + teflon	0.01				3
Rubber+teflon+compound	0.01	1	1		
Rubber+compound	0.01				1

5.2.3.3 High speed camera

Three plates were filmed with the high speed camera: TT21, TT22 and TT23. Their fracture patterns are depicted in Figure 5.12. It turned out that the camera is not quite fast enough; the fracture origin of TT22 and TT23 was not captured. TT21 was more succesful. In Figure 5.13 it can be seen fracture started from the bottom at the support ring. However, it seems some luck is required for the moment of fracture and total fracture to take place in different frames and be captured. It is therefore concluded a faster camera would be needed to capture all fracture origins. For this research, such a camera was not at hand.

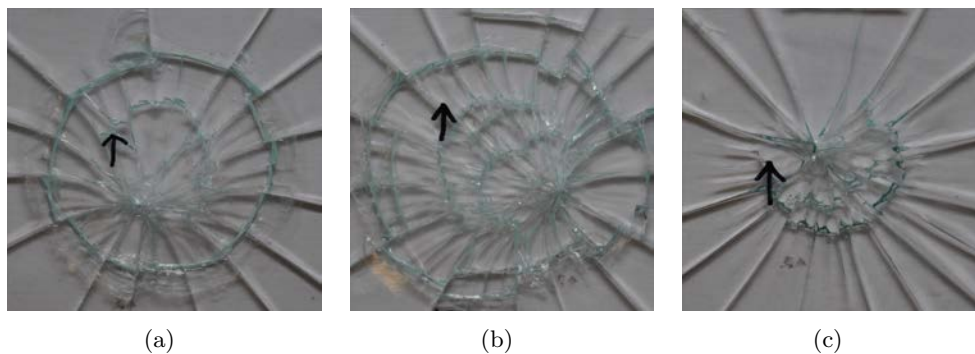


Figure 5.12: Fracture patterns of (a) TT21 (b) TT22 (c) TT23

5.2.3.4 Compressive tensile test

Three plates were tested in the compressive tensile test. A compressive load of 2 kN was applied. The failure stress is reported in Table 5.8. The fracture patterns are displayed in Figure 5.14. In the fourth test the load was increased to 4 kN. However, the test was aborted because one

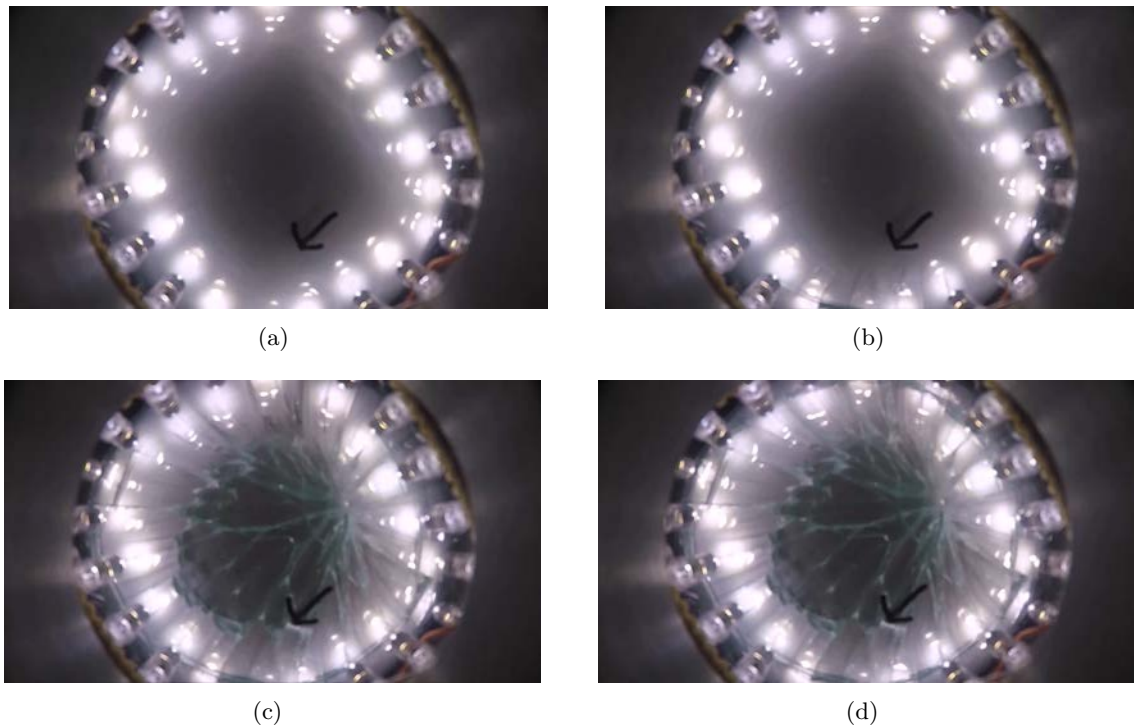


Figure 5.13: High speed video of the fracture of TT21

side of the plate was lifted upwards. See Figure 5.15. This was not noticed in the first three tests, but might have happened to a smaller degree. From the stress values it is guessed that it did happen in the first two tests, but not in the last. Either way, the set up needs to be improved before further compressive tensile tests are performed. Adding guiders that hold the u-profiles in place would solve the problem. Another improvement is placing a steel strip behind the u-profiles to assure a more even stress distribution.

Table 5.8: Failure stress in compressive tensile test

Plate	σ [Mpa]
CT1	52.34
CT2	57.09
CT3	131.95

5.2.3.5 3mm thick glass

30 out of 53 plates in the biaxial tensile test on 4 mm glass contained circumferential cracking at the support ring. If all of these fractured due to punching shear, the test was not as succesful as hoped. 10 glass plates of 185 by 185 mm and 3 mm thickness were RoR tested. The load rate was 0.01 mm/s. The interface was cut foil, sharpened rings and hinged. The results are surprisingly good. See Table 5.9 and Figure 5.16. None of the plates show circumferential cracking at the support ring. All pictures can be found in Appendix A. Moreover, with a lowest failure stress of 63.06 MPa and a highest of 120.08 MPa the strengths lie closer together (although, for a smaller test group this was to be expected). It seems this group works much better than the group of 53 specimens. There are three possible reasons:



Figure 5.14: Fracture patterns of (a) CT1 (b) CT2 (c) CT3

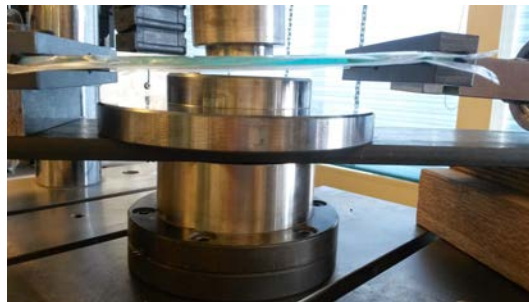


Figure 5.15: The u-profile moves upwards

Table 5.9: Results RoR tested 3 mm thick glass

#	Fracture	Failure load [kN]	Failure stress [Mpa]
X1	I	1.74	102.57
X2	I	1.07	63.48
X3	I	1.54	91.27
X4	R	1.77	104.76
X5	I	1.10	65.12
X6	I	1.44	84.84
X7	I	2.20	120.08
X8	R	1.32	77.83
X9	R	1.80	106.57
X10	I	1.07	63.06

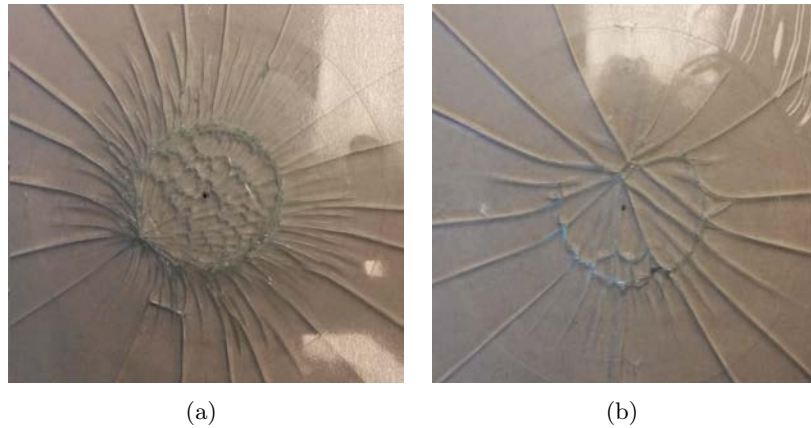


Figure 5.16: Fracture patterns of (a) X4 (b) X10

- A thickness of 3 mm instead of 4 mm.
- The shape and size of the specimen with a much smaller overhang.
- The manufacturer of the glass. The 4 mm glass originated from a factory in China, the 3 mm glass from a factory in Europe.

To the author, the first two options seem the most plausible. This is interesting because recommended ratios from the literature were used based on RoR testing on ceramics. This might mean different ratios apply to glass. It is unclear to the author if the European standards [29, 30] have a fundamental basis for the ratios applied. However, an article [44] that came to the attention of the author at a late stage in the research seems to have explored these further and could be a good starting point in future research.

5.2.4 Conclusions

From the strain measurements it followed that the calculated failure stress is not the actual failure stress that occurred in the glass. Moreover, the deviation is quite variable. This is thought to be caused by friction between the rings and the glass. Because of this variability no correction factor is chosen and the results presented use the formula's stress value. Again, this is not the actual value. However, it does give an indication of which plate has a low or a high strength.

30 out of 53 plates tested in the RoR test showed circumferential cracking at the support ring. This type of cracking is not expected from RoR fracture patterns, as reported in literature. There are two possible mechanisms behind this feature:

- Punching shear, thought to be caused by friction between the rings and glass.
- A more complex mechanism where dynamic effects, that occur in the glass microseconds before and after fracture, cause stress concentrations at the support ring.

The last test of 10 alternative glass specimens did not show circumferential cracking at the support ring. It seemed different recommended ratios apply to glass than to ceramics. This needs to be explored in future research. It is recommended to use [44] as a starting point.

Lastly, a RoR test with a high speed camera and a compressive tensile test were performed. For the former a faster camera than 240 fps is needed. For the latter guiders are required to keep the compressive stress horizontal.

5.3 Fractographic analysis

5.3.1 Test outline

This analysis consists of 2 parts. All plates were examined by eye to draw initial conclusions from their fracture patterns. The second step was to examine a selection of these plates by microscope. This step is actually quite special. Rather than the fracture surface, first the fracture pattern was analysed underneath the microscope. The author did not find reportings of such a research in the literature. The microscope used for this step is a Leica DM2500P petrographic microscope equipped with polarization accessories and semi-apochromat (fluorite) objectives. Optical photomicrographs of the glass specimens were acquired with a Leica DFC310FX digital camera at 1392 times 1040 uninterpolated resolution. In order to overcome the limited depth of field of the compound microscope, images were acquired through Leica LAS Live Z-Builder software which enabled dynamic emergence of the single in-focus image. The resulting image has a significantly large depth-of-field which renders the microstructural features of a glass specimen on a two dimensional final image. The advantage of this technique is that it makes all flaws and fracture markings that exist throughout the depth of the glass visible in a single field of view. This is what made this step special, as will become clear from the results. Two light settings were used:

- Transmitted light: polarised light enters the specimen from underneath illuminating all flaws inside the glass.
- Reflected light: the specimen is lighted from above, mainly illuminating the surface.

A third step would have been the microscopic analysis of the fracture surface. However, this did not fit in the time frame of this research.

5.3.2 Results

5.3.2.1 Fracture pattern analysis

Part of the fracture pattern analysis was performed right after the strength tests by sorting the plates in fracture pattern categories.

As was stated in the literature, the fracture origin can be determined from the branching of the cracks. In the images in the next paragraph the origin is indicated by a red arrow.

5.3.2.2 Microscopic analysis - qualitative

Six plates were selected to be examined with the Leica microscope. TT3, TT40 and TT10 were chosen because they had the smallest failure stress: 41.79 MPa, 56.16 MPa and 57.59 MPa respectively. (TT2 was not selected because too much fracture grit had developed during transportation and storage for it to be examined properly). They are interesting to examine because their low strength is thought to have been caused by a line defect. Microscopical examination might prove this. The other three plates form a good representation of the fracture pattern categories. Their fracture pattern analysis and photomicrographs are depicted on the next pages. The white circles mark the location of contact of the loading and support ring. The red arrows mark the origin crack of the fracture, concluded from the fracture pattern analysis. Based on the photomicrographs an analysis of each plate was made:

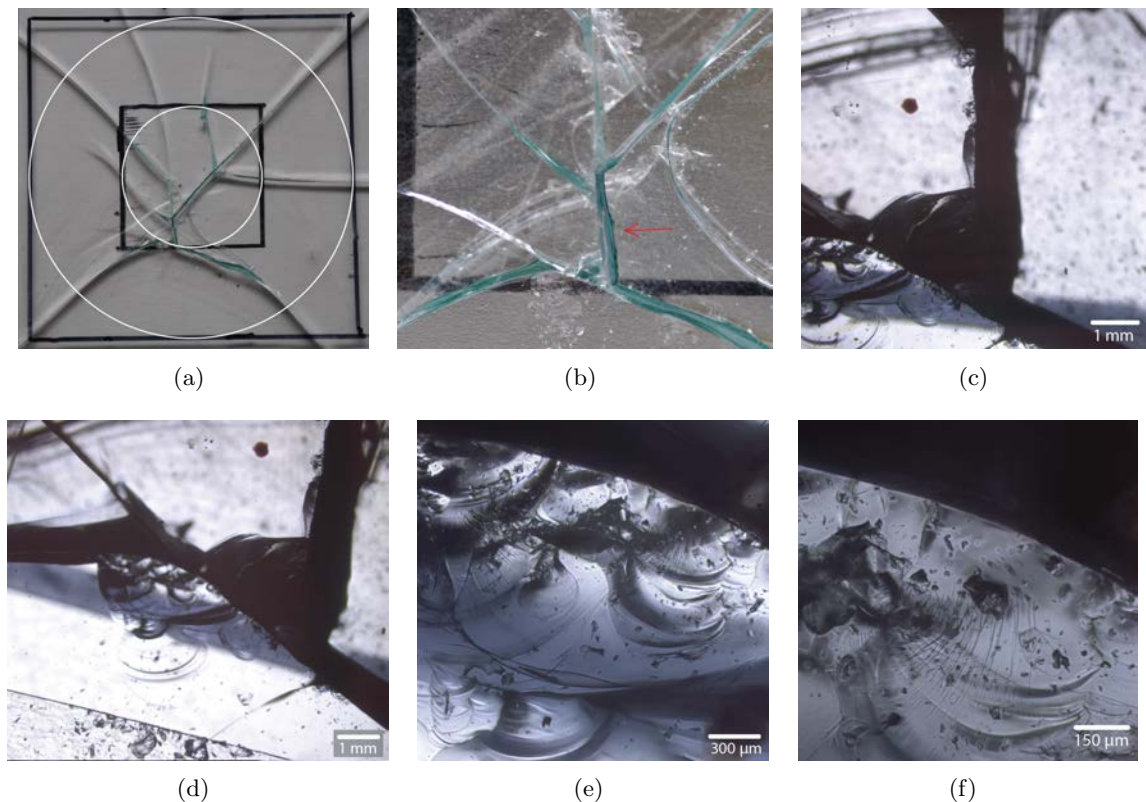


Figure 5.17: Fractographic analysis of TT3

TT3: In the first magnification of the likely origin crack nothing much is seen. However looking at the left bottom, a lot of fracture marks are seen, see Figure 5.17c and 5.17d. Quinn states that the greater the failure stress at fracture, the higher the stored elastic energy and the richer the fracture marks [5]. Therefore it is concluded that on this line the actual origin point lies. Apparently the branching of the cracks was interpreted wrongly. In Figure 5.17e several marks seem to confirm this, such as beach and hackle marks. Where beach marks represent stable crack growth and hackle marks unstable growth. Which of these marks actually started the first cannot be deduced from this image, but it does show multiple cracking processes followed up on one another. The last figure zooms in on one of them.

TT10: This specimen gave quite a straightforward analysis. At the origin crack a clear beach mark can be seen in Figure 5.18c. In Figure 5.18d stable crack growth is observed. Interestingly, at the arrow a point where unstable crack growth commences is marked. Figure 5.18e zooms in at a magnification at the centre of the beach mark where the cracking process started. Analysis of the fracture surface will have to conclude whether it is the actual point of origin.

TT40: In Figure 5.19c, made with reflected light instead of transmitted light, the crack branching is clearly seen which suggests this is the origin crack. In transmitted light in Figure 5.19d no starting point can be marked. There are two explanations for this. Either the light settings are not installed correctly for this specimen or the fracture surface is orientated 90 degrees to the direction of observation and no fracture markings were formed in this view. Looking at Figure 5.19e twist hackle marks are observed at the sides, both with their propagation direction (marked by arrows) towards the origin crack. This is special because mostly crack propagation runs away from the origin point. Whether this is a coincidence or the origin point is actually located somewhere else cannot be concluded from this analysis alone.

TT6: The location of the fracture origin is clearly visible in this specimen. However, under

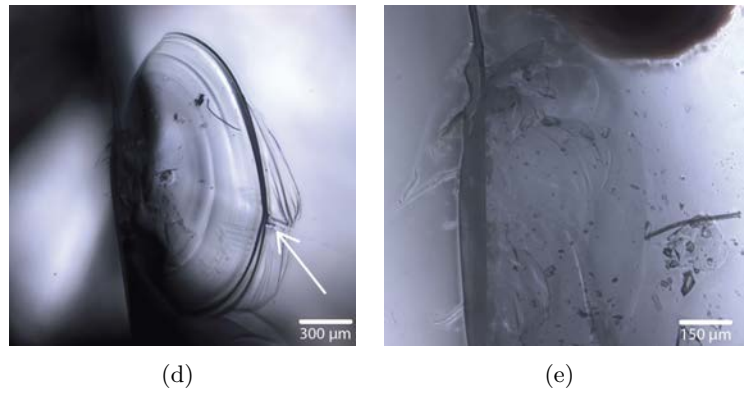
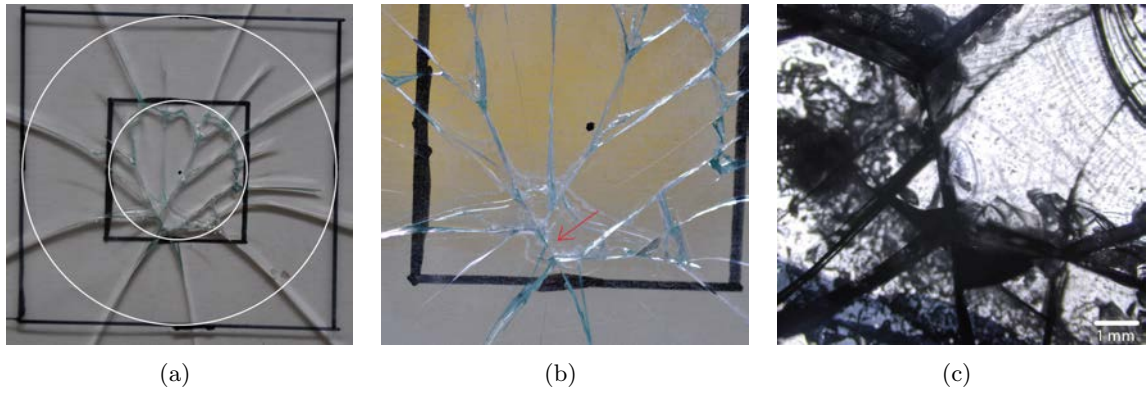


Figure 5.18: Fractographic analysis of TT10

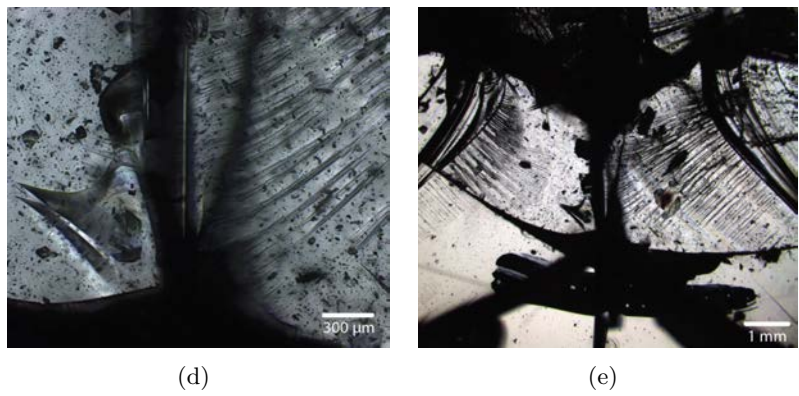
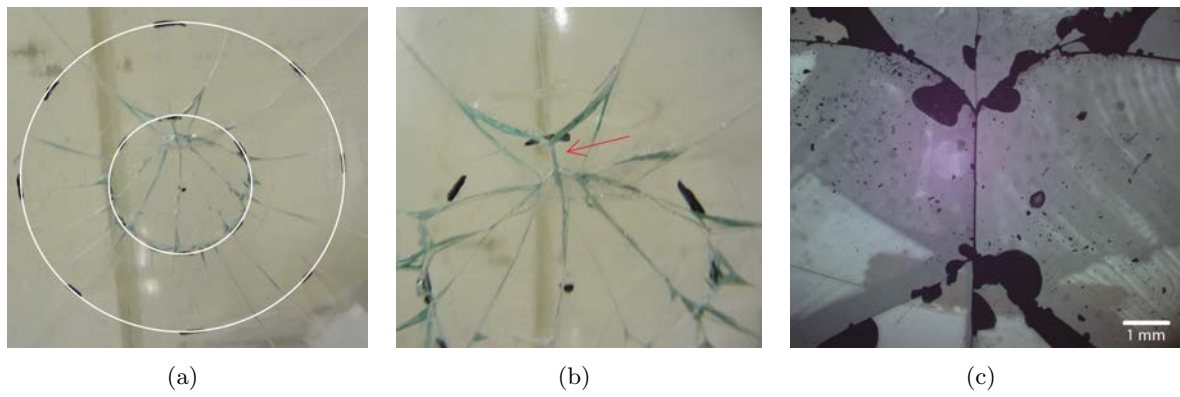


Figure 5.19: Fractographic analysis of TT40

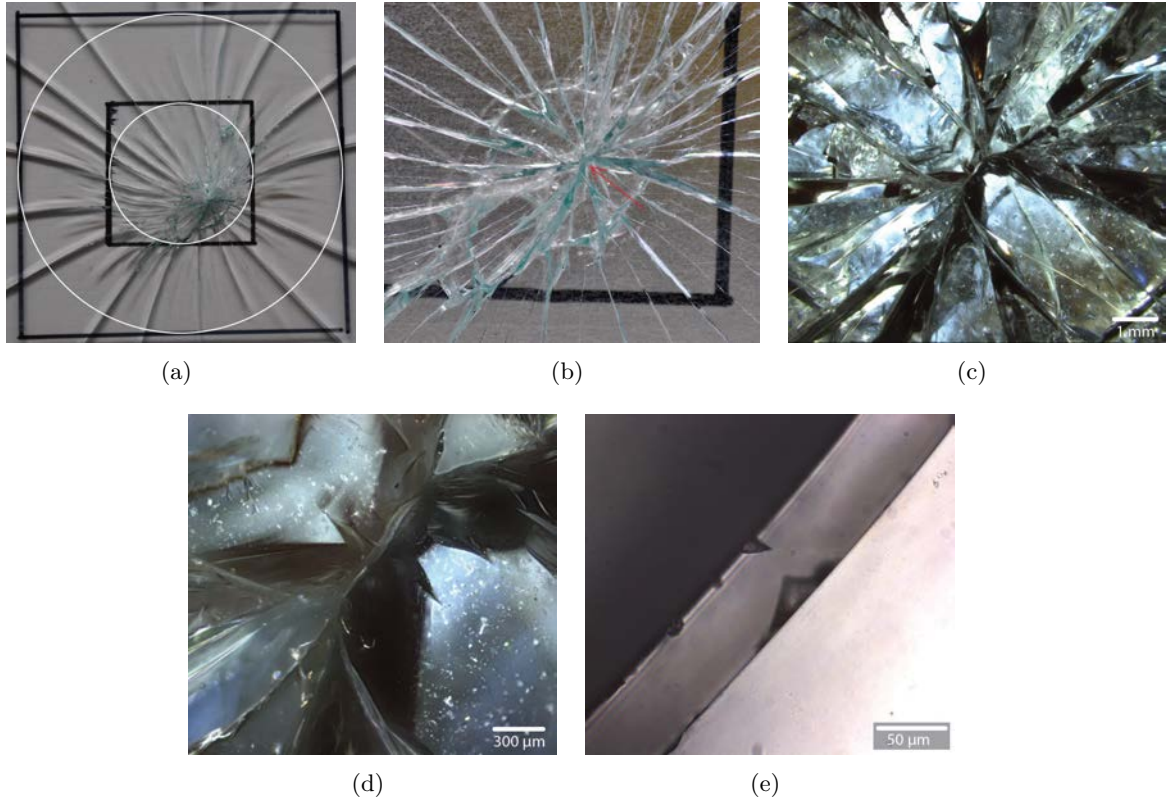


Figure 5.20: Fractographic analysis of TT6

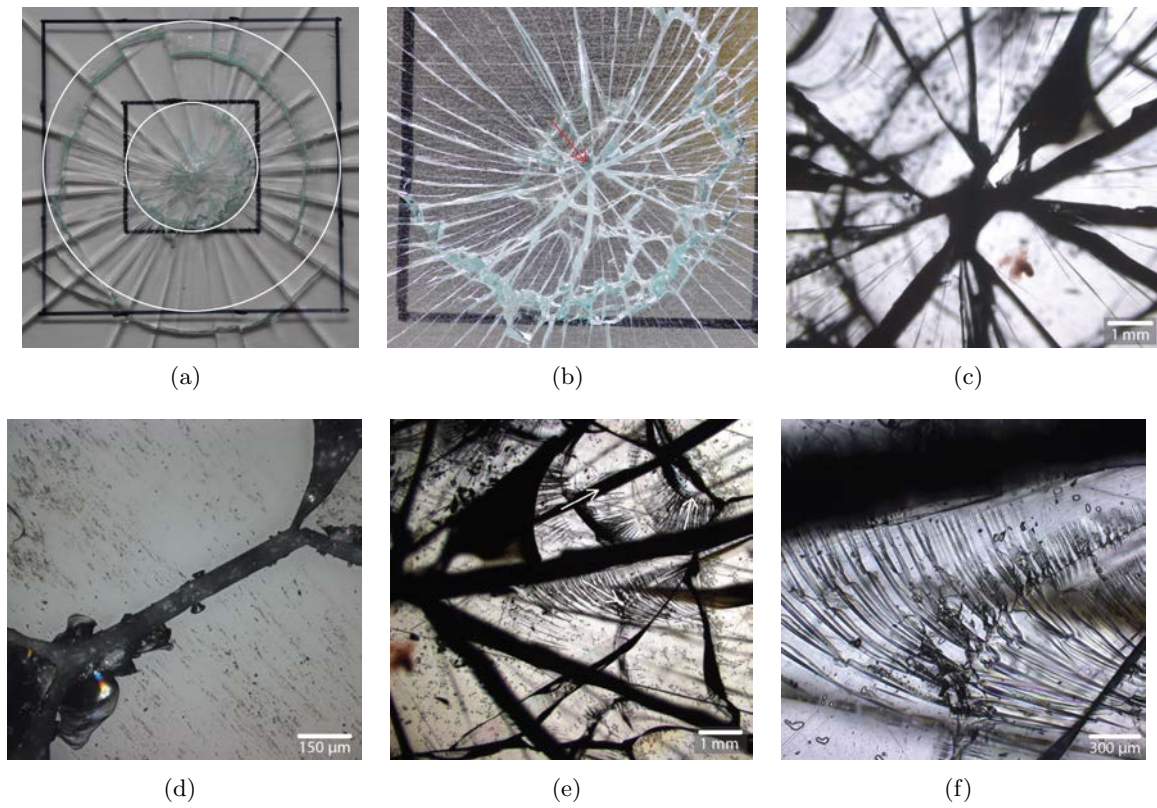


Figure 5.21: Fractographic analysis of TT8

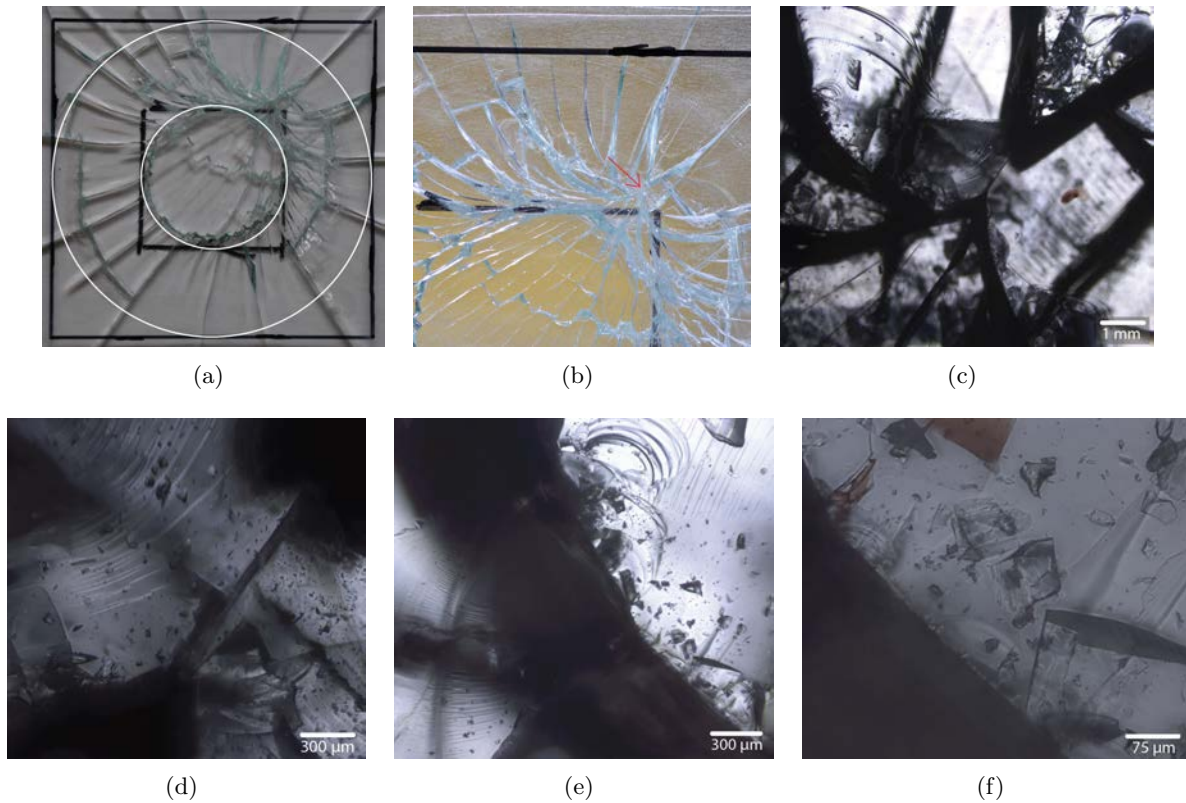


Figure 5.22: Fractographic analysis of TT16

the microscope so much light was coming through a gap at the crack of interest that the image was too bright. Therefore Figure 5.20c was taken in crossed polarised light. Despite giving a spectacular picture, in this light it is harder to distinguish the fracture marks, so it is less suitable to draw conclusions about the fracture pattern. On a sidenote, crossed polarised light can be useful in determining the composition of a material's components.

TT8: In this specimen the transmitted light was blocked at the crack of interest. Therefore Figure 5.21d was taken with reflected light only. Especially to the left, crack growth marks are observed. The origin of fracture might be found there. Figure 5.21e is taken to the right from the origin crack (the red dot can be used as a reference). Here twist hackle is captured that gives an indication of the ongoing crack propagation

TT16: The origin crack seemed to have been found but under the microscope hardly any fracture marks were observed, nor at a larger magnification in Figure 5.22d. Looking back at Figure 5.22c a lot more marks are observed to the left, which are shown at a larger magnification in Figure 5.22e. Interestingly, stable crack growth is seen in the form of beach marks but they seem to be taken over by unstable crack growth in the form of hackle. At the centre of this hackle, next to the crack more stable crack growth marks were captured in Figure 5.22f. The fracture may have originated there instead. Fracture surface analysis would have to conclude this.

Firstly, it should be stressed that these are all 2D images of features that are located at different depths in the glass. While interpreting them this should be borne in mind to make sure the right conclusions are drawn. This can be aided by making photographs of just the glass surface before building the 3D images, so that it can be checked whether a certain feature is at the surface or inside the glass.

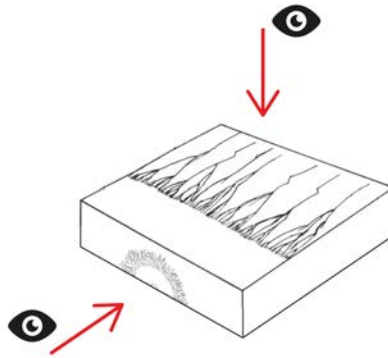


Figure 5.23: Different angles of observation

It is the opinion of the author that this technique works best in combination with fracture surface analysis, but definitely is a valuable addition. For TT3 and TT16 it seems the wrong origin crack was concluded from the visual fracture pattern analysis. In a fracture surface analysis this would have been discovered by following the Wallner lines at the fracture surface to the right origin point. However, by looking at the fracture pattern by transmitted light microscopy this can be seen in one glance and immediately gives a direction at which point to look in the fracture surface analysis. Therefore, these Z-axis scanned images can be used as an overview to contemplate during the fracture surface analysis. For example for TT10 a very clear spot is marked where the fracture origin can probably be found. When having found the fracture origin at the fracture surface the researcher then can use the Z-built image to gain an understanding of the rest of the cracking process. This process cannot be deduced in one view by examining only the fracture surface. As is seen in the case of TT8 where twist hackle marks the crack propagation at several location in the glass in one image.

This technique on its own does not give the final conclusion or even the desired images as was the case for TT40 and TT6. It turns out it depends on the position of the shards in the glass whether enough or too much light is let through and a good image can be made. Although it might be possible to improve this by exploring all settings of the polarised microscope.

It should be stressed that fracture pattern analysis by microscope is suggested as an intermediate step and not as a substitute of fracture surface analysis by microscope. The strength lies in the combination of these methods. By changing the angle of observation 90 degrees, fracture marks are revealed that would otherwise have been overlooked. This is illustrated in Figure 5.23. It depends on the angle of the fracture surface in the plate and to the shape of the fracture marks which of them were visible in this analysis and which will only become visible when the fracture surface analysis is performed. For example, it is possible that the fracture surface in TT40 is orientated parallel to the direction of observation. It could be the case that TT40 fractured due to a line defect creating two-dimensional fracture markings. Furthermore, for example TT10 might have fractured due to a spherical flaw creating three-dimensional fracture markings which could be clearly seen from this point of view. Further research will have to point this out.

5.3.2.3 Microscopic analysis - quantitative

Looking back at the images made with the Leica microscope, another thing that can be noted is that the higher the stress the more fracture marks seem to have developed. In this paragraph, it is explored if a relationship can be found. In Table 5.10 the marks are counted and described per specimen. A composition of several overlapping marks is counted as one. These values

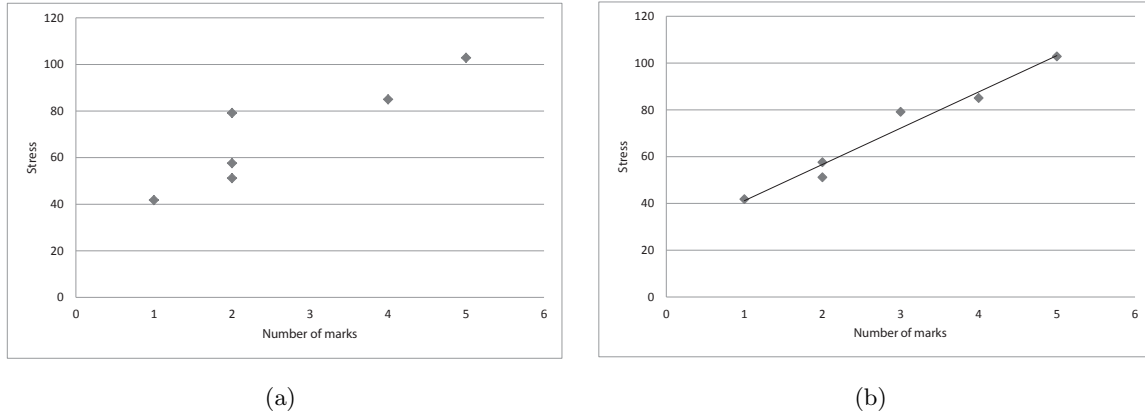


Figure 5.24: Stress plotted versus number of fracture marks

are plotted in a graph in Figure 5.24a. In this graph, TT6 forms an outlier. However, the microscopic image of TT6 was quite unclear. It is therefore quite possible TT6 has 3 markings, as is assumed in Figure 5.24b. On the other hand, it should be considered to omit TT6 from the results entirely. Either way, a tentative line can be drawn through the points.

The fractographic analysis with the Leice plates focused on the origin of fracture of the plates,

Table 5.10: Number of fracture marks per plate

Plate	N	Type	σ [MPa]
TT3	1	Composition	41.79
TT40	2	Hackle marks	51.16
TT10	2	1 beach and 1 hackle mark	57.59
TT6	2	Slight hackle marks	79.14
TT16	4	3 hackle marks, 1 composition	85.02
TT8	5	1 origin mark, 4 hackle marks	102.83

so not all marks were captured. Therefore, a second analysis was performed with a stereo microscope. The results are presented in Table 5.11 and Figure 5.25. TT6 was omitted from the results because it seems that the fracture surfaces are in such an angle in the plane of the glass that the fracture marks cannot be observed by the attempted methods. Again straight

Table 5.11: Number of fracture marks observed with stereo microscope

Plate	N	N Hackle	σ [MPa]
TT3	5	3	41.79
TT40	6	5	51.16
TT10	5	4	57.59
TT16	8	6	85.02
TT8	10	10	102.83

lines can be drawn through the points. It is recognised that these are not enough plates to draw the conclusion of a relationship between the number of marks and the failure stress, but this could be an interesting topic of a future research. Also the size of the marks could be explored. Another interesting notion is that TT8 showed only hackle marks. This could indicate barely any stable crack growth occurred.

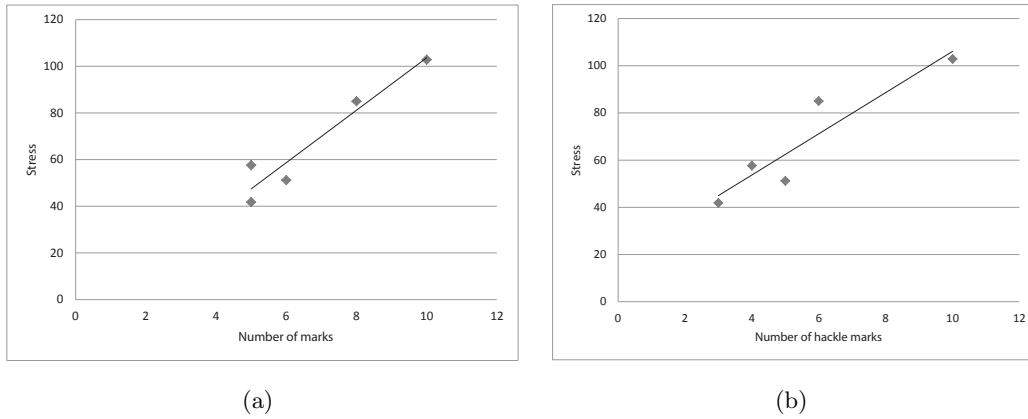


Figure 5.25: (a) New plot stress versus number of fracture marks (b) Stress versus number of hackle marks

5.3.3 Conclusions

A transmitted light microscopy analysis combined with Z-axis scanning software gives the glass researcher an overview of all fracture markings throughout the depth of the glass plate in one image. In combination with the fracture surface analysis this image can be used as a map which guides the researcher in their search of the fracture origin. More importantly, it reveals fracture markings that give new insights into the crack propagation and the local failure process that are overlooked in traditional glass fractography.

Therefore, transmitted light microscopy together with Z-axis scanning software is a valuable addition to glass fractography.

Application in Practice

6.1 Introduction

The strength of a structure is assessed by the formula:

$$\gamma_f S \leq \frac{R}{\gamma_m} \quad (6.1)$$

In which S is the solitude, R the resistance, γ_f the load factor, taking into account insecurities in the load and γ_m is the material factor incorporating impurities of the material that affect its properties. The material factor is quite large for glass. This is understood looking back at Section 2.4 in which the uncertainty of defects in glass was elaborated and their effect on the strength. For that reason material factors of 5 to 7 are used. This is unfortunate, because compared to steel and concrete, which have material factors between 1 and 1.5 respectively, a lot of material goes to waste. It is therefore desirable more insight is gained on which defects cause a lower strength. A similar system as timber might be applied, where the pieces with few defects are sorted into higher strength classes, gaining more confidence about the material factor. The importance of getting a more secure material factor will be shown by two practical cases: a portal and a window pane. The former was chosen because for this case the safety factors are highest, so the difference has the most impact. The latter was chosen because for this case the surface and volume strength of glass are most important. These were tested in the RoR test, whereas the edge strength (which is also important for the portal) was not. Both cases will be calculated twice. The first time according to the current standards and the second time according to an estimation of what the standards might be when it is possible to determine the strength of glass more accurately.

6.2 Safety philosophy

The strength of glass is very uncertain. When annealed float silica lime soda glass comes from the manufacturer, it is unknown if it has a strength of 20 MPa or 150 MPa. Therefore the lowest known strength value of 20 MPa is chosen for structural purposes. On top of that, a safety factor as high as 5 to 7 is often applied. This follows from the uncertainty, yet is a bit exorbitant, because already the lowest strength possible is applied. Fortunately, it can be justified to apply a lower safety factor by pursuing a proper design philosophy.

For the Ultimate Limit State, it is important to note that glass is a brittle material. This means that when it fails, this happens suddenly and without warning. Warning behaviour is important to give people a chance to get out of a building before it collapses. For glass, this can be achieved by:

- Applying steel reinforcement which adds ductile behaviour, as is described in [9].
- Laminating glass and adding redundancy. When a glass pane breaks in a laminated component, the fractured glass will stay in place because it is glued to other glass panes. Redundancy is added by placing sacrificial layers at the sides, which are nonbearing.

For the case of the portal the second option is chosen and therefore a safety factor of 4 is applied. For the case of the window pane a safety factor of 1 is applied [45], because window panes are not part of the main bearing structure.

When more certainty in the strength of glass is acquired, a higher strength can be assumed and the safety factor can be lowered. By working together with glass manufacturers, volume flaws caused by the production process can be detected, documented and even reduced. Surface and edge flaws are mostly caused after the production process. Again, detection and documentation brings more certainty. Moreover, protection can prevent flaws and repair can reduce them.

For the improved case, a strength of 50 MPa is assumed. The author feels like this is a fair assumption. Strength values as high as 150 MPa have been recorded, so it seems 50 MPa should be possible in the near future. When the flaws in a glass plate are inspected, a lot more certainty is gained. The safety factor is guessed to be 2 for the portal. Again, the safety factor for the window pane is 1.

That means that for Case I version A a strength of $20/4 = 5$ MPa is assumed and for Case I version B a strength of $50/2 = 25$ MPa. For Case II version A a strength of 20 MPa is applied and for Case II version B 50 MPa.

6.3 Case I

6.3.1 Portal design

The below sizes have been arbitrarily chosen. The portal consists of columns of 3 meters high and beams that span 6 meters long, see Figure 6.1

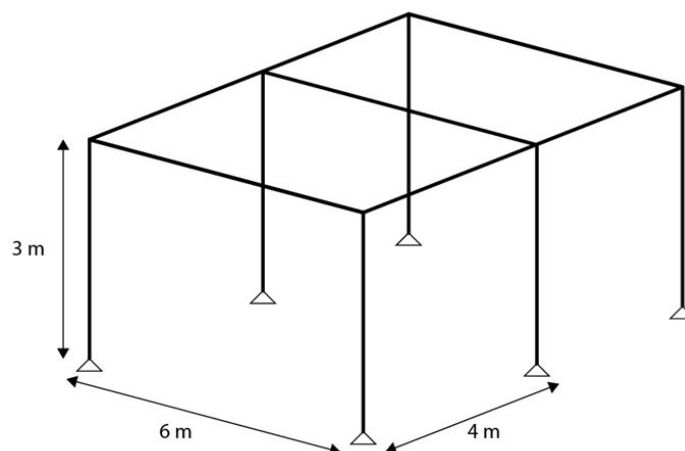


Figure 6.1: Schematic of the portal

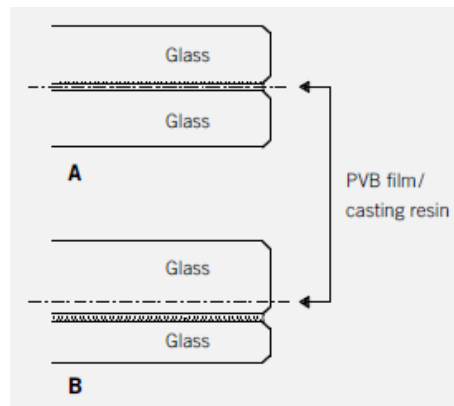


Figure 6.2: (a) In a symmetric cross-section the neutral axis runs through the glue line (b) In an asymmetric cross-section it goes through the glass [1]

The portal is part of a structure with a roof that spans 4 meters. The roof is supported at the sides as well. Since the main purpose of this case is to show differences for the construction, it is assumed that the climatic design is of no importance.

As type of glass annealed soda-lime glass is chosen, because that is the type of glass that was tested in the experiments. It should be noted that often in practice, heat strengthened is opted because of its additional strength. Tempered glass is less desirable as, despite the glue, the glass fragments fall down when fracture occurs.

In this case only the roof, beam and column are designed and calculated. However, it should be stressed that a proper design and calculation of the connections between those elements are crucial in achieving a successful glass structure. Nevertheless, for assessing the materials savings they are not necessary and therefore lay out of the scope of this thesis.

6.3.1.1 Beam design

A common and sound way of constructing with glass is by laminating glass plates. This method yields some advantages:

- The thicker a glass element, the more residual stresses are introduced in the material which affect the performance. By laminating thinner glass plates, the required thickness is achieved without having to deal with unwanted residual stresses.
- When one of the plates breaks, the failure will be contained in that plate because it is separated from the others by the glue layer. A one piece beam would fail entirely.
- Additionally, the broken glass will stick to the glue layer, instead of falling down where it could lead to injuries.

Glass manufacturers retain certain standard thicknesses for float glass. The most common for structural glass are: 8, 10, 12 and 15 mm. These can be glued together to make various compositions. It should be made sure that the neutral axis of the beam goes through a glass plate rather than through a glue line, see Figure 6.2. Also, to increase the redundancy of the structure, sacrificial layers will be applied. These can be thinner than the laminated plates, such as 4 mm. These layers should protrude a little to protect the beam properly [1], see Figure 6.3.

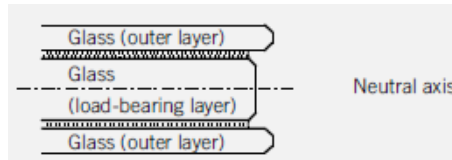


Figure 6.3: The outer sacrificial layers protrude past the load-bearing layer protecting it sufficiently [1]

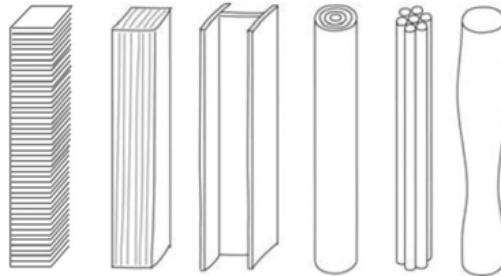


Figure 6.4: Ways to build a glass column [46]

6.3.1.2 Roof design

Since climatic design is not considered, single glazing can be used. The roof will be composed of one or more glass plates laminated together by PVB foil. Depending on the calculations more or thicker glass will be used. Additionally, a sacrificial layer will be applied at the top of the roof. It is assumed that it is highly unlikely that something will break the roof from below. For instance, a high vehicle would sooner hit a beam than hit the roof. The top layer should be thin as to not increase the weight too much. For example, 4 mm. This layer will be bonded to the roof by silicon, which does not bond as well as PVB. Thereby, it is easier to replace the layer when it is broken.

6.3.1.3 Column design

There are several ways to compose a glass column. A schematic of the options is depicted in Figure 6.4. The first two options are produced by stacking glass plates. Aesthetically, this is not a desirable option, because the side of glass is not very transparent. Also it is not a material efficient solution. The third option is making a profile of glass plates, which works well as long as the load is properly introduced over the entire cross-section. The last three options are respectively: layered cylinder, bundled column and poured in formwork. The latter does not work well because of the bubbles and residual stresses that are created when making such a thick shape with glass. The other two are good options. However, since flat glass was tested in this research a profile of glass plates seemed the most suitable. Then arises the question of which profile to choose. In her graduation work, Ouwerkerk considered five possible profiles [47], see Figure 6.5. The difficulty with composed profiles is how to compensate for misalignments of the glass plate. Configuration 1 and 2 can be problematic for this because if one of the vertical plates is wider than the others it will be hard to close the cross-section. This is easier to incorporate in the remaining configurations. Configuration 4 is chosen as for this profile only 1 side of all the plates needs to be aligned. To protect the column, a barrier will be placed around it so that sacrificial layers are not necessary. The barrier can be merged in the interior in the form of a bench or a lighting object.

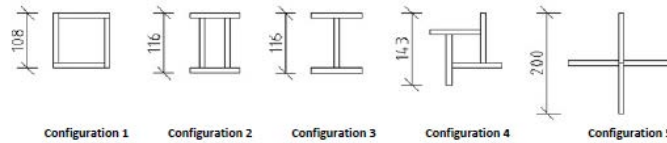


Figure 6.5: Possible configurations for a column made of glass plates [47]

6.3.1.4 Loads and factors

The portal will carry permanent and incidental loads. The permanent load depends on the dimensions of the beam and the dimensions of the roof. The weight of the PVB foil will be neglected. The load factors are material independent and were taken from the Eurocode.

Table 6.1: Loads

Category	Description	Value
pG1	Permanent Weight roof	Density*thickness = ? kN/m ²
pQ1	Variable Roof (according to EC)	1 kN/m ²
pQ2	Snow load Snow (according to EC)	0.8*0.7*1 = 0.56 kN/m ²

Combining the loads allows for making some other loads zero, because when it snows the variable load is not likely to occur. See Table 6.2. Combination 2 will be governing when the weight roof

Table 6.2: Load combinations

Description	Combination 1	Combination 2	Combination 3
Load case 1 Permanent	1.35	1.2	1.2
Load case 2 Variable	0	1.5	0
Load case 3 Snow load	0	0	1.5

is smaller than 10 kN/m². Only the results of the governing combination will be considered. So to calculate the load the following formula should be used:

$$p = 1.2q_{G1} + 1.5q_{Q1} \quad (6.2)$$

For deflections the load factors are 1.0.

6.3.2 Calculation portal version A

In practice, it is preferable to find the optimal combination of the number of plates and one glass thickness. However, here only the total glass thickness is taken. This was done so that the two versions of the case have similar unity checks in stress, which makes them more suitable for comparison. So in reality, it would be insufficient to use different thicknesses to get to the total applied thickness, but as the purpose of this case is to show the general improvement, it is now neglected.

6.3.2.1 Roof

The bending stress in the middle of a simply supported rectangular panel is given by the formula:

$$\sigma_{center} = \beta * p * \frac{a^2}{t^2} \quad (6.3)$$

b/a	1.0	1.2	1.5	2.0	3.0	4.0	5.0
β	0.270	0.360	0.474	0.602	0.711	0.740	0.748
α	0.047	0.065	0.089	0.116	0.140	0.147	0.149

Linear interpolation can be adopted to determine the α and β should the b/a value be other than listed.

Figure 6.6: Linear interpolation can be adopted to determine the α and β should the b/a value be other than listed

in which:

p is the uniform load

a is the length of the short side of the rectangle $\rightarrow a = 3m$

t is the glass thickness.

β is a parameter determined based on the ratio of longer side to the shorter side (b/a, where b is the longer side) as shown in Figure 6.6. By linear interpolation: $b/a = 4/3 = 1.33 \rightarrow \beta = 0.414$

The permanent part of the uniform load is dependent on the thickness, so an iterative calculation was necessary. This resulted in a final thickness of 50 mm and a sacrificial layer of 4 mm.

$$p = 1.2 * ((50 + 4) * 0.025) + 1.5 * 1 = 3.18 \frac{kN}{m^2} = 0.00318 \frac{N}{mm^2} \quad (6.4a)$$

$$\sigma_b = 0.414 * 0.00312 * \frac{3000^2}{50^2} = 4.66 \frac{N}{mm^2} \quad (6.4b)$$

$$U.C. : \frac{4.66}{5} = 0.93 < 1 \rightarrow OK \quad (6.4c)$$

The maximum deflection of the middle of the glass pane is given by the formula:

$$\delta = \alpha * p * \frac{a^4}{Et^3} \quad (6.5)$$

in which

δ is the deflection

α is a parameter that is determined using Figure 6.6. For $b/a = 1.33 \rightarrow \alpha = 0.076$

E is the elastic modulus of glass, $E = 73,000 \frac{N}{mm^2}$

This yields:

$$\delta = 0.076 * .00312 * \frac{3000^4}{730000 * 50^3} = 1.58mm \quad (6.6a)$$

$$\delta_{max} = L/200 = 4000/200 = 20mm \quad (6.6b)$$

$$U.C. : 1,58/20 = 0,08 < 1 \rightarrow OK \quad (6.6c)$$

The unity check for the deflection is much lower than that for the stress. This can be explained by the high safety factor, which is only applied to the strength not to the deflection, since it is a service criterion not a safety criterion.

6.3.2.2 Beam

Again, an iterative calculation was performed. This resulted in a beam with thickness 98 mm and a height of 950 mm. Two sacrificial layers of 4 mm are added, bringing the total thickness to 106 mm. Only the final calculation is shown. First the loads were determined: The same load combinations as in Table 6.2 apply, so Load combination 2 is once more governing, so that:

$$q = 1.2 * qG1 + 1.5 * qQ1 = 15.501 \frac{kN}{m} \quad (6.7)$$

Table 6.3: Beam loads

Category	Description	Value
qG1 Permanent	Weight roof	$25*0.106*0.95+1.35*4 = 7.9175 \text{ kN/m}^2$
qQ1 Variable	Roof (according to EC)	$1*4 = 4 \text{ kN/m}^2$
qQ2 Snow load	Snow (according to EC)	$0.8*0.7*1*4 = 2.24 \text{ kN/m}^2$

First the unity check for the stress is performed.

$$M = \frac{1}{8}qL^2 = 69.7545 \text{ kNm} = 69,754,500 \text{ Nmm} \quad (6.8a)$$

$$W = \frac{1}{6}bh^2 = 14,740,833 \text{ mm}^3 \quad (6.8b)$$

$$\sigma = M/W = 4.73 \frac{\text{N}}{\text{mm}^2} \quad (6.8c)$$

$$U.C. : \frac{4.73}{5} = 0.95 \rightarrow OK \quad (6.8d)$$

Finally, the deflection unity check easily suffices.

$$w_{max} = L/250 = 24 \text{ mm} \quad (6.9a)$$

$$I = \frac{1}{12}bh^3 = 7.002 * 10^9 \text{ mm}^4 \quad (6.9b)$$

$$w = \frac{5 * q * L^4}{384 * E * I} = 0.393 \text{ mm} \quad (6.9c)$$

$$U.C. : \frac{0.393}{24} = 0.016 \rightarrow OK \quad (6.9d)$$

6.3.2.3 Column

The strength of the column is assessed by the Euler strength.

$$F_{euler} = \frac{\pi EI}{l_{buc}^2} \quad (6.10)$$

It should be noted that the Euler equation overestimates the strength. In reality, a more safe approach should be applied, but for now the equation is utilised to make the comparison.

It is assumed the column is hinged at the top and the bottom. The column will have to be able to carry the following maximum load, according to Load combination 2: The permanent weight

Table 6.4: Column loads

Element	Load [kN]
Beam, perm	18.126
Roof, perm	38.88
Roof, variable	36
<i>Total</i>	93.006

of the column is neglected, therefore there is no need of an iterative calculation. To carry this load the column profile should have a moment of inertia of:

$$I = \frac{F_{euler} * l_{buc}^2}{\pi EI} = 1,161,799 \text{ mm}^4 \quad (6.11)$$

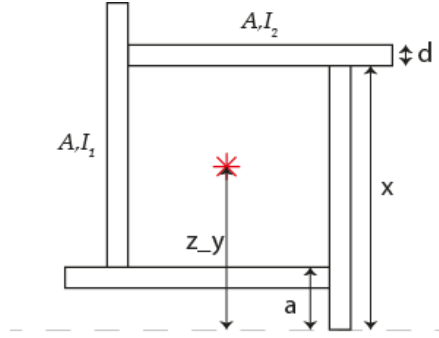


Figure 6.7: Profile configuration 4

The moment of inertia for profile configuration 4 is calculated below, see Figure 6.7

$$I_y = \sum I_i = A_i z_i^2 (I_1 + A) \left(\frac{\sum A_i z_i}{\sum A_i} \right) = \frac{A(\frac{1}{2}x + a) + A(x + \frac{1}{2}d) + A(a - \frac{1}{2}d) + A(\frac{1}{2}x)}{4A} = \frac{1}{2}x + \frac{1}{2}a \quad (6.12)$$

In which:

$$z_y = \frac{1}{2}x + \frac{1}{2}a \quad (6.13a)$$

$$I_1 = \frac{1}{12}dx^3 \quad (6.13b)$$

$$I_2 = \frac{1}{12}xd^3 \quad (6.13c)$$

To make a proper comparison value a and d are set and x is the variable. This resulted in:

$$x = 55mm \quad (6.14a)$$

$$d = 12mm \quad (6.14b)$$

$$a = 10mm \quad (6.14c)$$

$$I_y = 1,453,760mm^4 \quad (6.14d)$$

$$UC = \frac{1161799}{1453760} = 0.80 \rightarrow OK \quad (6.14e)$$

6.3.3 Calculation portal version B

As was stated, the calculation is performed again, only now a safety factor of 2 is applied. The same load combinations and variable loads apply. Only the permanent loads will be different. The calculations are not repeated in detail, only the unity checks are shown.

6.3.3.1 Roof

The roof has a total thickness of $19 + 4 = 33mm$. The thickness of 19 mm can only be built up by using different thicknesses of glass plates. This inconvenience is neglected because it yields similar unity checks as version A, so that a valid comparison can be made.

$$UC_{stress} = \frac{22.63}{25} = 0.91 \rightarrow OK \quad (6.15a)$$

$$UC_{deflection} = \frac{19.35}{20} = 0.96 \rightarrow OK \quad (6.15b)$$

The unity check for the deflection is now even larger than the unity check for the stress. This is quite an interesting notion because it means that for the roof the reduction of material by an increase of the strength stops here, due to the limits of glass' stiffness. A further reduction in glass could be reached by increasing the stiffness with reinforcing steel or fibers.

6.3.3.2 Beam

The beam is made with a total thickness of $19 + 2 * 4 = 27mm$ and a height of 750 mm.

$$UC_{stress} = \frac{23.67}{25} = 0.95 \rightarrow OK \quad (6.16a)$$

$$UC_{deflection} = \frac{2.36}{24} = 0.10 \rightarrow OK \quad (6.16b)$$

For the beam a lot more material reduction can still be achieved by increasing the strength.

6.3.3.3 Column

The following parameters are applied:

$$x = 46mm \quad (6.17a)$$

$$d = 12mm \quad (6.17b)$$

$$a = 10mm \quad (6.17c)$$

$$I_y = 871,424mm^4 \quad (6.17d)$$

$$UC = \frac{702093}{871424} = 0.81 \rightarrow OK \quad (6.17e)$$

6.4 Case II

In this case, a window pane is calculated. The material savings achieved in this case are expected to be lower than for the portal because no improvement in the safety factor is made, since it is set at 1. However, it is a representative case for this research because for a window pane only surface and volume flaws are of importance. For the portal, edge flaws can be critical too, but those were not explored during the experiments.

6.4.1 Window pane design

The Faculty of Civil Engineering building at the TU Delft campus is chosen as a case. See Figure 6.8 for its dimensions and orientation. The window is at the top floor of the south west façade. The dimensions of the window pane are shown in Figure. The window mainly has to resist a wind load which is modelled as a line load.

6.4.2 Calculation window pane version A

The wind load on the window can be calculated by the following formula:

$$q_{wind} = c_s c_d c_f q_p(z_e) H \quad (6.18)$$

In which q_{wind} is the line load on the window, $c_s c_d$ is a structural factor, c_f is the force coefficient for the structure, $q_p(z_e)$ is the peak velocity pressure at height (z_e) and H is the height of the

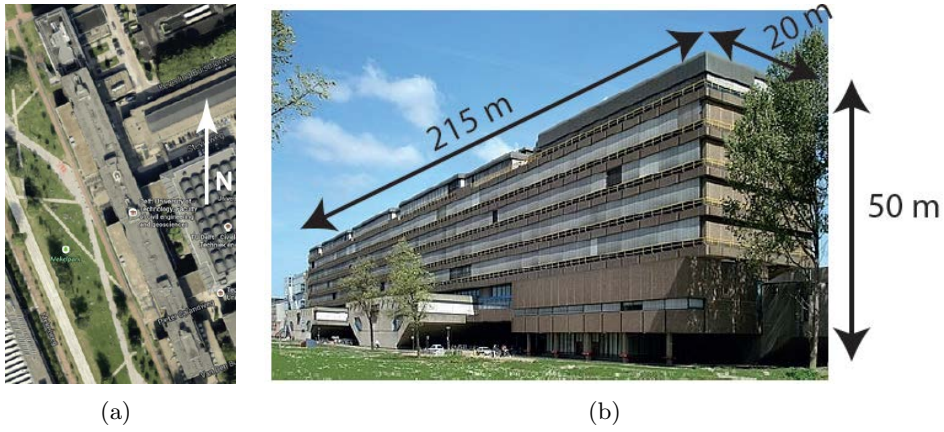


Figure 6.8: The orientation and dimensions of the Faculty of Civil Engineering

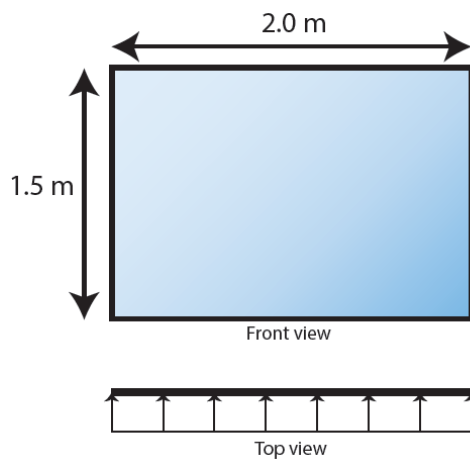


Figure 6.9: The dimensions of the window pane

window which is $1.5m$. $c_s c_d$ can be taken as 1, because the faculty falls under the category of a regular, low-rise building. The factor c_f depends on the value of:

$$e = 2h = 2 * 50 = 100m \quad (6.19)$$

In which h is the height of the building. It depends on the value of e which wind zone can be assumed for the building, see Figure 6.10 In this case:

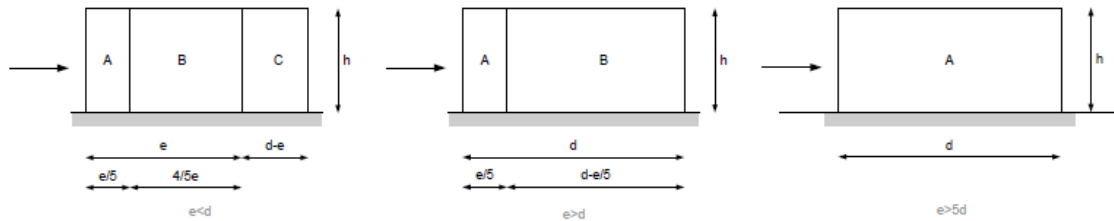


Figure 6.10: Wind zones for different values of e

$$e > 5d = 5 * 20 = 100m \quad (6.20)$$

So wind zone A applies. Table 6.5 shows which c_f should be taken for its corresponding value of $h/d = 100/20 = 5$ and wind zone. In this case $c_f = -1.2$ which can be taken as 1.2. Lastly,

Table 6.5: Value of c_f

Façades	c_f for wind zone				
	A	B	C	D	E
h/d					
5	-1.2	-0.8	-0.5	0.8	-0.7
1	-1.2	-0.8	-0.5	0.8	-0.5
≤ 0.25	-1.2	-0.8	-0.5	0.7	-0.3

q_p at a height z_e of 50 m is $1.21 \frac{kN}{m^2}$ in urban surroundings in Area II, which is the area Delft is located in. So the wind load is:

$$q_{wind} = 1 * 1.2 * 1.21 * 1.5 = 2.178 \frac{kN}{m} \quad (6.21)$$

The moment the windowpane has to take is:

$$M = \frac{1}{8}QB^2 = 1.089kNm \quad (6.22)$$

The area resistance of the glass is:

$$W = \frac{1}{6}Ht^2 \quad (6.23)$$

In which t is the thickness of the glass. The stress the glass has to withstand is:

$$\sigma = \frac{M}{W} \quad (6.24)$$

The strength of non-prestressed glass is determined by [46]:

$$f_{mt;u;d} = \frac{k_a k_e k_{mod} k_{sp} f_{g;k}}{\gamma_{m;A}} \quad (6.25)$$

In which: k_a is the area effect. In this situation: $k_a = 1$, because the calculation is linear. k_e is the factor for the edge quality. For non-prestressed glass: $k_e = 0.8$. k_{mod} is the modification factor for the load duration. For wind load: $k_{mod} = 1$. k_{sp} is the factor for the surface structure of the windowpane. For float glass: $k_{sp} = 1$. $f_{g;k} = 20MPa$. $\gamma_{m;A}$ is the material factor. For situations where wind load is the main variable load, $\gamma_{m;A} = 1.6$. This yields:

$$f_{mt;u;d} = \frac{0.8 * 20}{1.6} = 10MPa \quad (6.26)$$

An iterative calculation shows that the needed thickness is 22 mm. For the calculations $t = 21.7mm$ was applied, because glass is always produced a little bit thinner. This results in:

$$W = 0.00012m^3 \quad (6.27a)$$

$$\sigma = 9.25MPa \quad (6.27b)$$

$$U.C. = 0.93 \quad (6.27c)$$

6.4.2.1 Biaxial bending

The same equations as for the roof in Case I were applied. So for the biaxial bending stress:

$$\sigma_{center} = \beta * p * \frac{a^2}{t^2} \quad (6.28a)$$

$$\sigma_{center} = 1.33 * 1.452 * \frac{1.5^2}{21.7} = 2.88 \frac{N}{mm^2} \quad (6.28b)$$

$$U.C. = \frac{2.88}{10} = 0.29 \quad (6.28c)$$

And for the biaxial deflection:

$$\delta = 0.076 * 1.452 * \frac{1500^4}{730000 * 13.7^3} = 0.75mm \quad (6.29a)$$

$$U.C. = \frac{0.75}{6} = 0.12 \quad (6.29b)$$

6.4.2.2 Double glazing

However, 22 mm is not a common thickness made for float glass. It is possible but more expensive. It is cheaper to opt for double glazing. The set-up could be a single outer pane and a laminated inner pane. The pressure is distributed on these panes by ratio of stiffness. For a short wind load the cooperation is 100%. The single glazing calculation gave an indication of the amount of glass needed. If the outer pane is 6 mm thick and the inner pane is laminated glass of 2 times 8 mm, the total thickness is 22 mm, so that could be a good guess. The ratio of stiffness is:

$$\alpha_{out} = \frac{5.8^3}{5.8^3 + (7.7 + 7.7)^3} = 5\% \quad (6.30a)$$

$$\alpha_{in} = \frac{(7.7 + 7.7)^3}{5.8^3 + (7.7 + 7.7)^3} = 95\% \quad (6.30b)$$

Which gives:

$$M_{inner} = 0.05 * 1.089 = 0.05445kNm \quad (6.31a)$$

$$\sigma = 0.495MPa \quad (6.31b)$$

$$U.C. = 0.05 \quad (6.31c)$$

$$M_{outer} = 0.95 * 1.089 = 1.035kNm \quad (6.31d)$$

$$\sigma = 9.41MPa \quad (6.31e)$$

$$U.C. = 0.94 \quad (6.31f)$$

6.4.3 Calculation window pane version B

To make a comparison for the reduction of material use, simply the total thickness is considered. A thickness of 14 mm (13.7 mm in the calculations) yields:

$$f_{mt;u;d} = \frac{0.8 * 50}{1.6} = 25MPa \quad (6.32)$$

$$UC_{stress} = \frac{23.21}{25} = 0.93 \rightarrow OK \quad (6.33)$$

For biaxial bending:

$$U.C._{stress} = \frac{7.21}{25} = 0.29 \quad (6.34a)$$

$$U.C._{deflection} = \frac{2.97}{6} = 0.50 \quad (6.34b)$$

As was the case for the roof in Case I, the unity check of the deflection in the improved calculations surpasses the unity check of the stress.

6.5 Material use

Now that the structural dimensions have been determined, also the amount of glass needed is known. This will be used to compare the improved calculations of each case against the current calculations and show how much material can be saved. See Table 6.6 and Table 6.7.

It can be seen that for the beam the highest improvement is achieved when a more certain

Table 6.6: Comparison of material use of Case I. Values are in m^3

	Case I	Case II	Difference	Percentage
Roof	1.2960	0.5520	0.7440	57.41%
Beam	0.6042	0.1215	0.4827	79.89%
Column	0.0158	0.0132	0.0026	16.36%
Total	1.9160	0.6867	1.2293	64.16%

Table 6.7: Comparison of material use of Case II. Values are in mm

	Case A	Case B	Difference	Savings
Single glazing	21.7	13.7	8	36.87%

strength value is found.

Table 6.8: Results of the practical cases

	Case I A	Case I B	Case II A	Case II B
Strength	20 MPa	50 MPa	20 MPa	50 MPa
Safety factor	4	2	1	1
UC_strength roof	0.93	0.91	-	-
UC_strength beam	0.95	0.95	-	-
UC_strength column	0.80	0.81	-	-
UC_deflection roof	0.08	0.96	-	-
UC_deflection beam	0.02	0.10	-	-
UC_strength pane	-	-	0.93	0.93
UC_deflection pane	-	-	0.12	0.50
Material savings roof	-	57.41%	-	-
Material savings beam	-	79.89%	-	-
Material savings column	-	16.36%	-	-
<i>Total material savings</i>	-	<i>64.16%</i>	-	<i>36.87%</i>

6.6 Conclusions

Table 6.8 summarises the results from both versions of the two cases. The improvement for horizontal plate glass is limited by glass' stiffness. This is seen for both the window pane in Case II as the roof and beam in Case I. In the improved calculations of the roof in Case I, the point was already reached where the deflection is governing. Moreover, the unity check was only just sufficed. So from that point onwards an increase of strength would not lead to a reduction of material. To achieve this reduction the stiffness would have to be increased by applying reinforcement, such as steel bars or fibers.

The biggest improvement was made for the beam and even more improvement is possible there, because the unity check for the deflection was still quite low. This shows the importance of edge strength research. Although, it should be noted that the improvement will be slightly smaller because the roof will not be made of less material.

The strength of the column was determined with the Euler equation. This overestimates the strength. The material savings are expected to be slightly higher with a safer method. For now, an indication was given.

Lastly, it should be stressed that these improvement numbers are specifically derived from these two cases. It depends on the structural design how much improvement can be made. However, it is safe to say that in any case the improvement by a more certain glass strength assessment will be huge.

Conclusions

The main question reads:

How can the biaxial strength of float glass be understood through a mechanical and fractographic research?

This question can be answered through its subquestions which are presented below:

Which factors influence the strength of float glass?

The strength of glass can be attributed to deliberate and non-deliberate factors. The deliberate part includes factors that can be controlled. Flaws are the non-deliberate factors that influence the strength of glass. The first controllable factor is choosing the glass recipe. Soda silica lime glass has a stiffness ranging from 70 to 74 GPa depending on its additives. If the manufacturer does his job well, no residual stresses exist in the glass after the production process. For float glass, the side that was floating on the tin is slightly stronger than the side that was in contact with air.

Further processing can increase the strength of glass. This can be done by thermal processes such as heat-strengthening and tempering or mechanical processes such as grinding and polishing.

Glass researchers collectively agree flaws cause the uncertainty in the strength of glass. Flaws can be categorised by their locations (edge, surface and within the volume) and are caused by:

- Grinding and polishing, which is ironic as they are meant to improve the glass strength. However, it is possible that the point of deep cracks remain within the volume of the glass, forming a weak spot. Or even worse, if the grinder hits a flaw that is close to the surface this can induce additional cracks, which decrease the strength instead of increase it.
- Mishandling can cause scratches, pits or dents at the surface or edge.
- Environmental conditions can weather the glass.
- During the production process air bubbles are created in the melt and some of them remain there. Additionally, inclusions can be formed. These range from local crystallisations of glass components to pieces of broken off furnace.

How can models describe the strength of glass?

Three types of models were considered: materials failure, fracture mechanics and statistics.

It is quite hard to describe material failure without ending up with numerous parameters. The models that exist illustrate how complex materials are.

With fracture mechanics it is possible to describe the crack propagation and the influence of flaws. This could be used to verify findings from the fractographic analysis. It can also be of help in predicting which flaw would be most critical to ensue an improved strength assessment. It is a matter of probability whether a critical flaw will lie in the highest stressed part. Weibull analysis has proven to be a good describer of the probability of the weakest link in a body. However, flaws in glass behave so differently that they do not result in a proper Weibull plot. This might be solved if the flaws are characterised and their corresponding strength data are plotted separately.

How can the biaxial strength be mechanically determined?

The ring on ring (RoR) test was selected as the most suitable as a large area of constant biaxial tensile stress is created. Adding compression yields the compressive tensile test. However, the test has proven to be more complicated than was expected. Strain measurements were performed to check if the stress from the RoR formula is the real stress. The results were variable and deviated considerably from the calculated stress. It is hypothesised that the variability can be accounted to friction between the rings and glass. The deviation was partly due to additional stiffness from the adhesive foil and strain gauge. The remaining deviation is most likely caused by the formula itself which assumes zero thickness for the rings and glass plate. Due to the variability, no correction factor could be formulated.

Another oddity in the results was that 30 out of 53 plates showed circumferential cracking at the support ring. One explanation is that friction causes a punching shear mechanism. Another more complex explanation involves dynamic effects that occur in the glass during fracture which can cause stress concentrations at the support ring.

Despite the underlying mechanism, the solution seems to lie in the dimensional ratios. To determine their values, recommended ratios from ceramics RoR testing had been applied. In a test of 10 specimens, no circumferential cracking at the support ring occurred. Three factors were changed in this test:

- The thickness of the glass was 3 mm instead of 4 mm.
- The specimens were 180 by 200 mm. The cruciform specimens had a much larger overhang of 160 mm.
- The glass originated from Europe. The cruciform specimens originate from China.

It is hypothesised that the first two might be the most likely candidates for achieving more successful RoR tests. If that indeed is the case, different recommended ratios should be formulated for RoR testing on glass.

How can the strength be fractographically interpreted?

Traditional fractography of glass involves a fracture pattern analysis by eye and a fracture surface analysis by eye and by microscope. In this research, it was suggested to include an additional step: Observing the fracture pattern underneath the microscope. A transmitted light microscope was used, which illuminated all flaws and fracture marks within the glass. Together with Z-building software, which shows all flaws throughout the depth in one image, this had the following benefits:

- The glass researcher is given an overview of the fracture mechanism of the glass, which can be used as a guide to the fracture origin.
- It reveals fracture markings, that were otherwise overlooked, which give insights into the crack propagation and the local failure process.

An example of one of those insights concerned the amount of fracture marks observed in the glass. It seemed there might be a relationship between the number of fracture marks and the failure stress. However, the number of 5 plates is too small a group to draw final conclusions. Further research will have to further examine this theory.

What is the benefit for structural purposes?

More certainty of glass' strength will reduce the safety factor and increase the maximum stress value that can be applied. This is convenient for a structural designer, as it will save material and allow the freedom to make more slender structures. This was shown in two cases of a portal and a window pane. It was concluded that even with an improvement of glass' strength from 20 to 50 MPa and of the safety factor from 4 to 2 64% of material can be saved. The largest saving was made for the glass beam, namely 80%. The savings can be even larger when a higher strength and a lower safety factor are applied. However, it was also concluded that the saving is limited by glass stiffness when the unity check for the deflection reaches 1. By applying reinforcement such as steel bars or fibers, this can be further improved.

To summarise, the main question is answered:

How can the biaxial strength of float glass be understood through a mechanical and fractographic research?

Glass strength is mainly dependent on flaws. For this reason, Weibull plot of glass do not properly fit strength data. The biaxial strength can be determined by a ring on ring test. A fractographic analysis can give information on how the glass fractured and why. A full overview of the fracture marks and flaws is obtained by performing both a fracture pattern analysis and a fracture surface analysis by microscope.

Fracture mechanics can be used to understand the local mechanisms at a flaw. It is expected that by relating the strength data to their corresponding flaw type, more sensible Weibull plots can be drawn and glass' strength can be better predicted.

When this is achieved, in practice, a lot of material can be saved and more slender structures can be built.

Recommendations

This thesis provides a contribution to improving the strength assessment of glass. During this research several issues were encountered that have not yet been resolved, but can play a substantial role to achieve a better strength assessment. The following recommendations are made for several topics covered in this thesis.

Biaxial testing

Biaxial testing has proven to be quite complicated. Therefore, several improvements are still to be made on this test. One issue that needs to be further explored is that the strain measurements did not correspond to the calculated stress. The large deviation was concluded to be due to the basis of the formula itself. It is recommended to determine a correction factor for the formula. In this research, it was not possible to do this because there was also some variability between the results. More experiments are needed and it might be necessary to make a finite element model of the ring on ring test, which could be used to optimise the formula to the actual situation.

The variability in the strain measurements' results is thought to be caused by friction, but this will have to be further explored with strain gauges. This can be done by testing multiple glass plates under the same conditions to examine whether the strain values are similar.

A second issue that occurred in the RoR test was circumferential cracking at the support ring. However, this type of cracking no longer occurred when the following parameters were changed:

- 3 mm thickness instead of 4 mm.
- Square specimens with a smaller overhang.
- Glass originated from Europe instead of China.

The initial dimensions of 4 mm thickness and a larger overhang were based on recommended ratios formulated by RoR testing on ceramics. It appears that these ratios do not apply to glass. It is therefore suggest to reformulate these ratios for glass.

Moreover, it is recommended to use these parameters as a starting point in a more extensive strain measurement research.

The compressive tensile test can be improved by adding guiders which keep the pressure cell vertically in place.

Fractographic analysis

A traditional fractographic analysis includes a fracture pattern examination by eye and a fracture surface analysis by microscope. It is recommended to add an additional step inbetween in which the fracture pattern is examined by microscope as well, because this reveals fracture marks that would otherwise be overlooked. This works best with a transmitted light microscope that illuminates the flaws and markings inside the glass well and that is combined with Z-axis building software. This software allows all flaws and markings to be captured in one image, despite that they occur throughout the depth of the glass.

In future research, especially the combination of this technique and the fracture surface analysis should be addressed, because only then a total overview of all flaws and fracture marks in the glass is obtained.

Flaws in glass

It is expected to get significantly better Weibull plots when the strength data is separated by flaw type. This may be the start of a more accurate prediction of glass' strength. The flaw types can be characterised by microscopic research and the impact of a flaw type on the glass' strength can be calculated with fracture mechanics. By working together with glass manufacturers this can be used to optimise the glass recipe in such a way, that critical volume defects are prevented. Glass does not need to be flawless. It is mainly important to know which flaws are present in a glass component to determine its strength. The author hypothesises that a similar system as is used for timber can be conducted. A research by Molnár [12] showed that more flaws occur in float glass at the sides of the furnace and less in the middle. When that research is combined with flaw characterisation and strength determination it could turn out that glass from the middle is assigned a higher strength and glass from the sides a lower strength.

Quality control of glass for the building industry focusses on reducing flaws that are visible by eye. However, other fields are much more advanced in reducing flaws in glass, such as glass used in the screens of smartphones or tablets or glass used in optical microscopy. These fields apply much stricter rules on the amount and size of flaws in the glass. Research performed in these areas might also be useful for structural glass.

Improving the production process will mainly benefit volume flaws. However, surface and edge defects are created after the production process, due to, among others, mechanical processing, transportation, mishandling and influences during glass' lifetime.

It is therefore suggested that the quality control of glass should take place at least a second time after the mechanical processing. This way the grinding and polishing procedure that took care of all the flaws can be controlled. The volume should be checked too, because mechanical processing can induce or leave behind inner flaws as well.

In the end, additional defects created during the lifetime of glass will be inevitable. An interesting research by Overend and Louters shows repairing glass flaws is taking a promising turn [28]. Periodic maintenance of glass would ensure its strength. Another approach could be to perform a long term study on the quality during the service life of glass, which could be used to predict the degradation of glass over time. This is more uncertain than repairing the glass, but it depends on the application and cost consideration which approach is most suitable.

List of Figures

2.1	A silicon atom bonded to four oxygen atoms [2]	4
2.2	A silicon dioxide network [2]	4
2.3	(a) A crystalline SiO ₂ network, (b) an amorphous SiO ₂ network, (c) A soda silica glass network [2]	5
2.4	Water molecules deteriorating the glass structure [8]	6
2.5	Corroded glass [2]	7
2.6	(a) A sheet of molten glass is pulled through rollers (b) Molten glass is pulled vertically from the melt into a sheet [1]	8
2.7	A schematic overview of the float glass process [2]	8
2.8	(a) The surface is put under compression when glass is tempered (b) Heat-strengthening has the same effect but less intense [1]	10
2.9	A tensile load in the outer fibers is compensated by the compressive stress [1]	10
2.10	Fracture pattern of heat-strengthened (a) and tempered glass (b)[1]	11
2.11	Laminated glass with sacrificial outer layers [1]	11
2.13	The distribution of flaws over the surface of a float glass plate [12]	13
2.12	Size effect [2]	13
2.14	Three types of flaws [3]	14
3.1	Failure envelope according to the Von Mises and the Tresca criterion [13]	18
3.2	Failure theory based on Mohr and Coulomb [13]	19
3.3	Failure envelope according to Drucker and Prager	19
3.4	Paraboloid resulting from Christensen's polynomial-invariants criterion [13]	20
3.5	Paraboloids for different values of T/C [13]	21
3.6	T/C =1/8, glasses [13]	21
3.7	The three modes of crack surface displacements [16]	22
3.8	Crack in an infinite plate [16]	22
3.9	Polar coordinates for stresses near the crack tip [16]	23
3.10	Plasticity zone at the crack tip [16]	25
3.11	The strip-yield model [16]	25
3.12	The loading-unloading curve shows the specimen has deformed plastically [2]	26
3.13	Cavities develop ahead of the crack tip [18]	26
3.14	A Weibull plot of the strength of an aluminium. The points fit well on the line with slope m [5]	27
3.15	No straight Weibull line is achieved with the data from glass strength tests [4]	28

3.16	A fractographic montage of a ceramic [5]	28
4.1	Biaxial failure envelope of concrete [20]	30
4.2	Possible setups for biaxial testing [20, 21, 22]	30
4.3	Fracture pattern analysis of a disc broken in a biaxial tensile test [5]	33
4.4	The analysis of crack branching can supply useful information [5]	33
4.5	Typical fracture patterns in ring on ring tests [5]	34
4.6	Wallner lines at the fracture origin. The arrows indicate the crack propagation direction [31]	35
4.7	The reflection of light causes the ripples to look like lines [33]	35
4.8	Using Wallner lines in a fractography analysis [34]	36
4.9	Different crack fronts and Wallner lines per stress state [5]	37
4.10	Crack initiation marks	37
4.11	A schematic of a polarised light microscope [35]	38
4.12	An anisotropic material splits light in two rays, a slow and a fast one [35]	39
4.13	The interaction between the beam and the specimen [36]	39
4.14	Energy resolution of EDS vs WDS [36]	40
5.1	Ring on ring test values	44
5.2	Ring on ring test values	44
5.3	Ring on ring test set up	45
5.4	High speed camera set up	46
5.5	Compressive tensile test set up	46
5.6	Delrin rings were tried as they are more compliant than steel	48
5.7	Alteration of the steel rings to make a sharper edge	49
5.8	Graphs of the Young's Modulus of (a) TT1 (b) TT2 (c) TT27 (d) TT28 (e) TT29	50
5.9	Graphs of the Young's Modulus of (a) TT30 (b) TT26	51
5.10	Expected fracture patterns in RoR tested plates [5]	54
5.11	Fracture pattern categories	54
5.12	Fracture patterns of (a) TT21 (b) TT22 (c) TT23	55
5.13	High speed video of the fracture of TT21	56
5.14	Fracture patterns of (a) CT1 (b) CT2 (c) CT3	57
5.15	The u-profile moves upwards	57
5.16	Fracture patterns of (a) X4 (b) X10	58
5.17	Fractographic analysis of TT3	60
5.18	Fractographic analysis of TT10	61
5.19	Fractographic analysis of TT40	61
5.20	Fractographic analysis of TT6	62
5.21	Fractographic analysis of TT8	62
5.22	Fractographic analysis of TT16	63
5.23	Different angles of observation	64
5.24	Stress plotted versus number of fracture marks	65
5.25	(a) New plot stress versus number of fracture marks (b) Stress versus number of hackle marks	66
6.1	Schematic of the portal	68
6.2	(a) In a symmetric cross-section the neutral axis runs through the glue line (b) In an asymmetric cross-section it goes through the glass [1]	69
6.3	The outer sacrificial layers protrude past the load-bearing layer protecting it sufficiently [1]	70

6.4	Ways to build a glass column [46]	70
6.5	Possible configurations for a column made of glass plates [47]	71
6.6	Linear interpolation can be adopted to determine the α and β should the b/a value be other than listed	72
6.7	Profile configuration 4	74
6.8	The orientation and dimensions of the Faculty of Civil Engineering	76
6.9	The dimensions of the window pane	76
6.10	Wind zones for different values of e	77
1	Fracture pattern of TT3	99
2	Fracture pattern of TT4	99
3	Fracture pattern of TT5	100
4	Fracture pattern of TT6	100
5	Fracture pattern of TT7	100
6	Fracture pattern of TT8	101
7	Fracture pattern of TT9	101
8	Fracture pattern of TT10	101
9	Fracture pattern of TT11	102
10	Fracture pattern of TT12	102
11	Fracture pattern of TT13	102
12	Fracture pattern of TT14	103
13	Fracture pattern of TT15	103
14	Fracture pattern of TT16	103
15	Fracture pattern of TT17	104
16	Fracture pattern of TT18	104
17	Fracture pattern of TT19	105
18	Fracture pattern of TT20	105
19	Fracture pattern of TT21	106
20	Fracture pattern of TT22	106
21	Fracture pattern of TT23	106
22	Fracture pattern of TT24	107
23	Fracture pattern of TT25	107
24	Fracture pattern of TT27	107
25	Fracture pattern of TT28	108
26	Fracture pattern of TT29	108
27	Fracture pattern of TT30	108
28	Fracture pattern of TT31	109
29	Fracture pattern of TT32	109
30	Fracture pattern of TT33	109
31	Fracture pattern of TT34	110
32	Fracture pattern of TT35	110
33	Fracture pattern of TT36	110
34	Fracture pattern of TT37	111
35	Fracture pattern of TT38	111
36	Fracture pattern of TT39	112
37	Fracture pattern of TT40	112
38	Fracture pattern of TT41	112
39	Fracture pattern of TT42	113
40	Fracture pattern of TT43	113

41	Fracture pattern of TT44	113
42	Fracture pattern of TT45	114
43	Fracture pattern of TT46	114
44	Fracture pattern of TT47	114
45	Fracture pattern of TT48	115
46	Fracture pattern of TT49	115
47	Fracture pattern of TT50	115
48	Fracture pattern of TT51	116
49	Fracture pattern of TT52	116
50	Fracture pattern of TT53	116
51	Fracture pattern of TT54	117
52	Fracture pattern of CT1	118
53	Fracture pattern of CT2	118
54	Fracture pattern of CT3	118
55	Fracture pattern of X1	119
56	Fracture pattern of X2	119
57	Fracture pattern of X3	120
58	Fracture pattern of X4	120
59	Fracture pattern of X5	120
60	Fracture pattern of X6	121
61	Fracture pattern of X7	121
62	Fracture pattern of X8	121
63	Fracture pattern of X9	122
64	Fracture pattern of X10	122

List of Tables

2.1	Effect of flaws in glass	15
3.1	Fracture toughness of different types of glass [2]	24
4.1	Conclusions biaxial flexure tests [23, 24, 25, 26]	31
5.1	Dimensions	47
5.2	Ratios	47
5.3	Interfaces applied to minimise friction	48
5.4	Young's Modulus calculated by RoR stress and measured stress	50
5.5	Applied boundary conditions and resulting failure stress and fracture mechanism per specimen	52
5.6	Continuation of Table 5.5	53
5.7	Resulting categories for combinations of boundary conditions	55
5.8	Failure stress in compressive tensile test	56
5.9	Results RoR tested 3 mm thick glass	57
5.10	Number of fracture marks per plate	65
5.11	Number of fracture marks observed with stereo microscope	65
6.1	Loads	71
6.2	Load combinations	71
6.3	Beam loads	73
6.4	Column loads	73
6.5	Value of c_f	77
6.6	Comparison of material use of Case I. Values are in m^3	79
6.7	Comparison of material use of Case II. Values are in mm	79
6.8	Results of the practical cases	80

Bibliography

- [1] J. Wurm, *Glass structures: design and construction of self-supporting skins*. Walter de Gruyter, 2007.
- [2] E. Bourhis, *Glass: Mechanics and Technology*. Wiley, 2014.
- [3] G. Molnár, L. Molnár, and I. Bojtár, “Preparing a comprehensive analysis of the mechanical classification of structural glass,” *Materials Engineering-Materiálové inžinierstvo (MEMI)*, vol. 19, no. 2, pp. 71–81, 2012.
- [4] F. Veer, “The strength of glass, a nontransparent value,” *HERON*, vol. 52, no. 1/2, pp. 87–104, 2007.
- [5] G. Quinn, *Fractography of ceramics and glasses*. NBS special publication, NIST, 2007.
- [6] J. Shelby, *Introduction to glass science and technology*. Royal Society of Chemistry, 2005.
- [7] Y. Imanaka, *Advanced Ceramic Technologies & Products*. SpringerLink : Bücher, Springer, 2012.
- [8] M. Ciccotti, “Stress-corrosion mechanisms in silicate glasses,” *Journal of physics D: Applied physics*, vol. 42, no. 21, p. 214006, 2009.
- [9] C. Louter, *Fragile yet Ductile, Structural Aspects of Reinforced Glass Beams*. PhD thesis, Delft University of Technology, 2011.
- [10] F. Veer and J. Zuidema, “The strength of glass, effect of edge quality,” in *Glass processing days 2003*, (Tampere Finland), pp. 106–109, 2003.
- [11] G. Quinn, “A history of the fractography of glasses and ceramics,” in *Fractography of Glasses and Ceramics VI*, pp. 1–55, John Wiley & Sons, Inc., 2012.
- [12] G. Molnár and I. Bojtár, “Effects of manufacturing inhomogeneities on strength properties of float glass,” *Mechanics of Materials*, vol. 59, pp. 1–13, 2013.
- [13] R. Christensen, *The theory of materials failure*. Oxford University Press, 2013.
- [14] C. Hartsuijker, H. Welleman, F. of Civil Engineering, and Geosciences, *Mechanics of Structures: CT4145/CT2031 : Module: Introduction Into Continuum Mechanics*. TU Delft, 2007.

- [15] A. Verruijt and S. Van Baars, *Soil mechanics*. VSSD, 2007.
- [16] M. Janssen, J. Zuidema, and R. Wanhill, *Fracture Mechanics, Second Edition*. Taylor & Francis, 2004.
- [17] J. Mecholsky, “Quantitative fractographic analysis of fracture origins in glass,” in *Fractography of Glass* (R. Bradt and R. Tressler, eds.), pp. 37–73, Springer US, 1994.
- [18] F. Célarié, S. Prades, D. Bonamy, L. Ferrero, E. Bouchaud, C. Guillot, and C. Marlière, “Glass breaks like metal, but at the nanometer scale,” *Phys. Rev. Lett.*, vol. 90, p. 075504, Feb 2003.
- [19] W. Weibull, “A statistical distribution function of wide applicability,” *Journal of applied mechanics*, pp. 293–297.
- [20] H. Kupfer, H. Hilsdorf, and H. Rusch, “Behavior of concrete under biaxial stresses,” in *ACI Journal proceedings*, vol. 66, ACI, 1969.
- [21] M. Nooru-Mohamed, E. Schlangen, and J. van Mier, “Experimental and numerical study on the behavior of concrete subjected to biaxial tension and shear,” *Advanced cement based materials*, vol. 1, no. 1, pp. 22–37, 1993.
- [22] W. Yin, E. Su, M. Mansur, and T. Hsu, “Fiber-reinforced concrete under biaxial compression,” *Engineering Fracture Mechanics*, vol. 35, no. 1, pp. 261–268, 1990.
- [23] J. Kim, D. Kim, and G. Zi, “Improvement of the biaxial flexure test method for concrete,” *Cement and Concrete Composites*, vol. 37, pp. 154–160, 2013.
- [24] A. Börger, P. Supancic, and R. Danzer, “The ball on three balls test for strength testing of brittle discs: stress distribution in the disc,” *Journal of the European Ceramic Society*, vol. 22, no. 910, pp. 1425 – 1436, 2002.
- [25] H. Fessler and D. Fricker, “Multiaxial strength tests for brittle materials,” *The Journal of Strain Analysis for Engineering Design*, vol. 19, no. 3, pp. 197–208, 1984.
- [26] R. Morrel, “Biaxial flexural strength testing of ceramic materials,” *A National Measurement Good Practice Guide no. 12*, 1998.
- [27] J. Pepi, *Strength Properties of Glass and Ceramics*. SPIE Press monograph, SPIE Press, 2014.
- [28] M. Overend and C. Louter, “The effectiveness of resin-based repairs on the inert strength recovery of glass,” *Construction and Building Materials*, vol. 85, pp. 165 – 174, 2015.
- [29] “EN 1288-2: Glass in building - determination of the bending strength of glass - part 2: Coaxial double ring test on flat specimens with large test surface areas,” 2000.
- [30] “EN 1288-5: Glass in building - determination of the bending strength of glass - part 2: Coaxial double ring test on flat specimens with small test surface areas,” 2000.
- [31] N. Shinkai, “The fracture and fractography of flat glass,” in *Fractography of Glass* (R. Bradt and R. Tressler, eds.), pp. 253–297, Springer US, 1994.
- [32] T. Michalske, “Fractography of stress corrosion cracking in glass,” in *Fractography of Glass* (R. Bradt and R. Tressler, eds.), pp. 111–142, Springer US, 1994.

- [33] D. Hull, *Fractography: Observing, Measuring and Interpreting Fracture Surface Topography*. Cambridge University Press, 1999.
- [34] D. Dutt, “Mechanical properties and fracture analysis of glass.” Presentation at IES ALC Conference, Williamsburg, 2006.
- [35] O. Çopuroğlu, “Optical microscopy in concrete technology.” Lecture at Delft University of Technology, 2014.
- [36] O. Çopuroğlu, “Electron microscopy.” Lecture at Delft University of Technology, 2014.
- [37] O. Çopuroğlu, “X-ray analysis techniques.” Lecture at Delft University of Technology, 2014.
- [38] H. Fessler and D. Fricker, “A theoretical analysis of the ring-on-ring loading disk test,” *Journal of the American Ceramic Society*, vol. 67, no. 9, pp. 582–588, 1984.
- [39] J. Ritter, K. Jakus, A. Batakis, and N. Bandyopadhyay, “Appraisal of biaxial strength testing,” *Journal of Non-Crystalline Solids*, vol. 38, pp. 419–424, 1980.
- [40] M. Haldimann, A. Luible, M. Overend, I. A. for Bridge, and S. Engineering, *Structural Use of Glass*. Structural engineering documents, International Association for Bridge and Structural Engineering, 2008.
- [41] M. Overend Personal communication, 2015.
- [42] F. Veer Personal communication, 2015.
- [43] Y. Ha and F. Bobaru, “Studies of dynamic crack propagation and crack branching with peridynamics,” *International Journal of Fracture*, vol. 162, no. 1-2, pp. 229–244, 2010.
- [44] J. Swab, P. Patel, X. Tran, L. Gilde, E. Luoto, M. Gaviola, A. Gott, B. Paulson, and S. Kilczewski, “Equibiaxial flexure strength of glass: Influence of glass plate size and equibiaxial ring ratio,” *International Journal of Applied Glass Science*, vol. 5, no. 4, pp. 384–392, 2014.
- [45] “NEN 2608: Vlakglas voor gebouwen - eisen en bepalingsmethode,” 2014.
- [46] E. Ten Brincke, “Technoledge SD glass calculations.” Lecture at Delft University of Technology, 2015.
- [47] E. Ouwekerk, “Glass columns: A fundamental study to slender glass columns assembled from rectangular monolithic flat glass plates under compression as a basis to design a structural glass column for a pavilion,” Master’s thesis, Delft University of Technology, 2011.

Appendices

Appendix A

Of all the fractured plates photographs were taken of their fracture pattern. These are presented below. TT denotes the plates of 4 mm thick that were tested in the biaxial tensile test. CT denotes the plates of 4 mm thick that were tested in the compressive tensile test. X denotes the plates of 3 mm thick that were tested in the biaxial tensile test.

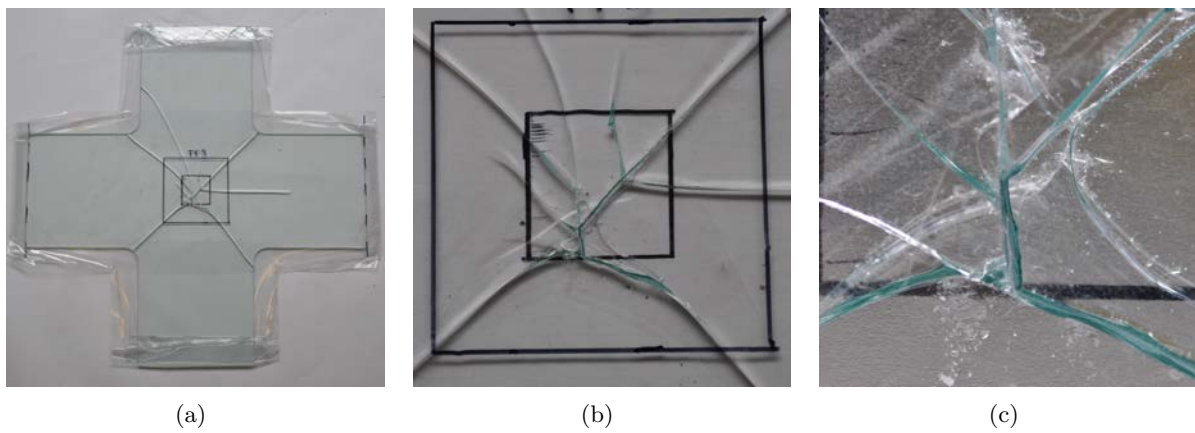


Figure 1: Fracture pattern of TT3

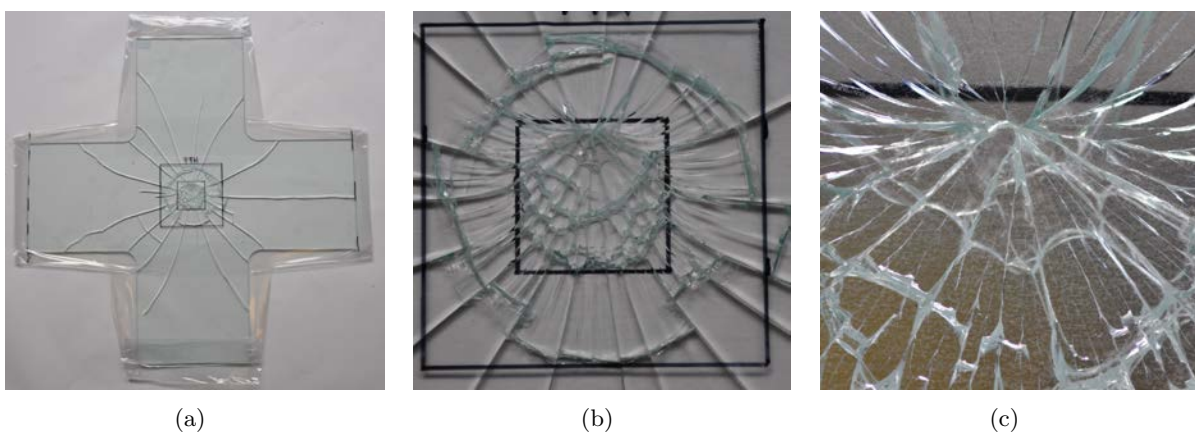
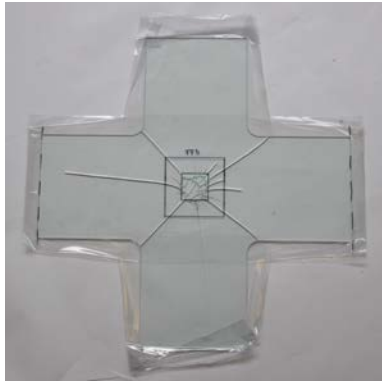
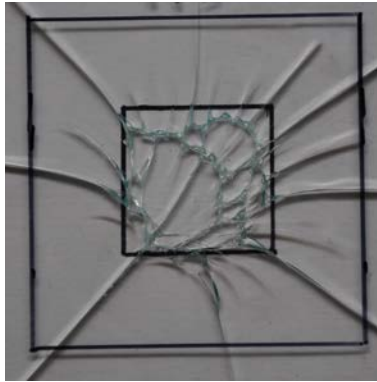


Figure 2: Fracture pattern of TT4



(a)

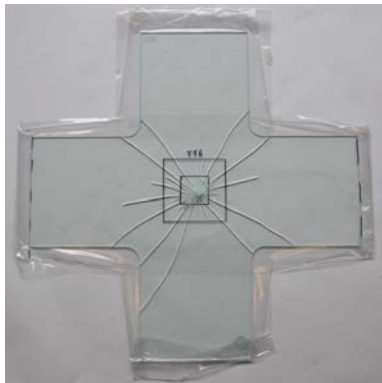


(b)

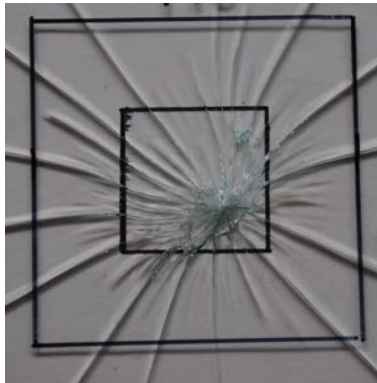


(c)

Figure 3: Fracture pattern of TT5



(a)

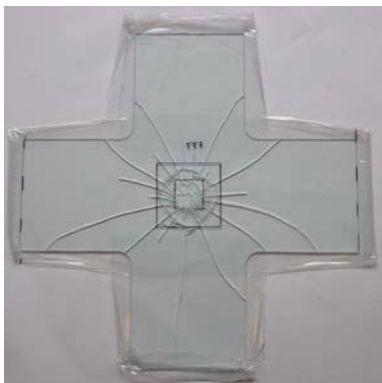


(b)

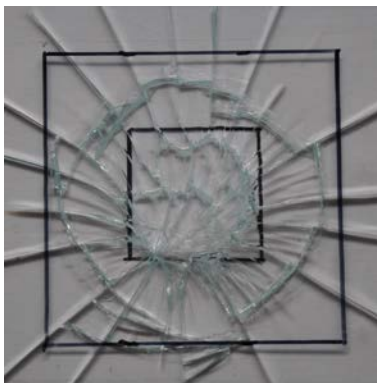


(c)

Figure 4: Fracture pattern of TT6



(a)

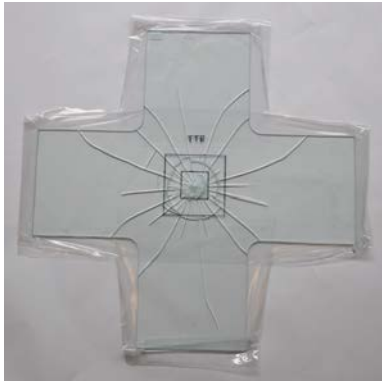


(b)

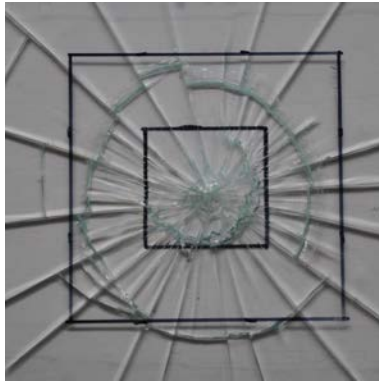


(c)

Figure 5: Fracture pattern of TT7



(a)

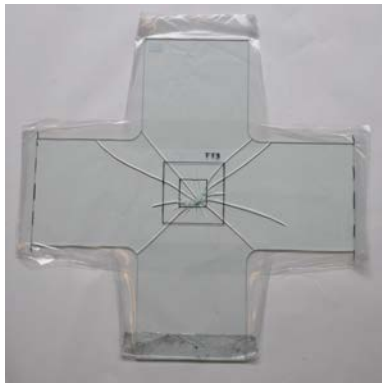


(b)



(c)

Figure 6: Fracture pattern of TT8



(a)

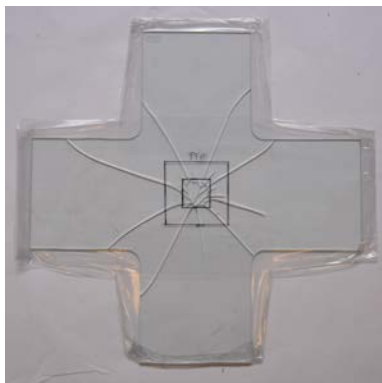


(b)



(c)

Figure 7: Fracture pattern of TT9



(a)



(b)



(c)

Figure 8: Fracture pattern of TT10



(a)

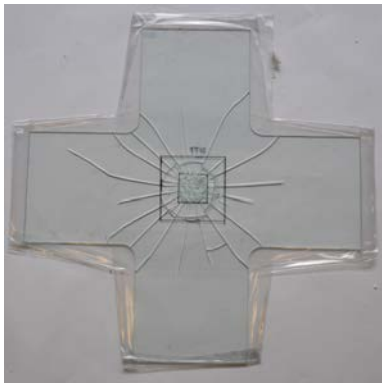


(b)



(c)

Figure 9: Fracture pattern of TT11



(a)



(b)

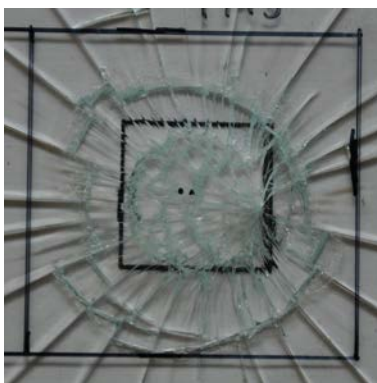


(c)

Figure 10: Fracture pattern of TT12



(a)

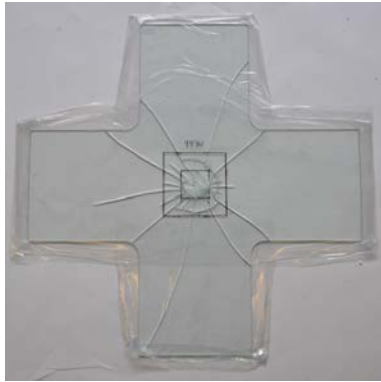


(b)



(c)

Figure 11: Fracture pattern of TT13



(a)

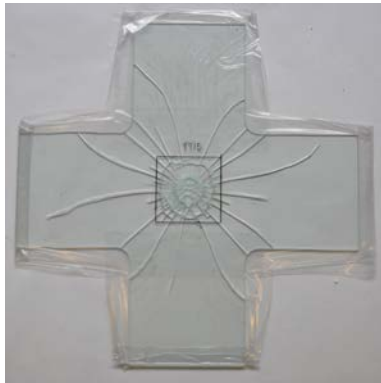


(b)



(c)

Figure 12: Fracture pattern of TT14



(a)



(b)



(c)

Figure 13: Fracture pattern of TT15



(a)

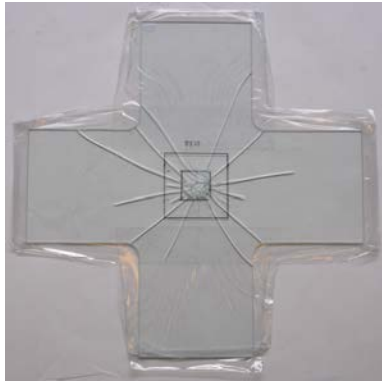


(b)



(c)

Figure 14: Fracture pattern of TT16



(a)

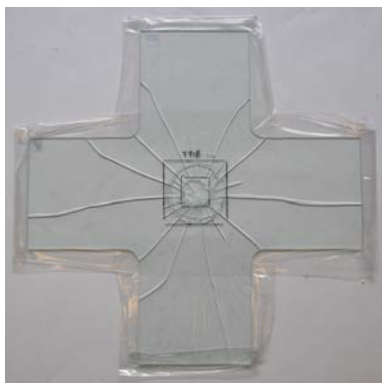


(b)



(c)

Figure 15: Fracture pattern of TT17



(a)



(b)



(c)

Figure 16: Fracture pattern of TT18



(a)

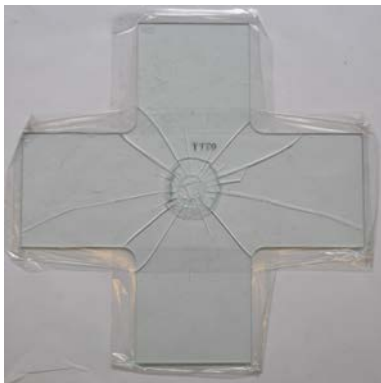


(b)



(c)

Figure 17: Fracture pattern of TT19



(a)



(b)



(c)

Figure 18: Fracture pattern of TT20

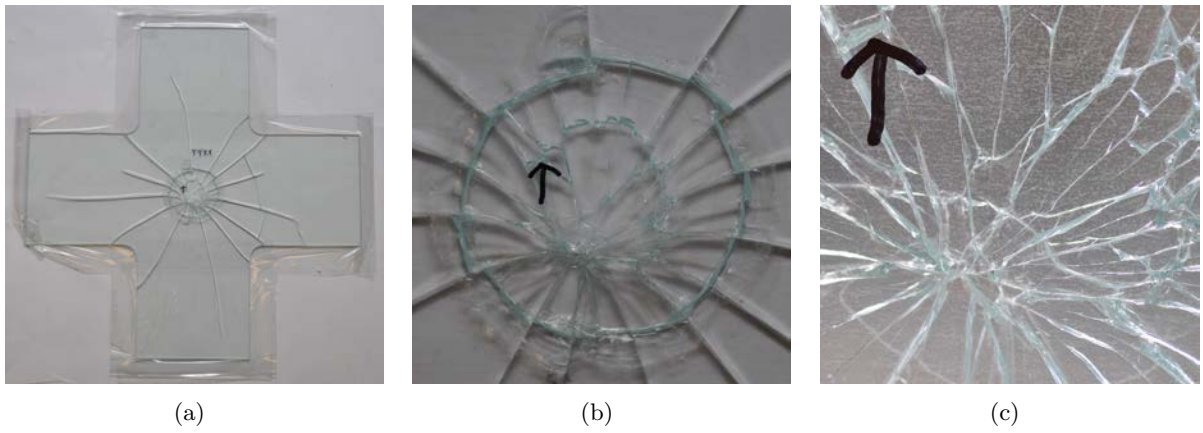


Figure 19: Fracture pattern of TT21

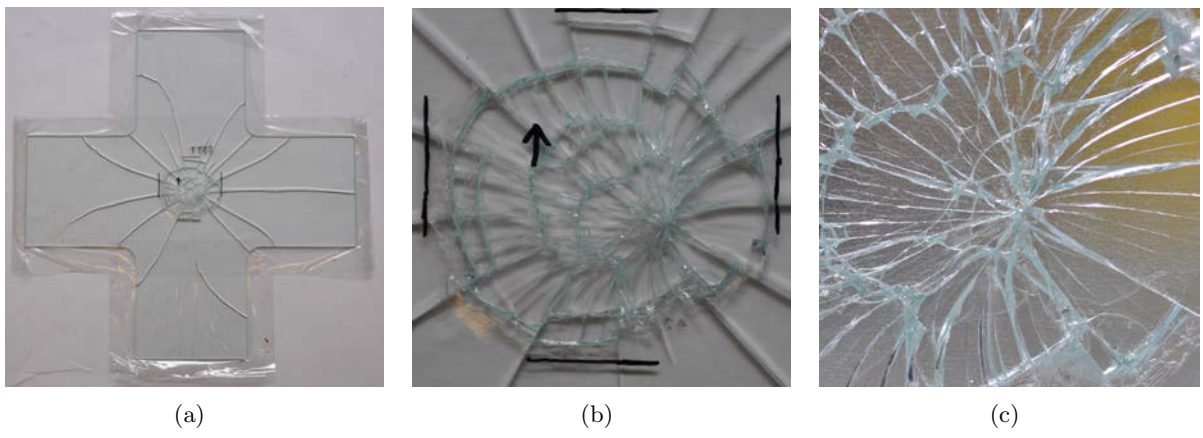


Figure 20: Fracture pattern of TT22

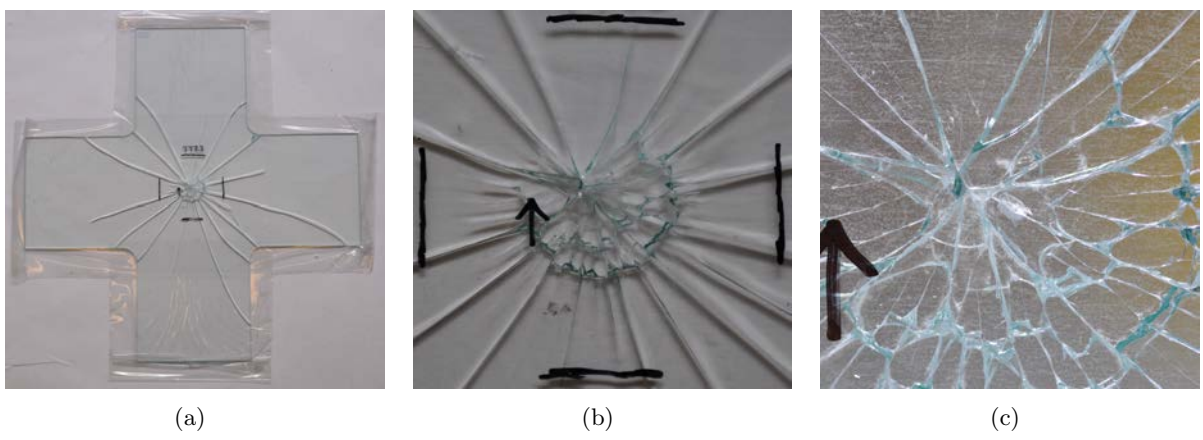


Figure 21: Fracture pattern of TT23

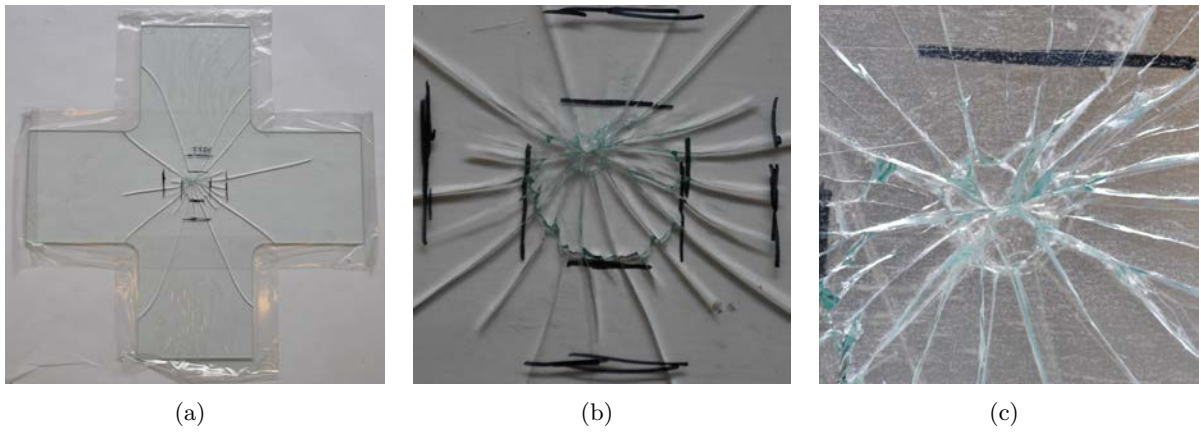


Figure 22: Fracture pattern of TT24

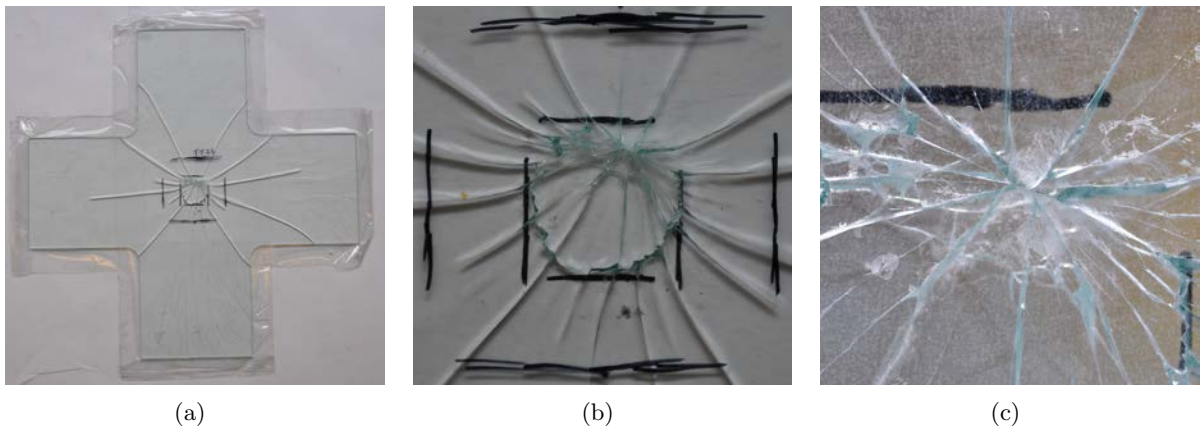


Figure 23: Fracture pattern of TT25

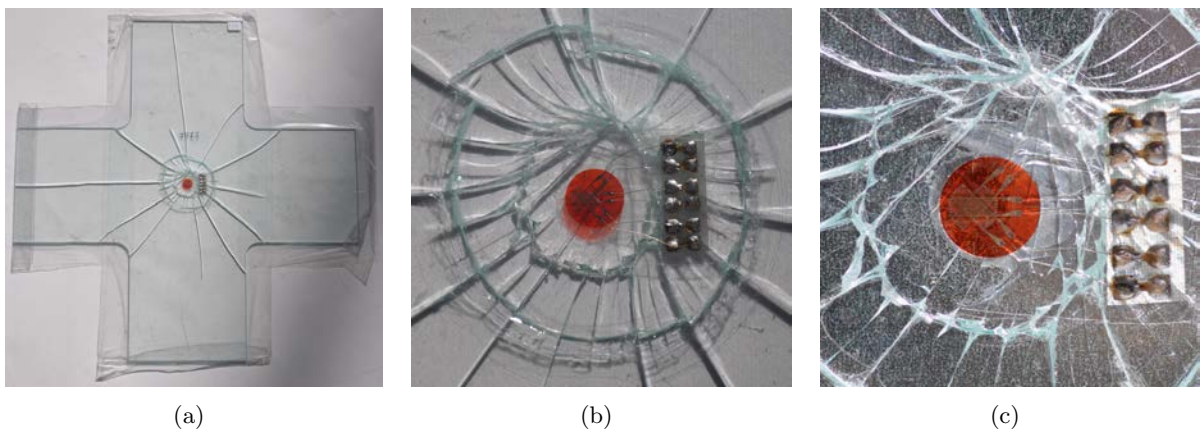
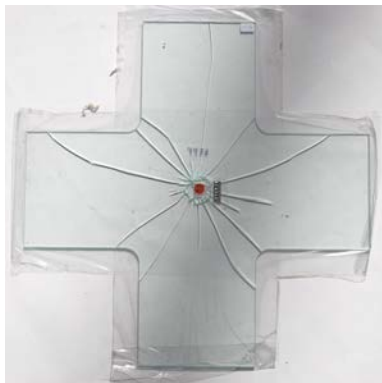
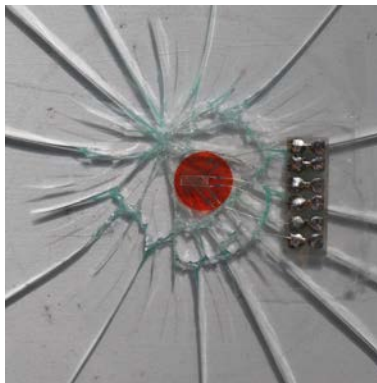


Figure 24: Fracture pattern of TT27



(a)

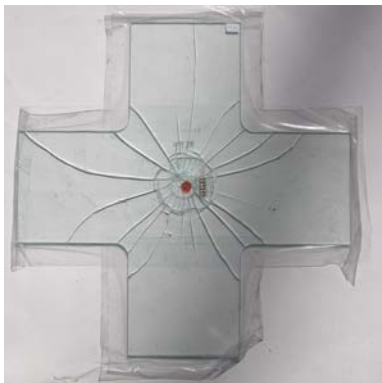


(b)



(c)

Figure 25: Fracture pattern of TT28



(a)

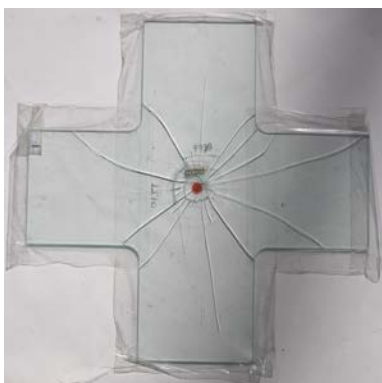


(b)



(c)

Figure 26: Fracture pattern of TT29



(a)

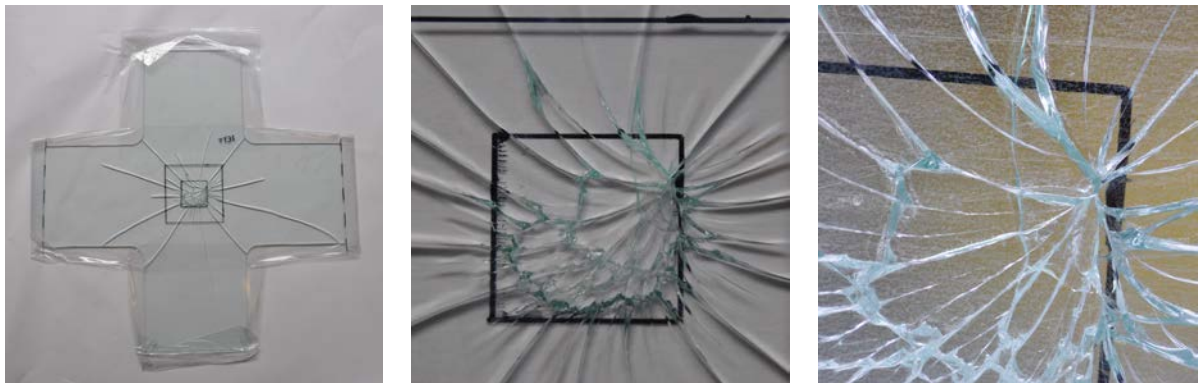


(b)



(c)

Figure 27: Fracture pattern of TT30

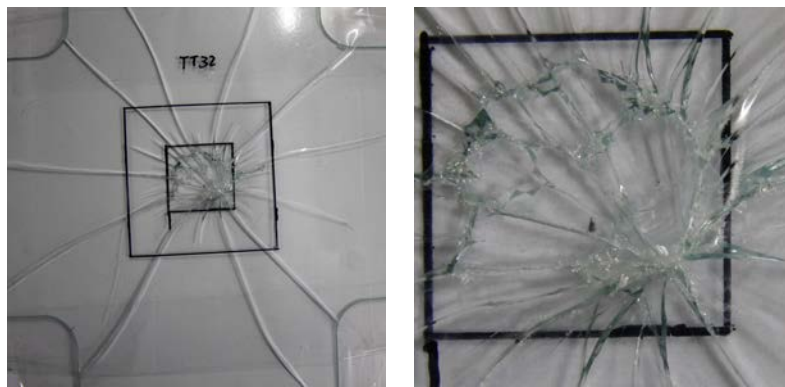


(a)

(b)

(c)

Figure 28: Fracture pattern of TT31



(a)

(b)

Figure 29: Fracture pattern of TT32



(a)

(b)

(c)

Figure 30: Fracture pattern of TT33

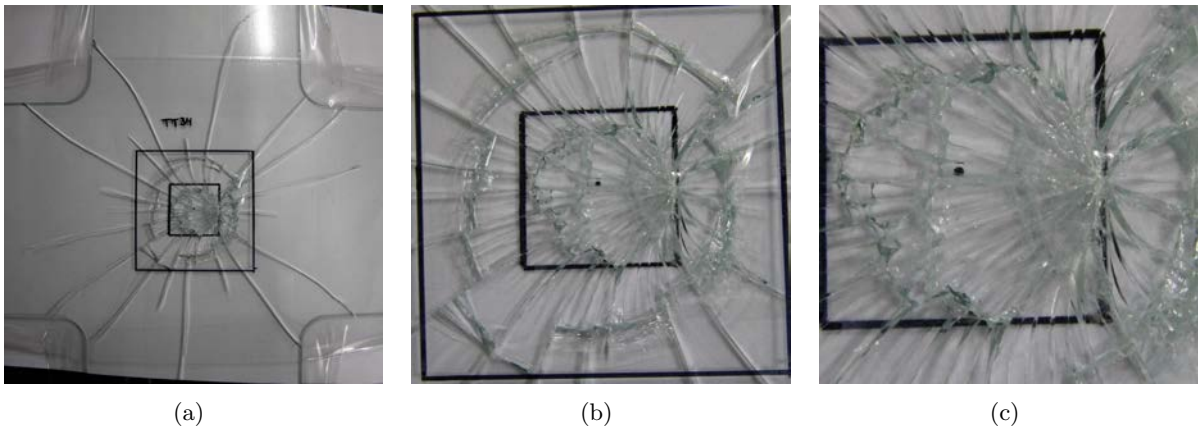


Figure 31: Fracture pattern of TT34

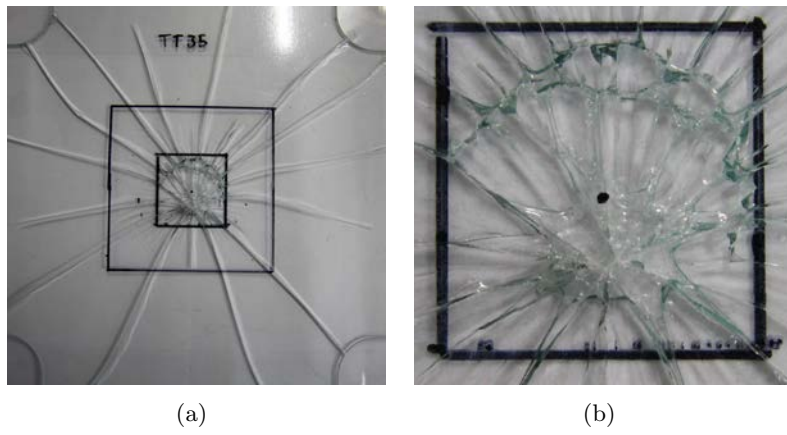


Figure 32: Fracture pattern of TT35

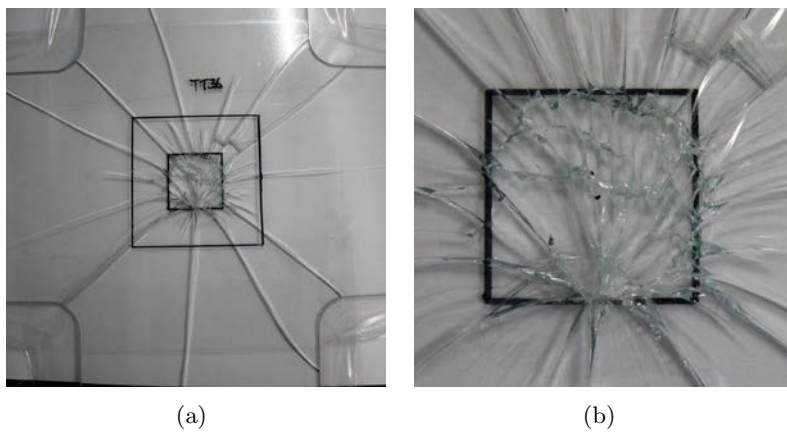
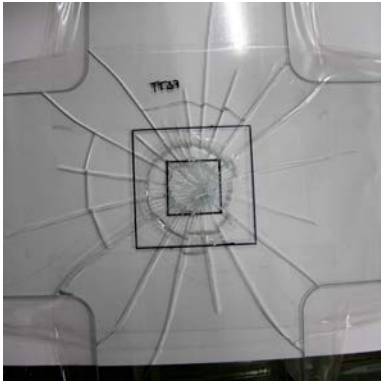


Figure 33: Fracture pattern of TT36



(a)



(b)



(c)

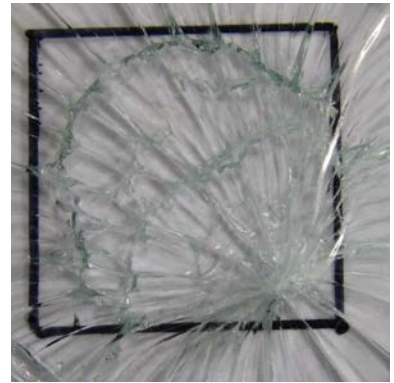
Figure 34: Fracture pattern of TT37



(a)



(b)



(c)

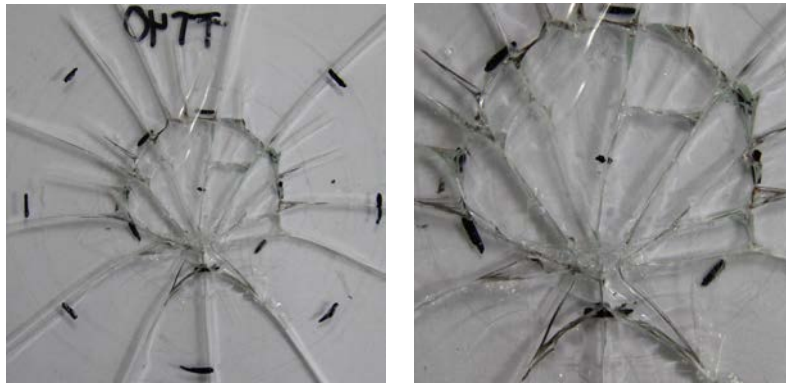
Figure 35: Fracture pattern of TT38



(a)

(b)

Figure 36: Fracture pattern of TT39



(a)

(b)

Figure 37: Fracture pattern of TT40



(a)

(b)

(c)

Figure 38: Fracture pattern of TT41



(a)

(b)

Figure 39: Fracture pattern of TT42

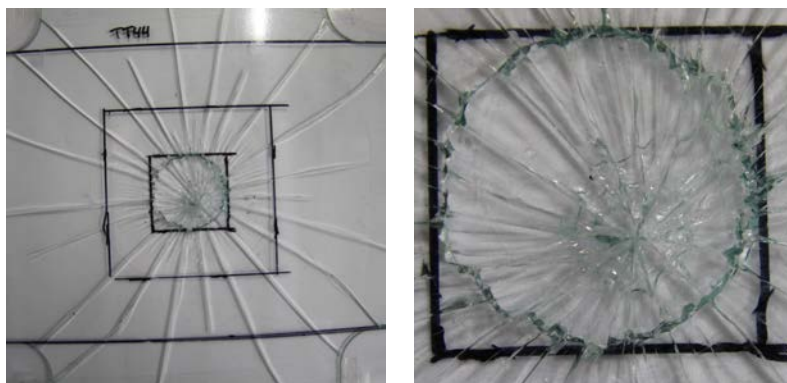


(a)

(b)

(c)

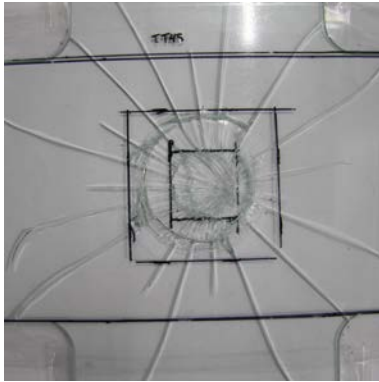
Figure 40: Fracture pattern of TT43



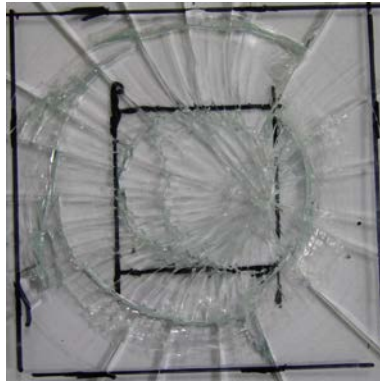
(a)

(b)

Figure 41: Fracture pattern of TT44



(a)

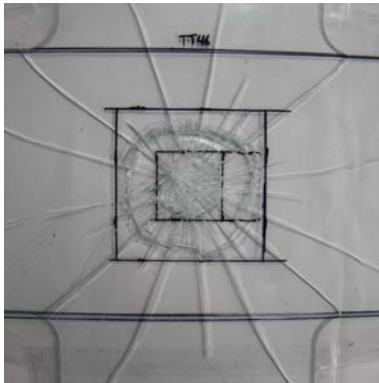


(b)

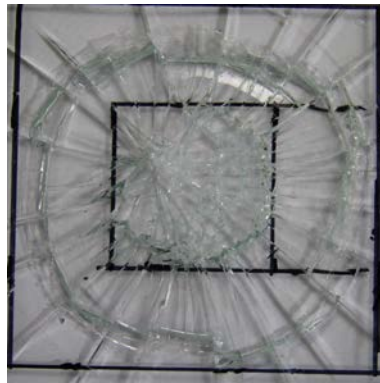


(c)

Figure 42: Fracture pattern of TT45



(a)



(b)

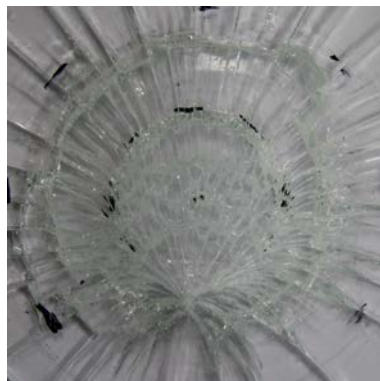


(c)

Figure 43: Fracture pattern of TT46



(a)



(b)



(c)

Figure 44: Fracture pattern of TT47

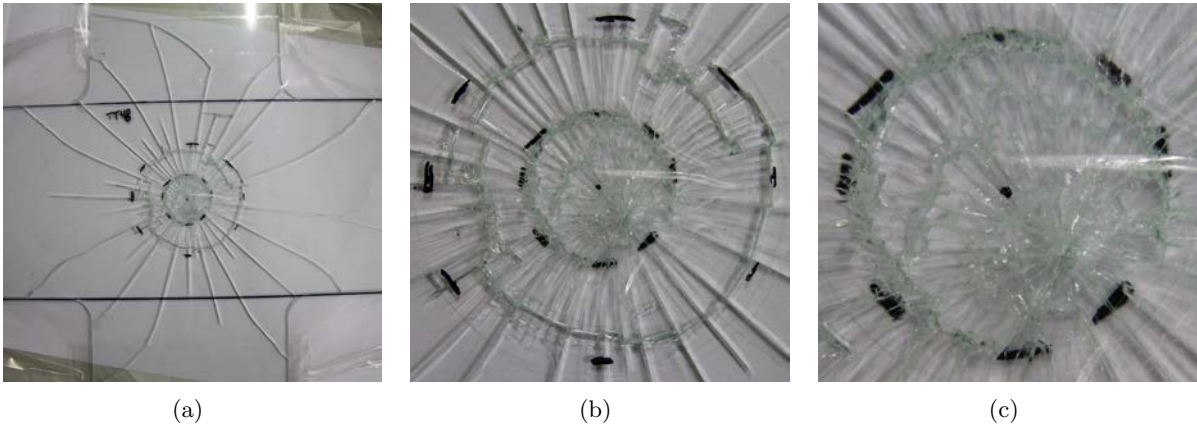


Figure 45: Fracture pattern of TT48

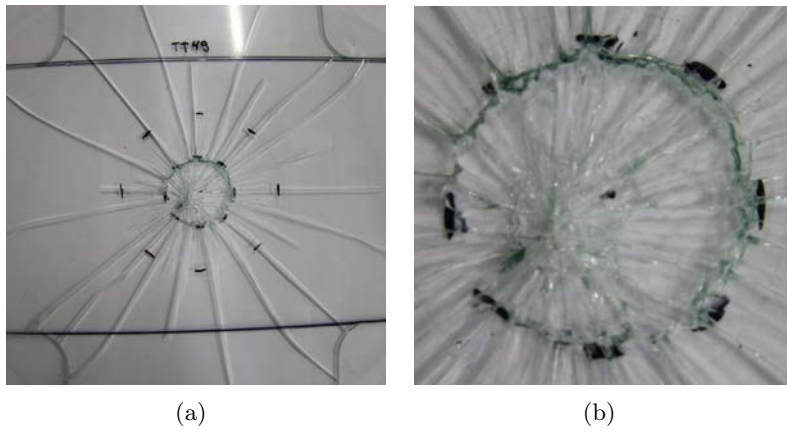


Figure 46: Fracture pattern of TT49

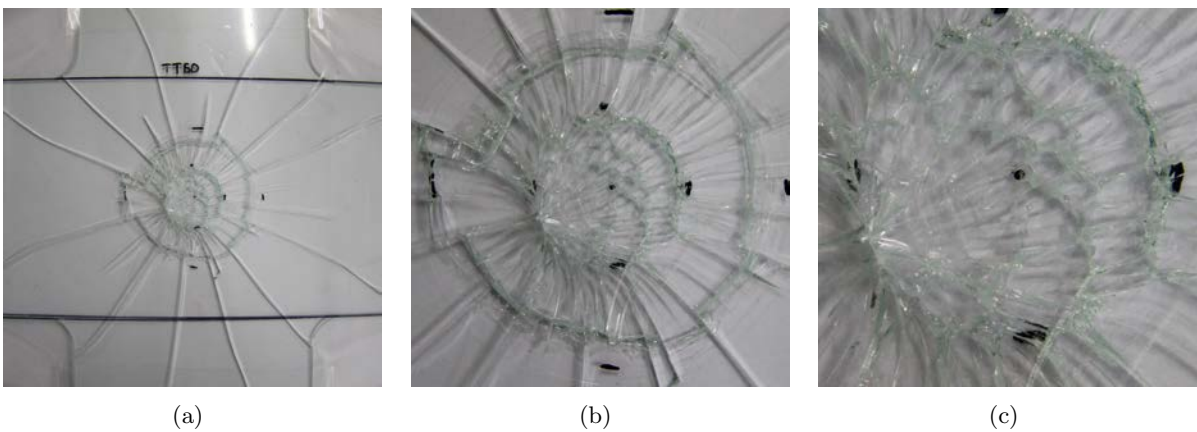


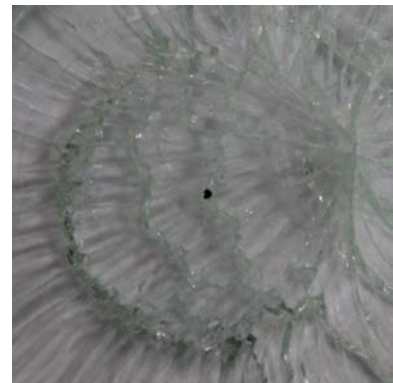
Figure 47: Fracture pattern of TT50



(a)



(b)



(c)

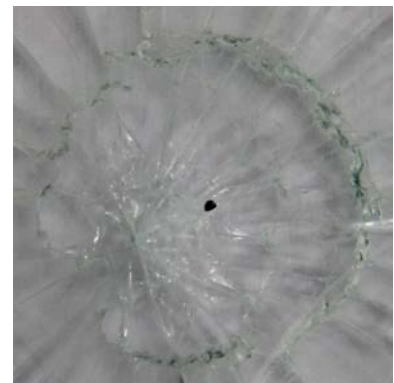
Figure 48: Fracture pattern of TT51



(a)



(b)



(c)

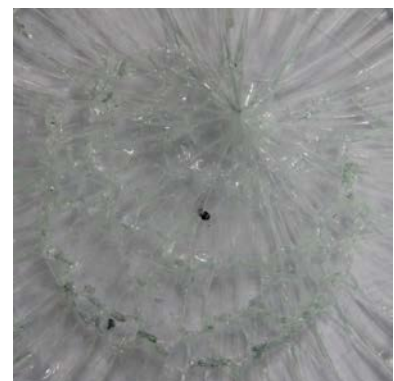
Figure 49: Fracture pattern of TT52



(a)

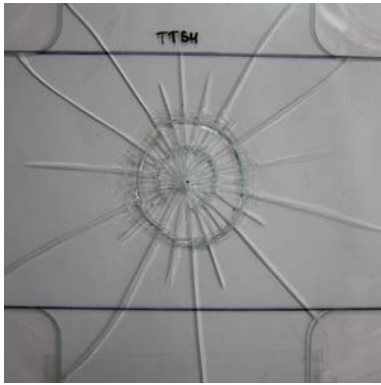


(b)

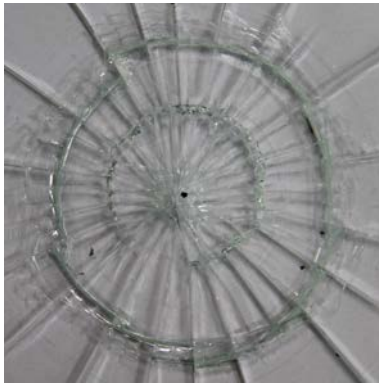


(c)

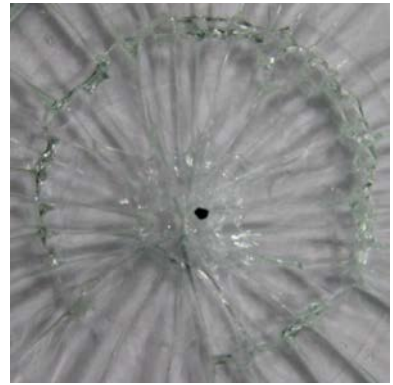
Figure 50: Fracture pattern of TT53



(a)



(b)



(c)

Figure 51: Fracture pattern of TT54



(a)



(b)

Figure 52: Fracture pattern of CT1



(a)

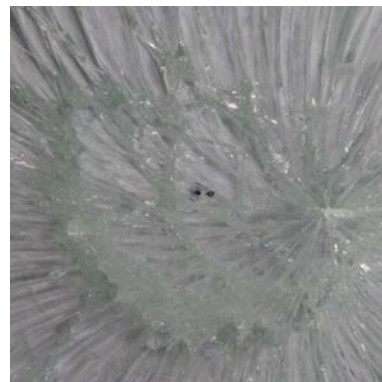


(b)

Figure 53: Fracture pattern of CT2

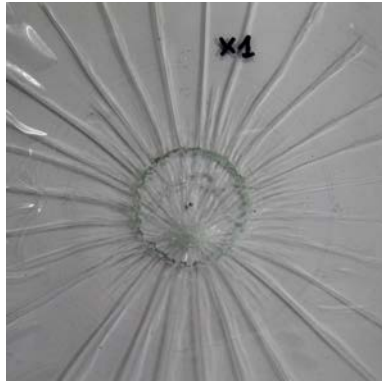


(a)



(b)

Figure 54: Fracture pattern of CT3



(a)

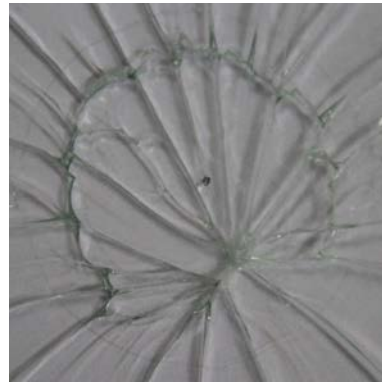


(b)

Figure 55: Fracture pattern of X1



(a)

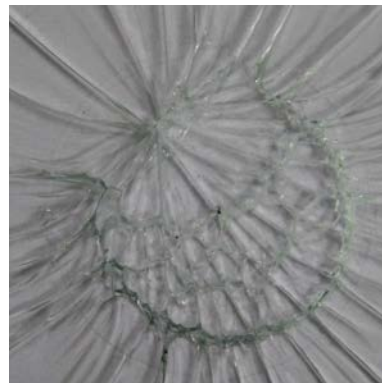


(b)

Figure 56: Fracture pattern of X2



(a)

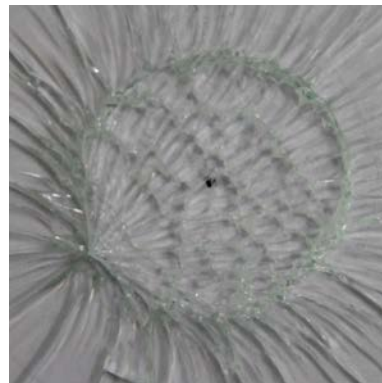


(b)

Figure 57: Fracture pattern of X3



(a)



(b)

Figure 58: Fracture pattern of X4



(a)

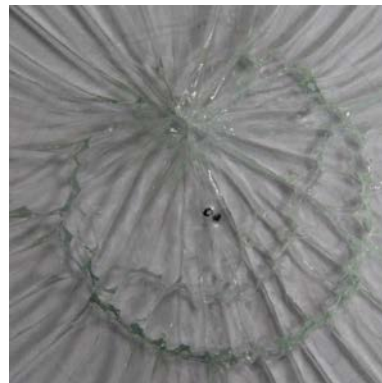


(b)

Figure 59: Fracture pattern of X5



(a)

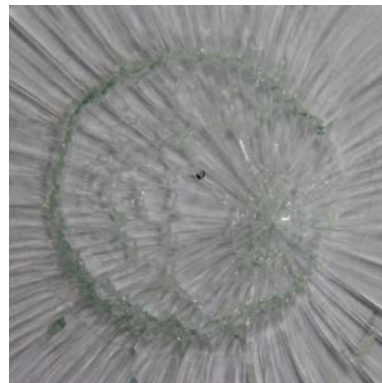


(b)

Figure 60: Fracture pattern of X6



(a)

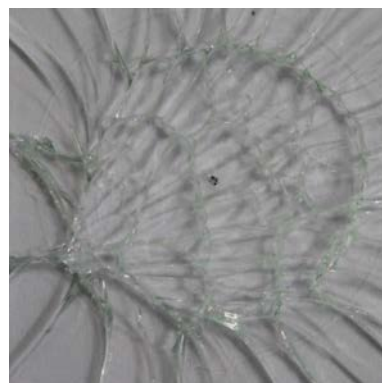


(b)

Figure 61: Fracture pattern of X7



(a)



(b)

Figure 62: Fracture pattern of X8

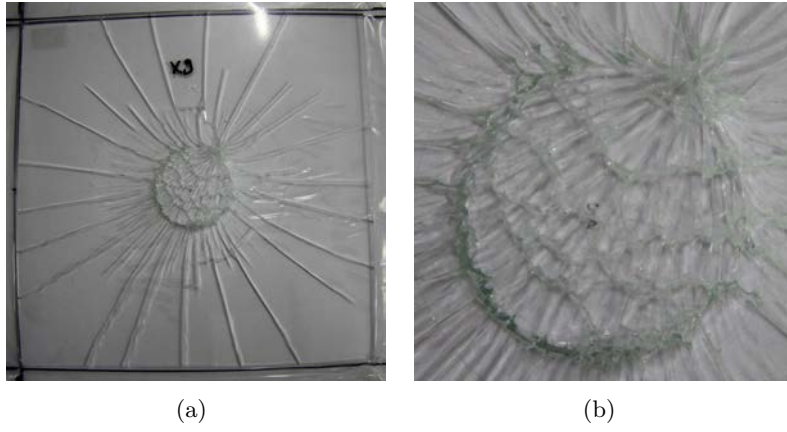


Figure 63: Fracture pattern of X9

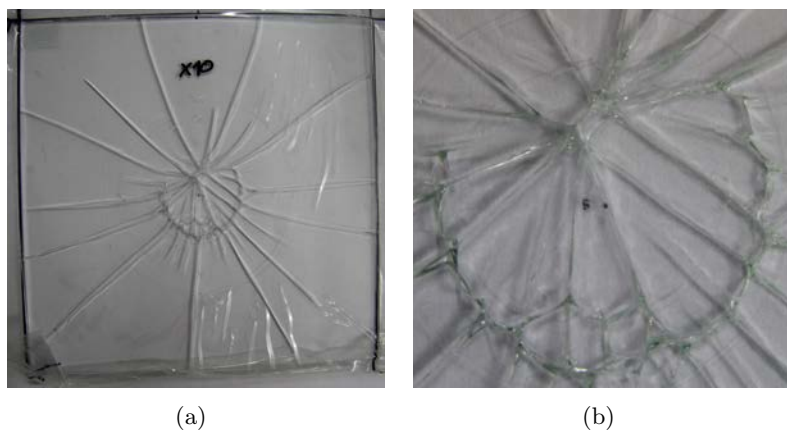


Figure 64: Fracture pattern of X10